PHYSIK–DEPARTMENT

Biophysical studies of radioiodine metabolism during therapy of Autonomous Functioning Thyroid Nodule

Doktorarbeit

von

Tilman Janzen

TECHNISCHE UNIVERSITÄT MÜNCHEN

TECHNISCHE UNIVERSITÄT MÜNCHEN

Fakultät für Physik
Fachbereich Strahlenphysik

Biophysical studies of radioiodine metabolism during therapy of Autonomous Functioning Thyroid Nodule

Tilman Janzen

Vollständiger Abdruck der von der Fakultät für Physik
der Technischen Universität München zur Erlangung des akademischen Grades eines

Doktors der Naturwissenschaften

genehmigten Dissertation.

Vorsitzender:	Univ.-Prof. Dr. Martin Zacharias
Prüfer der Dissertation:	
	1. Hon.-Prof. Dr. Herwig G. Paretzke
	2. Univ.-Prof. Dr. Franz Pfeiffer

Die Dissertation wurde am 16.11.2010 bei der Technischen Universität München eingereicht und durch die Fakultät für Physik am 21.03.2011 angenommen.

Contents

Zusammenfassung **vii**

List of acronyms and abbreviations **ix**

1 Introduction **1**

2 The thyroid **3**
2.1 Normal thyroid, physiology and metabolism 3
2.2 AFTN: disease, symptoms and diagnostics 5

3 Theoretical background of radioiodine therapy **7**
3.1 Introduction into nuclear medicine 7
3.2 Radiobiology and absorbed dose 8
3.3 Radioiodine therapy of AFTN 10
3.3.1 Basics of radioiodine therapy 10
3.3.2 Treatment planning 11

4 Materials and Methods **15**
4.1 Patients 15
4.2 Measurements 17
4.2.1 Measuring device and calibration 17
4.2.2 Measurement Schedule 18
4.2.3 Quantification of thyroid volume and mass 19
4.2.4 Quantification of activity in the thyroid 19
4.2.5 Quantification of activity in blood and urine samples 19
4.3 Biophysical modeling of radioiodine kinetics 20
4.3.1 Introduction into modeling 20
4.3.2 Approaches and software used in this work 22
4.3.3 Available models 27
4.4 Calculation of absorbed doses 31
4.4.1 Determination of half-life 31
4.4.2 Calculation of absorbed dose 33
4.4.3 Monte Carlo calculation of absorbed dose 33

4.5 Errors and uncertainties . . . 34
4.5.1 Uncertainties in time measurements . . . 34
4.5.2 Uncertainties in Gamma camera images . . . 35
4.5.3 Uncertainties in blood sample data . . . 36
4.5.4 Uncertainties in urine sample data . . . 36
4.5.5 Uncertainties in model parameters . . . 37

5 Measured data and model development 39
5.1 Measured data . . . 39
5.2 Development of a specific biophysical model structure for iodine in AFTN patients . . . 44
5.2.1 Model parameter estimation for the complete model . . . 47
5.2.2 Model parameter estimation: patients with blood samples . . . 51
5.2.3 Model parameter estimation: patients with urine samples . . . 54
5.2.4 Model parameter estimation: population analysis of reduced model 57
5.3 Comparison of biokinetics during diagnosis and therapy . . . 60
5.3.1 Differences between diagnostics and therapy - literature review . . . 60
5.3.2 Results of this study . . . 61

6 Optimization of the sampling schedule 65
6.1 Population analysis of the sampling schedule . . . 65
6.2 Individual analysis of the sampling schedule . . . 72

7 Absorbed dose and therapeutic outcome 77
7.1 Dose calculation for individual patients . . . 77
7.2 Dose calculation with Monte Carlo . . . 80
7.3 Evaluation of the outcome of the therapy . . . 82

8 Conclusions and outlook 85

Appendix 87

Bibliography 88

Acknowledgment 97

Zusammenfassung

Die Verwendung von Radioisotopen von Jod in der Diagnostik und Therapie von Schilddrüsenerkrankungen ist eine der ältesten klinischen Anwendungen in der Nuklearmedizin. Dabei ist der Schutz von Patienten und Personal vor ionisierender Strahlung ein wichtiger Aspekt. Einerseits soll dem Patienten so wenig Aktivität wie möglich verabreicht werden, andererseits muss eine für die Behandlung ausreichende Menge Aktivität in den zu behandelnden Organen oder Geweben akkumuliert werden. Dafür ist eine individuelle Behandlungsplanung für jeden Patienten notwendig, die auf der Kenntnis der jeweiligen Biokinetik des Radiopharmaceutikums beruht. Die dazu benötigten Daten müssen in einer patienten-spezifischen diagnostischen Studie gemessen werden, und die Kinetik muss mittels eines biophysikalischen Modells bestimmtwerden. Ein Ansatz für die Optimierung der Therapie ist die Entwicklung von biokinetischen Modellen, die in der Therapieplanung verwendet werden können.

Bei 43 Patienten mit autonomem Schilddrüsenadenom wurden sowohl während der diagnostischen Studie als auch während der Therapie die Aktivitätsverteilungen in der Schildrüse und die Aktivitäten in Blut- und Urinproben gemessen. Mit diesen Daten wurde in dieser Arbeit ein biophysikalisches Kompartmentmodell entwickelt, das spezifisch für die Biokinetik von Jod in Patienten mit autonomem Schilddrüsenadenom ist. Sowohl das gesunde als auch das kranke Schilddrüsengewebe wurden in eigenen Kompartments des Modells dargestellt. Auch die verschiedenen chemischen Zustände des Jods im Organismus, das elementare Jodid und das organisch gebundene Jod, wurden separat modelliert. Die Modellparameter wurden mit einem Populations-Kinetik Ansatz bestimmt.

Die während der Therapie im kranken Gewebe deponierte Energiedosis wurde berechnet und das Ergebnis mit einer Monte Carlo Simulation verifiziert. Der Ausgang der Therapie wurde mit der Dosis verglichen, um den Erfolg der therapeutischen Prozedur zu untersuchen. Die personalisierte Behandlung führte zu überaus guten Resultaten. Bei 90% der Patienten wurde die verschriebene Dosis verabreicht. Nur zwei der 43 Patienten litten nach der Therapie noch an einer Schilddrüsenberfunktion.

Mit dem in dieser Arbeit entwickelten Modell wurde ein optimierter Zeitplan für die Messungen erstellt, der die individuelle Behandlungsplanung weiter vereinfacht.

List of acronyms and abbreviations

AFTN	Autonomous Functioning Thyroid Nodule
ALARA	As Low As Reasonably Achievable
DIT	Diiodotyrosine
DNA	Deoxyribonucleic Acid
EANM	European Association of Nuclear Medicine
FDG	Fluorodeoxyglucose
FSD	Fractional Standard Deviation
fT3	free Triiodothyronine
fT4	free Tetraiodothyronine
IAEA	International Atomic Energy Agency
ICRP	International Commission on Radiological Protection
ICRU	International Commission on Radiation Units and Measurements
MIRD	Medical Internal Radiation Dose Committee
MIT	Monoiodotyrosine
MLEM	Maximum Likelihood Expectation Maximization
NIS	Sodium-Iodine Symporter
NNDC	National Nuclear Data Center
OMP	Fondazione IRCCS Ca' Granda - Ospedale Maggiore Policlinico
PET	Positron Emission Tomography
ROI	Region of Interest
SPECT	Single Photon Emission Computed Tomography
T3	Triiodothyronine
T4	Tetraiodothyronine
Tg	Thyroglobulin
TPO	Thyroperoxidase
TSH	Thyroid-Stimulating Hormone
WHO	World Health Organization

1 Introduction

One of the main peaceful uses of nuclear technology, next to energy production, is in the field of nuclear medicine. There, ionizing radiation is used for diagnostic and therapeutic purposes. The use of radioisotopes of iodine in the diagnostic and therapy of thyroid diseases is among the oldest procedures in nuclear medicine [Meier2002]. One of the procedures using radioiodine is the therapy of autonomous functioning thyroid nodules (AFTN). The procedure is divided into a treatment planning phase and and a therapy phase. Whereas the treatment planning phase includes a diagnostic scan with ^{123}I, the therapy phase mainly consists of the administration of a therapeutical activity of ^{131}I. In this thyroid disease some parts of the thyroid are producing excessive amounts of hormones unregulated. The treatment with radioiodine is very effective because the active cells in the thyroid gland accumulate iodine and thus the radiation from the decaying radioisotopes of iodine can destroy the diseased parts of the thyroid [Grzesiuk2006].

Since the introduction of nuclear medicine procedures into clinical practice in the 1940s, the radiation protection of patients and staff is one of the key issues discussed in this context. Several international organizations like the International Atomic Energy Agency (IAEA), the International Commission on Radiation Units and Measurements (ICRU) and the International Commission on Radiological Protection (ICRP) are concerned with this topic and have published guidelines and recommendations. Because ionizing radiation poses a potential threat to the health, a general principal in nuclear medicine is to keep the exposure to ionizing radiation "As Low As Reasonably Achievable"[ICRP1977]. This is simply referred to as the ALARA principle. Consequently there is an ongoing effort in clinical practice and research to optimize the use of ionizing radiation. The challenge is to minimize the exposure of patients while accumulating enough activity to get the wanted result: information on the condition of the patient in imaging or the administration of enough dose to control the respective disease during therapy.
One approach is to develop biophysical models of the radiopharmaceutical's kinetics using information on its physical, biological and physiological properties. These models can be used for treatment planning, dosimetric evaluations and to get further insight into the radiopharmaceuticals behavior in the human organism. They can also be used to optimize the clinical procedures in order to minimize the exposure of patients to ionizing radiation.

The aim of this work was to develop a biophysical compartmental model specific for the iodine kinetics in AFTN patients. This model should allow a physiologically realistic description of the administration, distribution, metabolism and excretion iodine. For this

purpose the model parameters can be estimated using the measured patient data collected during diagnostics and therapy in an extended clinical study.
In a next step the efficiency of the clinical procedures should be optimized with the help of the model to improve the measurement schedule for diagnostics. Thereto the minimal number and the optimal time points for diagnostic measurements should be investigated that are necessary to predict the kinetics during therapy. With this knowledge the optimal therapeutic activity can be determined for each patient individually.
Finally the absorbed doses administered to the thyroid should be calculated and the results validated with a Monte Carlo simulation. The outcome of the therapy can be compared with the absorbed dose to assess the success of the therapeutic approach.

2 The thyroid

2.1 Normal thyroid, physiology and metabolism

Because this work is aimed at developing a physiologically realistic biophysical model for a thyroid disease, a short introduction into the role and function of the thyroid is given here.

The thyroid is an endocrine gland that is found in the neck below the larynx (voice box) and in front of the trachea (windpipe). It is shaped like a butterfly with two lobes either side of the windpipe that are connected by the isthmus. The thyroid produces hormones that regulate the human metabolism and thus affect almost every function in the body. Thyroid hormones have an effect on the heart and the circulation. They lead to an increase in heart rate and blood pressure. The rate of sugar and lipid metabolism is increased and in the nervous system the excitability of the cells is raised. The general effect of the thyroid hormones is an increased basal metabolic rate and energy consumption of the organism.
The essential trace element iodine is a pivotal component of the thyroid hormones. The World Health Organization (WHO) recommends a daily dietary intake of iodine of 180-200 μg for adults [WHO2004]. Dietary iodine is generally ingested in the form of iodide. It is absorbed into blood from the small intestine and to a smaller degree from the stomach. Iodide is rapidly distributed in the extracellular fluid and is transferred to the stomach wall, to the gastric mucosa, to the salivary glands, to the kidneys and to the urinary bladder system but it accumulates primarily in the thyroid [Hays1965]. There it is metabolized during the synthesis of the thyroid hormones.
The following rough outline of the metabolism of iodine in the thyroid follows the description given in Werner & Ingbar's "The Thyroid" [Thyroid2000].
A schematic illustration of the thyroid cells and the metabolic processes of iodine in the thyroid is shown in figure 2.1. The thyroid cells are organized in spherical accumulations called the follicles. The space enclosed by these spheres is called the lumen and contains mainly the protein thyroglobulin (Tg). Iodide in the thyroid is transported through the thyroid cells into the follicular lumen and at the same time transformed to elemental iodine. The protein used for the transport is the sodium-iodine symporter (NIS). Neutral iodine atoms are formed by oxidation of iodide in a reaction that uses hydrogen peroxide (H_2O_2) and the thyroperoxidase (TPO) enzyme. In the lumen, residues of the amino acid

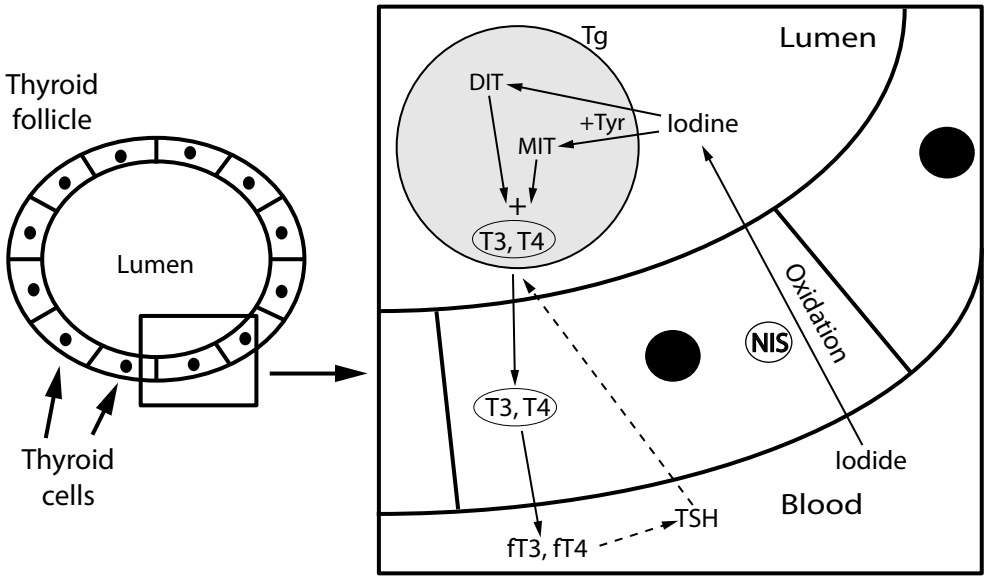

Figure 2.1: Schematic illustration of the synthesis and secretion of thyroid hormones adapted from internal ICRP communication; see text for details

tyrosine (Tyr) are iodinated within the Tg molecule. Depending on whether one or two iodine atoms are coupled to the tyrosine, monoiodotyrosine (MIT) or diiodotyrosine (DIT) are formed. These resulting iodotyrosine molecules are coupled within the Tg molecule to form the thyroid hormones triiodothyronine (T3 = MIT + DIT) and tetraiodothyronine (T4 = DIT + DIT). Free iodotyrosines (MIT and DIT) and iodothyronines (T3 and T4) are released by proteolysis of Tg and the iodothyronines T3 and T4 are then secreted into blood. The thyroid hormones T3 and T4 are taken up by various tissues in the whole organism and regulate metabolism and growth. Unbound T3 and T4 in the blood are referred to as "free" and called fT3 and fT4 respectively.

In healthy persons (defined as euthyroid, i.e. with normally functioning thyroid) the thyroid hormone production and release into blood are regulated by a negative feedback loop. It relies on the thyroid-stimulating hormone (TSH or thyrotropin) that controls the secretion of the hormones T3 and T4 from the thyroid gland and is produced in the pituitary gland. The levels of thyroid hormones in blood regulate the release of TSH. The more T3 and T4 in blood, the less TSH is released. Conversely, when the concentration of thyroid hormones is low, production of TSH is increased and secretion of T3 and T4 is promoted. The thyroid also reacts very sensitively to the available amounts of iodine. Low amounts of iodine can lead to overstimulation and overreaction of the thyroid tissue.

As thyroid hormones are very important for the human metabolism, diseases of the thyroid can have serious effects on the human constitution. Too low or too high levels of thyroid hormones can severely disrupt the metabolism and can lead to life threatening

symptoms. Patients whose thyroid is not able to produce sufficient amounts of thyroid hormones are called hypothyroid, while patients with excessive levels of hormones are called hyperthyroid. Common diseases are:

- Graves' disease, an autoimmune illness where the thyroid is enlarged and produces excessive amounts of hormones,
- thyroid cancer, a malign tumor and
- thyroid adenoma, a benign tumor, described in detail below.

2.2 Autonomous functioning thyroid nodule (AFTN): disease, symptoms and diagnostics

In this work a biophysical model is developed specifically for the biokinetics of iodine in patients suffering from AFTN. AFTN is a thyroid adenoma, a benign (non cancerous) tumor [Deleu2000]. It's development, symptoms and diagnostics are briefly described below.
In areas with a low presence of iodine in soil and water the deficiency of iodine in nutrition leads to a disturbance of thyroid function called the endemic goiter. It is in itself not a disease but rather a hypertrophy of the thyroid epithelial cells caused by prolonged TSH stimulation. Intrathyroidal iodine deficiency activates local growth factors (EGF, IGF-1, ...) that induce hyperplasia of the cells. Under continued TSH stimulation groups of thyroid cells can develop functional autonomy. Induced mutations of the TSH receptors lead to their permanent activation [Parma1993]. Single or multiple autonomous functioning nodules evolve that are no longer governed by the feedback loop. These are called autonomous functioning thyroid nodules. Depending on the hormone production rate of the adenoma and the functionality of the healthy thyroid the patient remains euthyroid or develops hyperthyroidism.
Hyperthyroidism is a severe disease and necessitates immediate treatment. Symptoms are tachycardia, nervousness, unwanted weight loss and increased sweating. Hyperthyroidism potentially aggravates cardiac diseases and the long term exposure to elevated levels of thyroid hormones can cause supraventricular arrhythmia. These complications may not be reversible after treatment of hyperthyroidism.
An AFTN can be diagnosed by palpation of the thyroid and it is often visible on sonographic (ultrasound) scans and in scintigraphic scans after administration of ^{99m}Tc pertechnetate. Blood samples are tested to check for hyperthyroidism and a low TSH level. Additionally, elevated serum fT3 and fT4 levels are indicators for the disease.

3 Theoretical background of radioiodine therapy

In this chapter background information is given on the radioiodine therapy of the autonomous functioning thyroid nodule. First the basics of nuclear medicine, radiobiology and dose calculation are described. Then the basics of radioiodine therapy and the most common clinical procedures for treatment planning are introduced.

3.1 Introduction into nuclear medicine

Nuclear medicine is the branch of medicine that deals with diagnostic and therapeutic procedures with unsealed radionuclides. These radionuclides, referred to as radiopharmaceuticals, can be either in elemental form, like radioiodine, or can be bound to molecules. After either oral or intravenous administration to the patient they are transported through the body and accumulate in certain tissues or organs. The choice of a radiopharmaceutical is based on its properties to accumulate only in specific areas, organs or tissues of the body.
The absorption, distribution, metabolism and excretion of a radiopharmaceutical are called the pharmaco- or biokinetics. The biokinetic behavior of a radiopharmaceutical is governed by its physical and chemical properties such as molecular size and structure. Depending on these properties a radionuclide or a molecule with an attached radionuclide can be used for various tasks. ^{18}F labeled fluorodeoxyglucose (FDG), for example, is used to monitor the metabolism of sugar and thus the energy consumption while ^{18}F labeled choline is used to screen for recurrence or metastasis in prostate cancer patients. In this way these specific regions of interest (ROI) can be imaged or treated. Further desired properties of radionuclides for medical use are a low chemical toxicity and a stable daughter-nuclide.

For diagnostic purposes the radiation leaving the body of the patient is of interest as it is used for imaging. When radiopharmaceuticals are used for imaging, the isotopes are preferably either pure gamma emitters or positron emitters. Isotopes with a gamma energy between 50 keV and 500 keV are chosen, so that only little energy is deposited within the patient's body because most rays leave the body. Photons in this energy range can be detected efficiently and can therefore be used for imaging. The most widespread devices

for imaging are gamma cameras, single photon emission computed tomography (SPECT) and positron emission tomography (PET) devices. While the latter two are specifically devised for three dimensional imaging, gamma cameras can be used for two dimensional and three dimensional imaging depending on operational mode and the technical set up.

For therapy, it is the radiation energy deposited within the patient that is of interest. Therapy in nuclear medicine is based on the biological effect of ionizing radiation. For therapy with radiopharmaceuticals, the radionuclide is targeted to accumulate in or near to diseased cells and to decay and to deposit its energy there. The preferred radionuclide for therapy is a β-emitter because electron radiation has a relatively short range. Therefore the radiation energy released during the decay is deposited near the site of the decay and can thus destroy the diseased cells.

3.2 Radiobiology and absorbed dose

To understand the effects of ionizing radiation on tissues and to implement radiation protection in medicine, first the properties of the interaction of ionizing radiation with matter have to be considered.

If the radiation energy absorbed by the tissue is large enough to ionize atoms, this ionization can lead to the destruction of molecular connections and to the alteration of biomolecules. Generally two kinds of ionizing radiation can be distinguished. The first is directly ionizing radiation, i.e. charged particles like electrons, protons and α-particles. These can ionize atoms directly through collisions. The second kind is indirectly ionizing radiation like neutrons and photons (x-rays and gamma rays). In this case secondary charged particles are created by interaction with the atoms of the irradiated tissue. Neutrons interact by collisions, but for photons the main interactions are the photoelectric effect, Compton scattering and pair production.
The destructive effect of ionizing radiation on a cell is mainly due to damage to the deoxyribonucleic acid (DNA) molecule in the cell nucleus, although membrane damage may also be a factor. There are two ways that ionizing radiation can damage the DNA: either by a direct hit or by ionization of a water molecule near the DNA molecule with the newly formed radical damaging the DNA. The most common damages are base damage, single- and double-strand breaks. Because most damages can be repaired, the most important mechanisms for the biological effect of ionizing radiation are not or not correctly repaired double-strand breaks. These lead, depending on the cell-type, either to apoptotic or mitotic death. This destructive effect can be used in medicine to destroy diseased tissues like cancer cells.

Because the biological effect is connected to the absorbed energy, a measure is defined to quantify the absorbed energy per mass. It is called the dose and its unit is the Gray

(Gy) defined as 1 Gy = 1 J/kg. The higher the dose the lower is the fraction of surviving cells. The ICRP and the Medical Internal Radiation Dose Committee (MIRD) both have published standard methods and mathematical schemata for the calculation of absorbed doses in nuclear medicine although with differences in terminology. Recently a unified terminology has been proposed [Bolch2009] that is adopted here. The mean absorbed dose $D(r_T, T_D)$ to a target tissue r_T from one or more source tissues r_S over a time interval T_D after the administration of a radiopharmaceutical is given by:

$$D(r_T, T_D) = \sum_{r_S} \int_0^{T_D} A(r_S, t)\, S(r_T \leftarrow r_S, t)\, \mathrm{d}t, \tag{3.1}$$

where $A(r_S, t)$ is the time-dependent activity of the radiopharmaceutical in the source tissue, and $S(r_T \leftarrow r_S, t)$ is the absorbed dose rate to a target r_T per unit activity in a source r_S. The time-dependent activity A in a source tissue can either be obtained from measurements or can be derived computationally e.g. from solutions of compartmental models describing the biokinetics of the radiopharmaceutical. It corresponds to the area under the time-activity-curve that describes the kinetics of the radiopharmaceutical's uptake, retention and excretion for a tissue. These can be very hard to estimate as they can differ widely between patients.
The S-value is specific to the radionuclide and the relative position of source and target region:

$$S(r_T \leftarrow r_S, t) = \frac{1}{M(r_T, t)} \sum_i E_i\, Y_i\, \phi(r_T \leftarrow r_S, E_i, t), \tag{3.2}$$

where $M(r_T, t)$ is the time-dependent mass of the target tissue, E_i is the energy of the i^{th} nuclear transition, Y_i is the number of i^{th} nuclear transitions per nuclear transformation, and $\phi(r_T \leftarrow r_S, E_i, t)$ is the absorbed fraction. The absorbed fraction is that fraction of the energy emitted in a source region r_S that is absorbed in a target region r_T. Besides the energy emitted, it is also dependent on the anatomical model chosen to represent the patient. This can be either a computational model [Snyder1975] or a segmented image of the patient [Zankl2003]. Additionally, S-values can not only be calculated for tissues or organs but also on a voxel level [Bolch1999]. As radiopharmaceuticals generally have a short half-life of up to a few days, S can in general be assumed to be independent of time because normally the masses don't change that fast. If time dependency can be neglected equation 3.1 can be simplified to the following time independent form:

$$D(r_T, T_D) = \sum_{r_S} \tilde{A}(r_S, T_D)\, S(r_T \leftarrow r_S, t), \tag{3.3}$$

where $\tilde{A}(r_S, t)$ is the total number of nuclear transformations (or time-integrated activity) in the source tissue over the dose integration time T_D; $\tilde{A}(r_S, t) = \int_0^{T_D} A(r_S, t)\, \mathrm{d}t$. This time-independence may not be true for tumors, so care must be taken when dealing with either fast growing tumors or with tumors that decrease in size during therapy.

3.3 Radioiodine therapy of AFTN

There are several treatments available for the therapy of AFTN and similar conditions like Graves' disease. The treatment with radioactive iodine isotopes is a long-standing, very common, safe and effective method. As with all nuclear medicine procedures, the only contraindications for the therapy with radioiodine are pregnancy and breast-feeding [Singer1995]. Alternative treatments that are also available are surgery and percutaneous injection of ethanol.

3.3.1 Basics of radioiodine therapy

The iodine isotopes used in clinical practice are ^{123}I, ^{124}I and ^{131}I. Information on the physical properties of the isotopes were obtained from the National Nuclear Data Center at Brookhaven National Laboratory [NNDC2010]. The nuclear decay data provided in ICRP publication 107 [ICRP2008] are based on the same source.
The isotope ^{123}I is used for imaging. It decays via electron capture and is a pure gamma emitter with a half-life of 13.22 hours. 83 % of the photons are emitted with an energy of 159.0 keV.
^{124}I is rarely used. It also decays via electron capture with a half life of 4.18 days. It can be used for PET imaging of the thyroid because, with an intensity of 22.7 %, it is a positron emitter.
The iodine isotope ^{131}I is generally used for radioiodine therapy. It is a β emitter with a half life of 8.02 days. The emitted electrons have a mean energy of 191.6 keV and a maximal energy of 606 keV. This corresponds to a maximal range of the electrons in tissue of about 2 mm. Additionally gamma radiation is emitted. Photons with an energy of 364.5 keV are emitted with the highest intensity (81.7 %).

The basic idea of radioiodine therapy is the destruction of the functionality of thyroid cells by radiation. The energy released during radioactive decay of ^{131}I is mainly absorbed in the diseased part of the thyroid because in AFTN the most iodine is accumulated there. Thus the effect of the therapy is directly connected to the absorbed dose [Grzesiuk2006].

There is an ongoing discussion about long-term effects of radioiodine treatment of hyperthyroidism. This issue has been addressed in several studies but with conflicting conclusions [Hoffman1982, Holm1991]. Tezelman et al. claimed in 1994 that radioactive iodine in doses suitable for treatment of Graves' disease may increase the risk of developing thyroid cancer and that these cancers are discovered at a later stage and appear to be more aggressive [Tezelman1994]. But the study design in this case prevents any conclusion about the causal relationship between the therapy with radioiodine and cancer. In a population-based cohort study in Finland, Metso et al. have recently reported an increased incidence and mortality for cancer and cardiovascular diseases in patients who had

undergone radioiodine treatment for hyperthyroidism [Metso2007a, Metso2007b]. But it is not clear whether this increase is related to the therapy and the authors conclude that it is rather the hyperthyroidism itself that is responsible for long term effects. In the light of these publications Lucignani concluded recently that there was no evidence that the administration of radioiodine induces cancer or other diseases [Lucignani2007].

3.3.2 Treatment planning

Every procedure in nuclear medicine is preceded by a treatment planning phase.
The first step in treatment planning is to determine what absorbed dose is needed to destroy the diseased tissue and cure the patient. However, this step is often omitted and the absorbed dose plays no role in many clinical protocols for radioiodine treatment of AFTN. The reason for this is that it is much easier and cheaper to give all patients the same predetermined activity [Weetman2007]. Less staff is needed and the machines are not blocked by the additional measurements.

In the protocols that consider the absorbed dose during treatment planning, several factors influence the choice of dose to be administered to the AFTN patient. One is the grade of the disease; the more advanced the disease is, the more dose is needed. Another factor is the desired functionality of the thyroid after the treatment. Depending on the dose the normal functionality of the healthy thyroid tissue is either preserved or it is lost if there is too much damage to the healthy tissue.
The desired outcome of the therapy is always to remedy hyperthyroidism. The higher the dose the better is the chance that the diseased tissue is destroyed and there will be no recurrence of hyperthyroidism. But as the healthy thyroid tissue is also irradiated during therapy it can be damaged [Reschini1999]. So the patient can become either euthyroid or hypothyroid after therapy, depending on the dose. Hypothyroidism is often not seen as a complication as it can be easily controlled by giving artificial thyroid hormones regularly to the patient.
The severity of the disease is also important in the choice of dose. The more advanced the disease the more dose is needed for cure [Franklyn1995, Alexander2002]. And also the volume of the autonomous tissue is correlated with the dose. For a bigger volume a higher dose is needed for successful treatment [Reinhardt2002, Erdogan2004].

After the desired absorbed dose is determined, the respective activity needed to deliver this dose to the AFTN has to be estimated. There are several different approaches but they can be divided into two main classes. One are protocols where the individual kinetics are neglected. The other are approaches where a small test activity of radioiodine is administered and the activity in the thyroid is measured for every patient. This second procedure is used to determine some individual biokinetic parameters and is referred to as the diagnostic approach.

The simplest approach is to give all patients the same, fixed activity that has evolved empirically. Some authors claim the results of this method are not worse than those with individually determined activities and because of its simplicity it is connected with very low costs [Franklyn1995, Leslie2003, Allahabadia2001]. But several authors have shown that this method can lead to severe over-dosage and thus unnecessary exposure of healthy tissue to high doses of radiation [Clerc1995, Matheoud2003, Jonsson2004, Mattsson2006].

In an alternative method a fixed activity per nodule volume (MBq/ml) is administered [Zingrillo2000, Kok2000]. Because this method, like the previous one, neglects the individually different uptake and retention of iodine in the nodule, it can lead to over- or underdosage and a failure of treatment.

The protocols including the measurement of the individual kinetics for diagnostic purposes come in a great variety of complexity. Usually, a small activity is administered and the activity accumulated in the thyroid is measured at different times. In this work this administration and measurements of a small test activity will be referred to as diagnostic procedure or as diagnostics.
Next to ^{131}I, also ^{123}I is used in some protocols. It is very well suited for imaging because its gamma energy of 159 keV is very close to that of ^{99m}Tc with 140.5 keV. As most commercially available gamma cameras are optimized for the imaging with ^{99m}Tc, radiation from the decay of ^{123}I can be detected more efficiently than radiation from ^{131}I. Furthermore, the yield of gamma radiation per nuclear transition of ^{123}I is larger than that of ^{131}I. Therefore a smaller activity is needed than with ^{131}I. Because of this and because ^{123}I emits no β-radiation the absorbed dose from imaging with ^{123}I is lower. Another advantage of ^{123}I over ^{131}I is that the spatial resolution in the images is better because a thinner collimator can be used. Thereby the structure of the thyroid can be better imaged and a differentiation between the AFTN and the healthy tissue is possible.
While some are contented with sole measurements of the 24 h uptake of radioiodine in the thyroid gland [Alexander2002], others measure additionally the volume and thus the mass of the gland [Ross1984, Nygaard1999, Haase2000, Erdogan2004]. In these cases the half-life is approximated by one empirical value for all patients and the activity to be administered is calculated so that at maximum uptake a certain activity per mass ratio (MBq/g) is reached.
A more complex procedure is to determine uptake and half-life for each patient individually. In this case several measurements over several days are necessary. This information combined with data on volume or mass is the best method to administer the desired dose to the diseased tissue and gives good treatment results [Guhlmann1995, Berg1996, Canzi2006].
One example for such a procedure is the one used at Fondazione IRCCS Ca' Granda - Ospedale Maggiore Policlinico (OMP) in Milan, Italy [Matheoud2003][Canzi2006] where the patients in this study were treated. There, the measurements made during the diag-

nostic study are used to calculate the activity needed to deliver the desired absorbed dose to the AFTN in the following way. The iodine uptake $U(t)$ in the thyroid is described using the relationship

$$U(t) = \frac{U_0 * \lambda_{in}}{\lambda_{out} - \lambda_{in}}(e^{-\lambda_{in}t} - e^{-\lambda_{out}t}) \tag{3.4}$$

with U_0 the fraction of administered iodine transferred to the thyroid, λ_{in} the rate of intake and λ_{out} the rate of biologic clearance. λ_{out} is assumed to be much smaller than λ_{in}. Because uptake data corrected for radioactive decay are used, this equation describes the biologic behavior of iodine independent of the isotope used. The parameters U_0 and λ_{out} are obtained from a fit of equation 3.4 to five uptake values $(t, U(t))$ collected during diagnostics. The activity A_0 of ^{131}I to administer is then calculated as:

$$A_0 = \frac{D * \lambda_{eff} * m}{U_0 * S} \tag{3.5}$$

where D is the desired absorbed dose, the effective decay constant $\lambda_{eff} = \lambda_{out} + \lambda_{phys}$ is the sum of the biologic clearance and physical decay constant, m is the mass of the target structure and S is the absorbed dose per unit activity defined in equation 3.2.

The different approaches were compared in several studies. Those favoring a fixed activity over the diagnostics approach either found that outcome was not significantly better with diagnostics [Catargi1999] or could not find a relation between the administered activity and the outcome of the treatment [Leslie2003, Metso2004] or could not find differences in the absorbed doses between the methods [Clerc1995]. Those in favor of an individualized treatment found that it yields better results as the kinetics can differ widely and only a personalized therapy can avoid over- or undertreatment [Matheoud2003, Reinartz2003, Jonsson2004]. It can be observed that the studies that see no difference between the methods and therefore favor the fixed activity approach consider mostly qualitative aspects like outcome and do not take actual absorbed doses into account. The authors favoring the diagnostic protocols do a more quantitative evaluation calculating the absorbed dose and finding severe over- or undertreatment in the fixed activity methods.

Because of this ongoing discussion the treatment is monitored in many clinics by measuring with gamma cameras or gamma counters over the thyroid. The general aim is to verify if the planned activity or dose is administered to the gland and to determine how much activity is accumulated in the healthy tissue. These studies are continuously evaluated to improve the clinical procedures.
If uptake measurements have been made for diagnostics and therapy, a common observation is that uptake is comparatively lower during therapy than it was during diagnostics [Bockisch1993, Reinhardt2002, Canzi2006].

4 Materials and Methods

4.1 Patients

All investigations in this work, like the model development and the dosimetric evaluations, were based on a set of patient data collected at Fondazione IRCCS Ca' Granda - Ospedale Maggiore Policlinico (OMP) in Milan, Italy during the years 1998-2009. Measurements in recent years were done in collaboration with the Department for Medical Radiation Physics and Diagnostics at the Helmholtz Center Munich. 43 patients (33 females and 10 males) suffering from AFTN gave their written informed consent to participate in the study. Patient age at referral to the hospital ranged from 43 years to 85 years with a median of 66 years. All patients were hyperthyroid with suppressed levels of TSH but in 25 patients (58 %) the condition was subclinical. 13 patients were previously treated with methimazole, 5 patients with ethanol injections, 2 patients with both methimazole and ethanol and one patient had been given levothyroxine. Medication was discontinued at least 14 days before radioiodine treatment started. 22 patients (51 %) did not have any previous treatment. The patients participating in this study are representative for the target population of the treatment.

Table 4.1: Statistics of the patients and the treatment; next to age and gender of the patients, the activities administered for diagnostics and therapy and the times of the last measurements are indicated.

Number	Age [a]	Gender	Diagnostics		Therapy	
			Act [MBq]	t_{max} [h]	Act [MBq]	t_{max} [h]
1	84	F	111	119	274	506
2	70	F	111	118	111	532
3	85	F	111	118	163	603
4	62	F	111	119	444	602
5	47	F	111	119	266	771
6	60	F	111	118	307	603
7	62	F	111	119	518	770
8	66	M	111	120	389	600

continued on next page...

Table 4.1: (continued)

Number	Age [a]	Gender	Diagnostics		Therapy	
			Act [MBq]	t_{max} [h]	Act [MBq]	t_{max} [h]
9	67	F	111	118	300	768
10	70	M	111	117	488	528
11	55	F	111	118	470	600
12	69	M	111	118	252	96
13	80	F	55	118	152	94
14	68	F	111	119	259	96
15	53	F	111	119	352	599
16	64	F	111	118	155	600
17	70	F	111	118	318	768
18	53	F	148	121	315	95
19	60	M	148	119	333	168
20	66	F	55	71	189	503
21	55	F	55	71	370	506
22	63	F	55	72	180	505
23	50	F	55	72	277	509
24	63	M	55	71	451	506
25	73	M	37	71	337	507
26	45	F	37	71	340	340
27	74	F	37	71	189	73
28	45	M	37	72	218	99
29	66	M	37	72	311	602
30	70	M	111	119	359	769
31	73	F	111	119	315	1103
32	75	F	111	119	196	359
33	63	F	111	119	274	675
34	72	F	111	120	315	551
35	55	M	146	120	611	721
36	65	F	105	122	197	1033
37	84	F	95	119	607	360
38	66	F	165	120	66	335
39	79	F	167	120	481	505
40	61	F	170	120	870	527
41	79	F	170	121	164	527

continued on next page...

Table 4.1: (continued)

Number	Age [a]	Gender	Diagnostics		Therapy	
			Act [MBq]	t_{max} [h]	Act [MBq]	t_{max} [h]
42	69	F	133	119	851	864
43	43	F	167	119	198	673
Females		33				
Males		10				
Mean (total)	65		67	108	331	524
Mean (Females)	66		108	110	318	544
Mean (Males)	64		90	100	375	460
Minimum	43		37	71	66	73
Maximum	85		170	122	870	1033

4.2 Measurements

The standard procedure used for radioiodine treatments at OMP has been described in detail previously [Matheoud2003, Canzi2006]. The following is a short summary of the procedure followed during this study. After diagnosis of AFTN, the patients were referred to the clinic. There they were injected with a small activity of ^{123}I for the diagnostic scan. Based on these measurements, the therapeutical activity of ^{131}I needed was determined and administered.

4.2.1 Measuring device and calibration

For each patient the syringe containing the activity for the diagnostic scan and the capsule containing the activity for the therapy were both measured before and after application to the patient in a calibrated well-counter. Thus it was possible to determine exactly the activity given to the patient.
A Picker (meanwhile bought by Philips) Irix 3 gamma camera was used during diagnostics and therapy for the scans measuring the activity in the thyroid. Measuring with a gamma camera is advantageous in patients with AFTN because the activities in the diseased nodule and the healthy lobe can be determined separately and the shapes and volumes of these structures can be determined.

Because two different isotopes, ^{123}I and ^{131}I, were used for diagnostics and therapy, the images were acquired with a low-energy and a high-energy, high-resolution, parallel-hole collimator, respectively. To calibrate the camera, the syringe and the capsule were also measured in the gamma camera before and after the application. For this purpose they were placed in a neck phantom made of an acryl cylinder with a 12.5 cm diameter and a hole, fitting the size of the syringe, situated 1 cm below the side facing the collimator. The phantom is used to simulate the attenuation and scattering of the radiation occurring in a human neck. Comparing the counts from the gamma camera with the value given by the well counter gives an absolute calibration of the gamma camera. For activities higher than 300 MBq a correction factor had to be introduced to account for dead time of the camera. All blood and urine samples were measured in a gamma counter Wizard 1480 manufactured by Wallac (Turku, Finland). Here too calibration factors were applied to account for the counting photon efficiencies at different energies.

4.2.2 Measurement Schedule

For the diagnostic study, the activity of ^{123}I injected ranged from 37 MBq to 170 MBq with a median of 111 MBq. The first measurement was taken 2 hours after injection. Then scans after about 4, 24, 48 and 120 h followed. In ten patients that got a lower amount of activity (37 or 55 MBq) the last measurement was taken 72 h after injection. Urine samples were collected in three patients. In two further patients blood samples were taken.

The therapeutic activity was determined according to the results of the diagnostics as described in chapter 3.3.2. The activity was administered orally. Therefore the patients were asked to fast the night before the treatment. The capsules containing the activity for oral administration are obtained from a commercial provider. They are only available from the manufacturer containing discrete amounts of activity increasing in steps of 1 mCi (1, 2, 3, ... mCi). These values are determined at the time of production. However, because the time needed for shipment may vary and radioactive decay reduces the activity during that time, it is not possible to know in advance exactly what activity will be available for treatment. The order for activity is made so that the activity determined during treatment planning is approximately met. However, there is no possibility to adjust the activity the patient gets once the capsule has arrived in the hospital other than wait for some time until radioactive decay has reduced the activity.

During therapy the activity was measured 5 to 9 times in each patient. A total of 301 measurements was made (which equates to an average of 7 measurements per patient). The first measurement was taken after about 2 hours, followed by measurements after about 4 h, 1 d, 2 d, 3 d, and 4 d. In one patient the last measurement was after 3 d, in five patients after 4 d, in one patient after 7 d, in four patients after 14 d and thirty three

patients had the last measurement later than 21 d after injection. Urine samples were collected in seven patients. In three further patients blood samples were taken.

4.2.3 Quantification of thyroid volume and mass

ROIs for the nodule and, if visible, the lobe were defined in the first image of the diagnostic scan for each patient. This was done with a special computer program, provided with the gamma camera, that displays the images and allows ROI definition by manually drawing the outline of the structures with the mouse cursor. Once defined on the first image these ROIs were saved and were used for all subsequent images of diagnostics and therapy of the same patient. The ROIs drawn for nodule and lobe generally have an ellipsoidal shape. By measuring the long and short axes a and b of this ellipsoid in the image, the volumes of nodule and lobe are determined as $V = \pi ab^2/6$. A mass density of 1 g/ml was assumed and the mass was calculated accordingly.

4.2.4 Quantification of activity in the thyroid

The ROIs for nodule and lobe were drawn as described above. Additionally a background region was defined in the first image. A rectangular area in one corner of the image was chosen, about half the size of the nodule, well separated from nodule and lobe and with no visible uptake. In the same program that was used for the ROI definition, the number of counts in each ROI in every image was automatically computed. The iodine uptake $U(t_i)$ in a ROI at time t_i of the i-th measurement corrected for radioactive decay was then calculated as:

$$U(t) = \frac{C_{ROI} - C_{Bkg}}{C_{SyrPre} - C_{SyrPost}} \, e^{\lambda_{phys} t} \tag{4.1}$$

with C_{ROI}, C_{Bkg}, C_{SyrPre} and $C_{SyrPost}$ the counts per second in the ROI, in the background ROI, in the syringe in the neck phantom before the administration and in the syringe in the neck phantom after injection, respectively; λ_{phys} is the physical decay constant of the respective isotope.
The decay corrected values were used to compute from the diagnostic measurements the activity needed for therapy. For this the procedure and the equations described on page 13 were used. For the pharmacokinetic and dosimetric modeling uncorrected uptake values were used and the physical decay was included in the model (see chapter 4.4.2).

4.2.5 Quantification of activity in blood and urine samples

In some patients blood or urine samples were collected. The blood samples taken had volumes between 0.3 and 2.5 ml and were measured in the vial they were collected in.

Urine was only collected while the patients were in the hospital. No urine samples were collected while the patients were at home. The patients were asked to collect all urine excretions in beakers. From each beaker an aliquot of 1 to 2 ml was taken in a test tube and measured.

4.3 Biophysical modeling of radioiodine kinetics

The approaches for treatment planning introduced in chapter 3.3.2 use simplified models to approximate the kinetics of iodine. Additional data acquired during diagnostic studies or during therapy can be used to set up more complex models that describe the kinetics more accurately. These models can help to improve diagnostic and therapeutic procedures.

4.3.1 Introduction into modeling

Pharmacokinetic models are used in medicine to describe the extent and rate of the absorption, distribution, metabolism and excretion of a drug. These mathematical models are built to relate the physiological parameters of interest to the measured data with the help of a set of equations. In nuclear medicine the parameters of interest are uptake, distribution, metabolism and excretion of a radioactively labeled substance, the radiopharmaceutical, in an organ or a ROI. The measured quantity is the concentration of radioactivity there. To get insight into the time-course of the distribution of the substance, repeated measurements of the same patient are necessary. If the substance is well chosen, the distribution of radioactivity in the examined tissues will be mainly influenced by its physiological properties like blood perfusion or receptor density.

The choice of a model is a very complex task and there are different approaches to achieve that. The conception of a model usually starts with some a priori information about the system and its physiology. Using all these, a very complex model emerges in most cases. This approach is called model-based as it includes the parameters as a priori information and can only be used to simulate and predict the outcome of an experiment. In order to calculate the parameters from measured data, the equations of the model simply have to be inverted. Then an iterative procedure is used to estimate the parameters from the data. But this inversion process only works if the model is identifiable with the given data. Identifiability is the property that the model can describe the measured data with a unique set of parameters, i.e. that there is a unique solution. This depends on the experimental set-up; the more parameters are modeled the more sets of data, each corresponding to a different part of the model, are needed to find a unique solution for the equations. So the limiting factor for the complexity of a model is the number of available data sets and the amount of data in each set. Therefore,

a model often has to be reduced in complexity to be identifiable and applicable to the experimental data. Another limiting factor in biokinetic modeling is the accuracy of the data and the uncertainty of the measurements. A model is only useful if its parameters can be estimated accurately and reliably. This depends on the accuracy of the data and the uncertainty of the measurements. The accuracy of the data is given e.g. by the reconstruction algorithm of tomographic data, the noise level in an image or the uncertainties of other measurements. So the model is practically limited by the number, the statistics and the circumstances, such as instruments and patient conditions, of the measurements.

A common approach in biokinetic modeling is based on the compartmental analysis. The following outline of the main concepts of first order kinetic compartment models is based on the book by Carson, Cobelli and Finkelstein [Carson1983]. Such a model consists of several compartments that represent selected organs, tissues or parts thereof. Each compartment is characterized by its state variable that generally corresponds to the time dependent amount or concentration of a substance. These compartments can represent the physiological or physical location or the metabolic or chemical state of the substance under investigation. Often some of these conditions are combined, e.g. free substance in blood or bound substance in a certain tissue. It is important to note that a compartment not necessarily represents a physiological entity like an organ, but is a far more abstract construct. That is due to the fact that in most cases the mathematical model is only a very simplified representation of the complex biological system.
The possible transformations and translocations are described by connections between the compartments that allow for exchange of the substance. The relation between compartments can be described by mass balance equations

$$\frac{dc_i(t)}{dt} = \sum_l R_{il} \; - \sum_m R_{mi}, \tag{4.2}$$

where $c_i(t)$ is the state variable of compartment i and $\sum_l R_{il}$ is the sum of all general transfer rates into compartment i from all compartments l. If the transfer rates are dependent on the substance concentration or amount c_l in compartment l, often the simplifying assumption is made that these general transfer rates can be described by $R_{il} = k_{il} * c_l(t)$. In these first order processes positive, constant rate coefficients k_{il} describe what fraction of substance molecules will move from compartment l to compartment i by a defined time. Equation 4.2 can then be rewritten as a set of first order linear differential equations:

$$\frac{dc_i(t)}{dt} = \sum_l k_{il} * c_l(t) \; - \sum_m k_{mi} * c_i(t). \tag{4.3}$$

This system of coupled differential equations can be solved given some initial values or boundary conditions for the $c_i(t)$. The solution are sums of exponential functions with constant coefficients.

This approach is implemented in several different computer programs with iterative algorithms to solve these differential equations and fit the model to measured data. The software used in this work is described in detail in chapter 4.3.2. With this method it is possible to determine the unknown values of the rate constants k_{il}. These are directly connected to the physiological parameters, e.g. the rate constant for the transition from the blood compartment to the AFTN compartment reflects the uptake rate of the radioiodine into the diseased tissue. A key element of the modeling is the input function, describing the application of the substance. A usual starting condition is the assumption of no substance in the system. The substance can then be applied at one or more times either as a rapid bolus or as a slower infusion over a certain period of time depending on the clinical protocol. If the substance is administered orally and then absorbed from the alimentary tract (GI), the total absorption fraction f_A is of special interest. It is defined in ICRP Publication 100 [ICRP2006] as the fraction of entering material that is absorbed to blood in the human alimentary tract in the absence of radioactive decay. So f_A describes the fraction of the administered iodine amount that is available for metabolism.

The measured quantity in nuclear medicine is activity or concentration of activity of a radiopharmaceutical in an organ, tissue or ROI. The biokinetic models are mainly devised for dosimetric purposes and describe the time course of activity or concentration of activity in any ROI. Therefore the $c_i(t)$ correspond to the time-dependent activity $A(r_S, t)$ in a source region S in equation 3.1.

Compartment modeling depends on a number of assumptions that are more or less met in the experiments. The first one is that mass is conserved, meaning that all influxes and losses can be accounted for in the model. Another one is that the radiopharmaceutical does not disturb the normal physiological and metabolic processes. This means that radioiodine is assumed to behave like stable iodine. Furthermore, as mentioned above, that the system is in steady state so that the parameters of the model will be constant over time.

Pharmacokinetic models are usually developed in the frame of a study involving several healthy volunteers or selected patients. The easiest way to evaluate a model is to fit the model to the data of each subject in a study individually and evaluate the resulting sets of model parameters. Another way to analyze a model is to consider all data of all patients simultaneously in a so called population kinetics analysis. The population kinetic approach will be described in detail in chapter 4.3.2.

4.3.2 Approaches and software used in this work

The modeling process used in this work consists of several steps:

- First a new model is devised or a previously existing model is modified according to a previous evaluation.

- This model structure is then checked for identifiability using the GLOBI2 software [Audoly1997].
- If the structure is identifiable, the model is translated into the format suitable for the software used for the fitting and initial values for the parameters are chosen.
- The model is then fitted to the sets of measured data. The goodness of fit is evaluated by appearance and by calculating several statistical criteria. If the model does not describe the data satisfactorily the process can be repeated.

In this modeling process two different software packages were used, SAAM II [Barrett1998] and ADAPT 5 [DArgenio2009]. This enables to verify the stability of the results depending on the algorithms and on the minimization techniques employed.

Both packages provide the possibility to do individual and population analysis of a model. In the individual analysis the model parameters are estimated for each patient separately while in the population approach the data of all patients are analyzed together and the mean population model parameters are estimated. This method, beyond providing the characteristic values of the population means and of the population standard deviations, can make better use of the whole set of data, compensating for partially incomplete individual sets of data.

In the following two sections some details of the softwares used are outlined to explain which options were chosen for the fitting and what parameters for the evaluation of the results are available.

SAAM II

SAAM II was originally developed for the development and solution of individual kinetic models. The following description of the computational features is taken from the SAAM II User's Guide and from tutorials provided with the software.
SAAM II fits a model to data in a series of iterations. In these it modifies the values of the adjustable parameters to obtain the best agreement between the calculated model predictions and the data. The best fit is produced by minimizing an objective function $R(\theta)$ that is calculated at each iteration:

$$R(\theta) = \frac{1}{M} \sum_{j=1}^{J} \sum_{i=1}^{N_j} (log[V_{i,j}(h_{i,j}(\theta), y_{i,j}, v_j)] + \frac{(y_{i,j} - h_{i,j}(\theta))^2}{V_{i,j}(h_{i,j}(\theta), y_{i,j}, v_j)}). \tag{4.4}$$

The terms in this equation are:

θ	(estimated) vector of adjustable parameters (transfer rates and blood volume)
M	total number of data points
J	number of data sets (measurements in nodule, lobe ...)

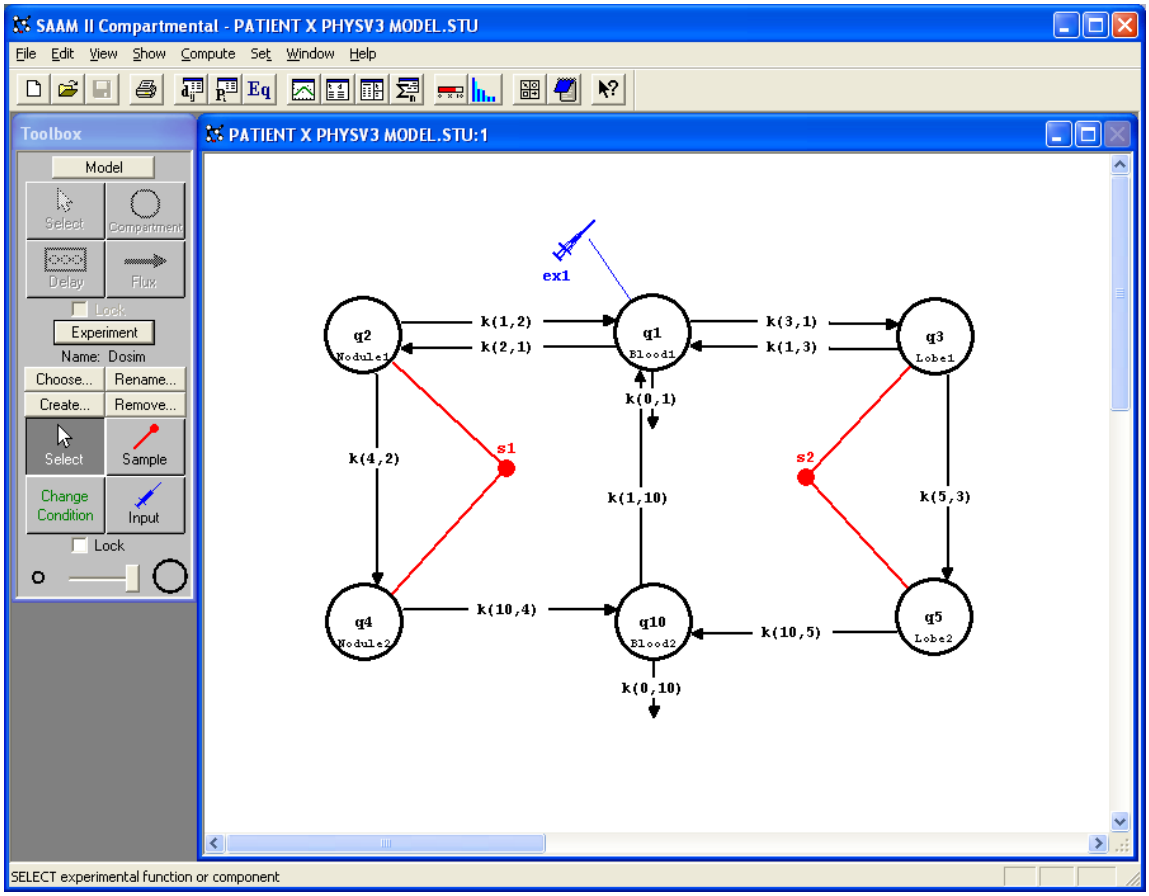

Figure 4.1: Screenshot of the SAAM II user interface: the circles are the compartments, the blue arrow with the syringe represents an input, the red dots connected to compartments represent measurements in these compartments connected with the respective data.

N_j	number of data points in the j-th data set
v_j	variance parameter for the j-th data set
$y_{i,j}$	the i-th datum of the j-th data set
$h_{i,j}(\theta)$	the model prediction corresponding to $y_{i,j}$

$V_{i,j}$ is the variance model that has to be chosen by the user. The fractional standard deviation (FSD) scheme was chosen that assigns a constant coefficient of variation as the variance to each datum

$$V_{i,j}(h_{i,j}(\theta), y_{i,j}, v_j) = v_j * \left(f^2 * \left| \begin{array}{c} y_{i,j} \\ h_{i,j}(\theta) \end{array} \right|^2 \right) \tag{4.5}$$

with $0 < f < 1$. This model was chosen because no absolute values for the uncertainties were available as discussed below in chapter 4.5. The variance model can be either based on the data $y_{i,j}$ or on the model prediction $h_{i,j}(\theta)$ and a second choice can be made between absolute and relative weighting. If absolute weighting is chosen v_j is set to 1 and the assigned uncertainty is used without further weighting. For relative weighting v_j is calculated for each data set as

$$v_j = \frac{1}{N_j} \sum_{i=1}^{N_j} \frac{(y_{i,j} - h_{i,j}(\theta))^2}{V_{i,j}(h_{i,j}(\theta), y_{i,j}, 1)} \tag{4.6}$$

The differences in the weighting factor v_j for the data sets can indicate the differences in their influence on the result of the fit. On the other hand each set of data can be assigned a different value for FSD, reflecting the assumed uncertainties connected with that data set.
For all modeling in this study the variance model was based on the model prediction with absolute weighting. So each set of data was assigned a specific coefficient of variation, given by the uncertainties derived in chapter 4.5, and no further weighting was applied.

For each adjustable parameter an initial value as well as upper and lower boundaries, in which the parameter value will be varied, have to be specified before the fitting process. The lower boundary was always set to zero while the upper boundary was chosen to be 10 times the initial value. If a parameter value is known a priori (like the physical decay constant) it is possible to indicate it as fixed and this parameter value is not changed during the fitting process.

During each iteration the algorithm searches for parameter values that result in a reduced value of the objective function relative to the previous iteration. This optimization is performed by a modified Gauss-Newton method, while the Rosenbrock integrator is used to solve the differential equations. The iteration process continues until the convergence criteria are satisfied or the maximum number of iterations is reached. As a result, the software gives the final parameter estimate and the associated covariance matrix.

ADAPT 5

The ADAPT 5 software was used to perform population kinetics analysis. The following description of the parametric population problem and its maximum likelihood (ML) solution with expectation maximization (EM) as implemented in the MLEM routine is taken from the ADAPT 5 User's Guide [DArgenio2009].
As mentioned in the introduction chapter 4.3.1, the main purpose of the modeling process is to determine the model system parameters. In ADAPT the system parameters for the i^{th} subject are a vector Θ_i. The Θ_i are assumed to be independent, identically distributed random vectors with a mean vector μ and a covariance matrix Σ describing the inter-individual variation. With Y_i the vector of all measurements for the i^{th} subject, $h_i(\Theta_i)$ the vector of model outputs (i.e. the model solution) and e_i the vector of the associated output error, the system can be written as

$$Y_i = h_i(\Theta_i) + e_i. \tag{4.7}$$

The output error e_i is assumed to be independent and normally distributed with a mean of zero and a covariance matrix $G_i(h_i(\Theta_i), \beta$: $e_i \sim N(0, G_i(h_i(\Theta_i), \beta)$, describing the intra-individual variation. So the solution of the population problem for subjects $i = 1, \ldots, N$ is to determine Θ_i and (μ, Σ, β) given the data Y_i for the population.

To get to the likelihood function for our problem we have to define the density functions

$$\begin{aligned} p(Y|\Theta_i, \beta) &= N(h_i(\Theta_i), G_i(\Theta_i, \beta)) \\ p(\Theta_i|\mu, \Sigma) &= N(\mu, \Sigma). \end{aligned}$$

The likelihood function is then given by:

$$L(\mu, \Sigma, \beta) = \prod_{i=1}^{N} \int p(Y|\Theta_i, \beta) p(\Theta_i|\mu, \Sigma)\, \mathrm{d}\Theta_i. \tag{4.8}$$

The maximum likelihood estimator is then: $\Phi_{ML} = \arg\max L(\Phi)$ with $\Phi = (\mu, \Sigma, \beta)$.

The EM algorithm solves this ML problem iteratively in two steps given initial estimates for the population mean, the error variance and the individual subject parameters $(\mu^{(0)}, \Sigma^{(0)}, \beta^{(0)}, \Theta_i^{(0)})$. In the first step the the conditional mean and the covariance for each subject's parameters are estimated. In step two μ, Σ and β are recalculated. The two steps are repeated until convergence is reached. ADAPT uses the differential equation solver LSODA (Livermore Solver for Ordinary Differential equations with Automatic method switching for stiff and non stiff problems). Next to the final population mean parameter and population covariance matrix, parameter estimates and covariance matrices for the individual subjects are also available as results of the fitting process.

ADAPT provides a graphical user interface only for the execution of the program, not for the creation of the model. The differential equations and other parameters characterizing the model are defined by the user in a Fortran file. Here the initial starting values for all parameters and the connection of compartments to measured data, called output, are also defined. Also the variance model can be defined here. The model chosen was the same as the "model absolute" option in SAAM II.
Next to the Fortran file with the model information a measurement data file with a specific format and a parameter file that also contains starting values for all parameters are needed for the execution of the software. Further details that have to be specified are if the full covariance matrix or only its diagonal components are used, the number of samples per EM iteration and total number of iterations. Also the assumed distribution of the estimated parameters was chosen to be normal.

4.3.3 Available models

One of the first compartmental models for iodine kinetics in humans was published by Berman et al. in 1968 [Berman1968]. The model is shown in figure 4.2. It will be used to give a general description of compartment models. The boxes represent the compartments and the arrows represent the exchanges between compartments. The arrow labeled Uptake stands for the input of radioiodine into the human organism. The arrows that do not end at a compartment stand for losses of substance from the system, e.g. iodine in feces, urine or sweat. The compartment Plasma Iodide contains the iodine in the body that is not organically bound. From this compartment iodine is taken up into the thyroid or excreted into Urine. The thyroid is separated into three subunits. All three produce the thyroid hormones T3 and T4 and release them into Plasma. This division was introduced to model the different time scales of hormone release. T3 and T4 in Plasma are modeled by separate compartments. These compartments for organically bound iodine have a recycling exit back to inorganic iodine in plasma and excretion into feces.

Over the past decades the ICRP has published a number of biokinetic models for iodine. These biokinetic compartment models are used in the recommendations for the calculation of absorbed doses. Historically the ICRP reports were mainly concerned with the protection of workers and the general public from ionizing radiation, but recently also the medical applications of ionizing radiation came into focus and there are now models specific for nuclear medicine.
The first ICRP model for the kinetics of iodine was published in ICRP Publication 30, Part 1 in 1979 [ICRP1979]. This model was slightly modified in ICRP Publication 53 in 1987 [ICRP1987] for use in nuclear medicine and in ICRP Publication 56 in 1989 [ICRP1989] for use with occupational and environmental exposure. It is depicted in figure 4.3. In this three compartment model the iodine is taken up directly into the Blood compartment.

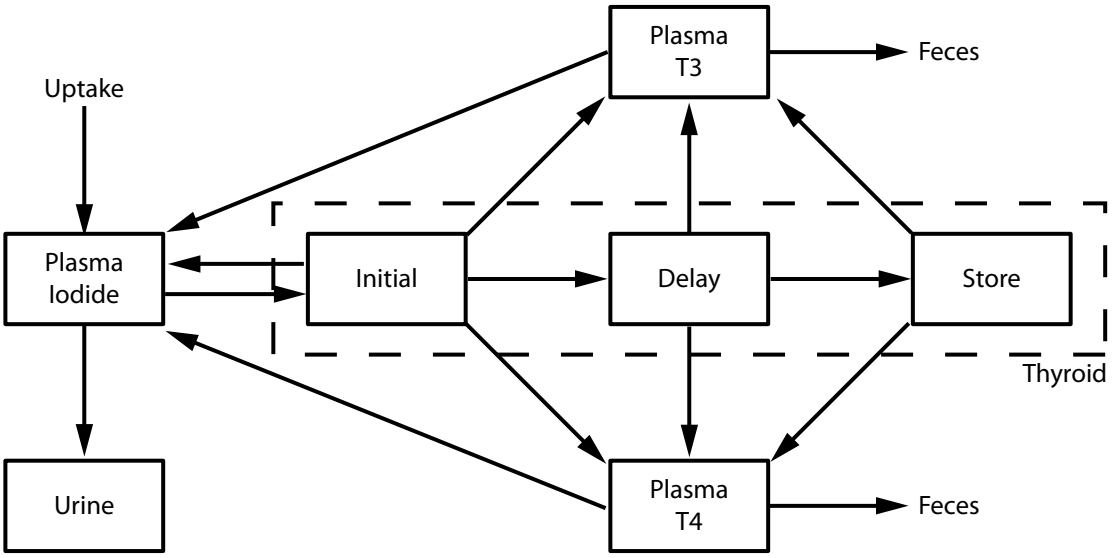

Figure 4.2: The (simplified) compartmental model proposed by Berman et al. in 1968

From there it is either transferred to Thyroid (30 %) or is excreted rapidly to Urine (70 %). The only exit from the thyroid compartment leads into Rest of Body. From there, there is a recycling transfer back to Blood (80 %) and an excretion into feces (20 %).

For the estimation of doses to fetus and mother during pregnancy a more complex model was published in ICRP Publication 88 in 2001 [ICRP2001], adopted from the models published by Berkovski [Berkovski1999a][Berkovski1999b](see figure 4.5). Next to compartments for the fetus there are compartments for blood thyroid and rest of body, as in the previous model for adults. To model the transfer of iodine from mother to fetus and to account for dose from iodine in non-thyroidal maternal tissues, additional compartments for ovaries, amniotic fluid and the utero-placental unit were inserted. The gastro-intestinal tract was also modeled in detail. Beside that, one key feature of the model is that iodide and organically bound iodine are modeled separately in most compartments.

In 2003 Johansson et al. [Johansson2003] proposed a refinement of the model published in ICRP 56 (fig. 4.4). It contains additional compartments for salivary glands and stomach as well as a specific compartment for organic iodine. It is intended for use in nuclear medicine and is therefore not as complex as the model in ICRP 88.

All these models provide reference values for the model parameters. These are based on data acquired in numerous studies in humans and animals published in the literature. In ICRP 53, 56 and for the model of Johansson these are provided for different age groups and thus allow the adaptation of the model. Also different values of the fraction of iodine taken up in the thyroid are considered and the respective dose coefficients are provided.

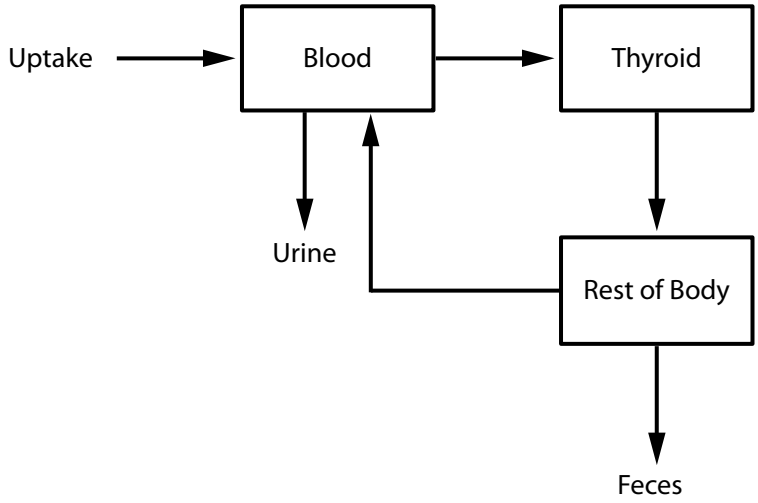

Figure 4.3: The compartmental model proposed by ICRP publication 56

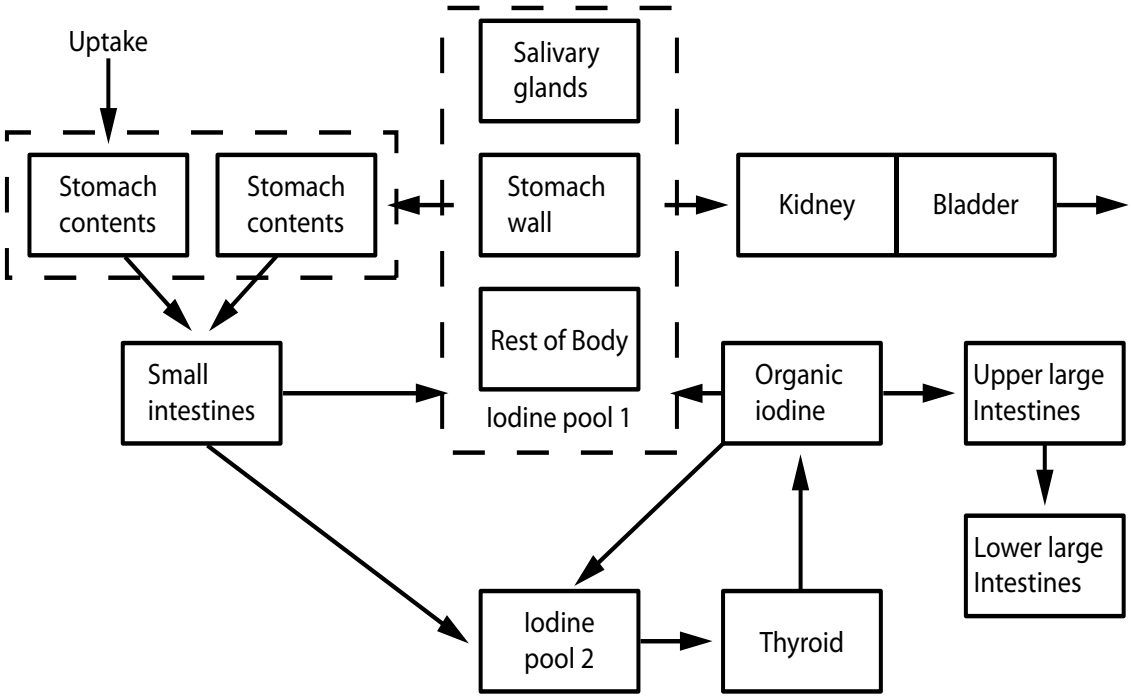

Figure 4.4: The compartmental model proposed by Johansson et al. in 2003

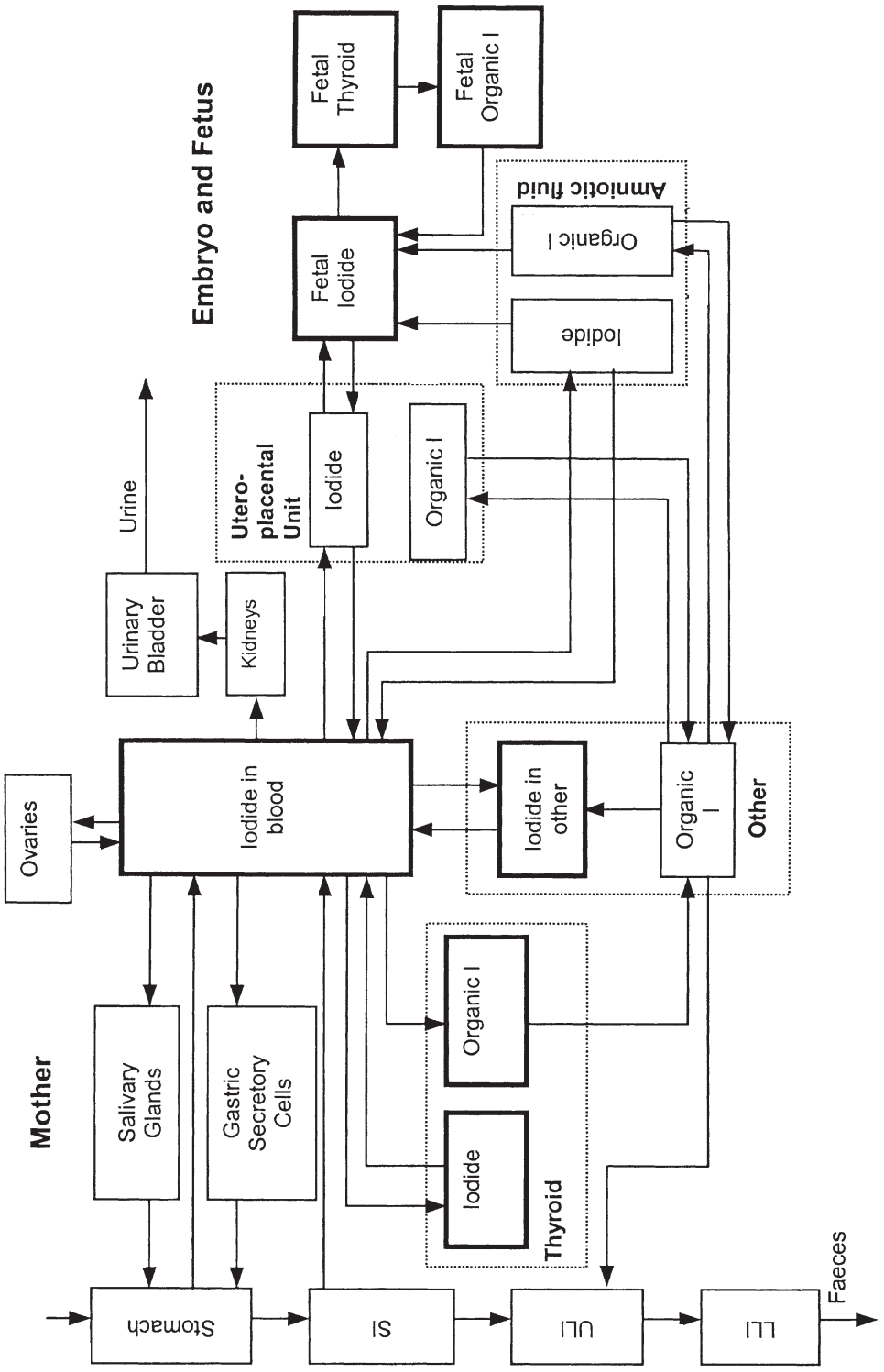

Figure 4.5: The compartmental model proposed by ICRP publication 88

4.4 Calculation of absorbed doses

4.4.1 Determination of half-life

There are many different values for the half-lifes of ^{123}I and ^{131}I available in the literature and in online databases. In ICRP publication 38 [ICRP1983] the values of 13.2 h and 8.04 d respectively are given but more recent measurements have added more precise values with corresponding uncertainties. ICRP publication 107 [ICRP2008] gives the values of 13.27 h and 8.0207 d respectively. These are based on data published in 2001 and 2003. More recent data published by the Brookhaven National Laboratory [NNDC2010], the main source of the ICRP values, give now the following values:

- ^{123}I: $T_{1/2} = 13.22\,\text{h}$; $\lambda_{\text{phys}} = 0.05242\,1/\text{h}$;
- ^{131}I: $T_{1/2} = 8.025\,\text{d}$; $\lambda_{\text{phys}} = 0.003599\,1/\text{h}$.

These were used for all subsequent calculations and for the modeling.

Table 4.2: Decay Data for ^{123}I according to NNDC [NNDC2010]; the radiation omitted each has a intensity of $< 0.1\%$

Radiation	Energy (KeV)	Intensity (%)
Auger electron L	3.19	95.1
Auger electron K	22.7	12.4
X-Ray 1	3.77	9.0
X-Ray kα2	27.202	24.7
X-Ray kα1	27.472	45.7
X-Ray kβ3	30.944	4.2
X-Ray kβ2	31.704	2.3
X-Ray kβ1	30.995	8.1
Gamma	158.97	83.3
Gamma	346.35	0.13
Gamma	440.02	0.43
Gamma	505.33	0.32
Gamma	528.96	1.4
Gamma	538.54	0.38

Table 4.3: Decay Data for ^{131}I according to NNDC [NNDC2010]; the radiation omitted each has a intensity of $< 0.1\%$

Radiation	Energy (KeV)	Intensity (%)
Beta -	69.36	2.1
Beta -	86.94	0.65
Beta -	96.62	7,2
Beta -	191.58	89.6
Beta -	283.24	0.39
Auger electron L	3.43	5.9
Auger electron K	24.6	0.68
X-Ray 1	4.11	0.63
X-Ray kα2	29.461	1.5
X-Ray kα1	29.782	2.8
X-Ray kβ3	33.562	0.26
X-Ray kβ2	34.419	0.15
X-Ray kβ1	33.624	0.51
Gamma	80.185	2.62
Gamma	177.214	0.27
Gamma	284.305	6.1
Gamma	325.789	0.27
Gamma	364.489	81.5
Gamma	503.004	0.36
Gamma	636.989	7.2
Gamma	642.719	0.217
Gamma	722.911	1.77

4.4.2 Calculation of absorbed dose

In each subject in this study the absorbed dose in the nodule and, if present, in the healthy contralateral lobe was calculated according to equation 3.3. Both are treated as sources, so the first thing to determine is the number of disintegrations in both structures to get $\tilde{A}(r_S, t)$. The data used in this work were used as they were measured in the patients, i.e. no correction for radioactive decay was implemented. Therefore the radioactive decay was included in the model. For this purpose a twin compartment was assigned to every compartment. The transfer from the original compartment to the twin compartment was modeled with a fixed rate corresponding to the radioactive decay constant λ.
Consequently the content of each decay compartment at a given time T_D represents the number of nuclear transitions $\tilde{A}(r_S, t)$ that have occurred in the original compartment until that time T_D. As T_D grows and gets larger than the physical and biological half-life, the content of the decay compartment reaches a plateau that represents the total number of decays that occurred in the original compartment.

In a second step the S-value (conf. equ. 3.2) has to be determined. The physical properties are well known for the different isotopes. The decay data with information on the released radiation of both isotopes are listed in tables 4.2 and 4.3. So only the mass of the target structure and the absorbed fraction (AF) $\phi(r_T \leftarrow r_S, E_i, t)$ have to be calculated. The calculation of the mass of nodule and lobe is described above in chapter 4.2.3. The absorbed fractions were calculated only for self-irradiation, i.e. the source and target are the same; crossfire was not considered. In 2000 Stabin and Konijnenberg [Stabin2000] published tables with absorbed fraction values for unity density spheres for certain weights and different energies of beta and gamma radiation. These absorbed fractions were linearly interpolated for weight to fit the actual weight of each patient and for energy to fit all energies emitted by the respective radioisotope. So for each patient's individual nodule and lobe masses a value for the absorbed fraction of each emitted radiation was calculated. With these values, the mass, the radiation energies and the respective yields, the S-value was calculated. With that and the number of nuclear disintegrations, the absorbed dose from self-irradiation in nodule and lobe could be calculated.

4.4.3 Monte Carlo calculation of absorbed dose

The calculations described in the previous chapter follow the standard method that only considers the self-absorbed dose. Therefore the S-value for the crossfire from one structure to the other were not calculated. To assess the validity of that method and to get an estimate for the dose contribution from crossfire, a Monte Carlo calculation in a three-dimensional voxel phantom was performed. A voxel phantom is a computational model

of the human body. It is divided into equal sized volume elements called voxels that can be given properties like density or composition individually according to the tissue they are to represent.
In a Monte Carlo calculation the transport and absorption of radiation, emitted by a large number ($> 10^6$) of nuclear decays in a source region, through a tissue can be simulated according to the laws of physics. The statistical accuracy of the calculation is determined by the number of simulated particle histories; usually several million histories are performed. This allows the realistic estimation of the dose absorbed in a selected part of the voxel phantom.
In this case the voxel model Visible Human [Zankl2002] was selected. In the thyroid structure of this phantom a nodule structure was defined representing the diseased tissue. Three different nodule masses were selected for the simulation: five, ten and twenty grams. The total mass (31.8 g) of the thyroid structure, i.e. the sum of the masses of nodule and healthy tissue, was constant in all three cases. A homogeneous activity distribution in the nodule was simulated. No activity was placed in the healthy part of the thyroid because the dose contribution from external irradiation of the nodule by the healthy tissue is inconsiderable compared to the dose contribution from self-irradiation. The Monte Carlo code EGS [Kawrakow2009] and the energy spectrum of the radiation emitted by ^{131}I was used. For each case five million histories were calculated.

4.5 Errors and uncertainties

As mentioned in chapter 4.3.2 the chosen variance model was based on the model prediction to allow for uncertainties introduced by the modeling process itself. To implement this in the model, both softwares require as input the uncertainties associated with each set of measured data.

In the following chapters the contributions to the uncertainties connected with the measured data are listed and explained. For most of the uncertainties no quantitative values can be determined but they can only be estimated qualitatively. In these cases a global estimate of the uncertainty is given that sums all contributions.

4.5.1 Uncertainties in time measurements

A possible source for uncertainties are the time measurements. For each measurement of activity or activity concentration the exact time point of the measurement is also recorded. These information are important because on the one hand the kinetics describe the time-dependency of the administration,distribution, metabolism and excretion of the radiopharmaceutical. On the other hand time is important for calculating the radioactive

decay. For most blood and urine samples some time elapsed between collection and measurement. The measured values have to be corrected for the radioactive decay that happened in that time therefore exact time measurements are important.
Most time measurements in this study were made with clocks that are not coordinated. The well-counter measuring the initially administered activity and the gamma camera measuring the uptake of activity in the thyroid use different clocks that are not necessarily sharing the same time. Furthermore, the urine and blood sample collection usually takes some time so that only an approximate middle value for the collection time can be given. These times are typically measured with the personal wristwatches of the staff which again are not coordinated.
These uncertainties are rather small and are only important for data acquired in the first few hours. At later times a difference of a few minutes does not have a large impact on the measurements. The uncertainties of the time measurements cannot be included into the model because both software packages used do not give that possibility. Therefore the uncertainties are included in the uncertainties of the measured values in our case.

4.5.2 Uncertainties in Gamma camera images

Uncertainties in the values of uptake in the thyroid measured in the gamma camera can have different origins. One is the uncertainty due to the counting statistics that is present whenever activity is measured with a single counting process. It is described by the square root of the number of counts. In this study this led to an uncertainty of 1 % or less for the values in the data sets used in this work.
Another source is the ROI definition on the first gamma camera image. The edge of the thyroid is not clearly defined in these images because it is blurred by scattering, background radiation and the limited spatial resolution of the camera. Therefore it can happen that the ROI is chosen too small or too large thus leading to an over- or underestimation of the uptake. Using the ROI that was defined on the first image for all subsequently acquired images can also lead to errors as the shape or size of the structure can change over time. In this study, the effect of these uncertainties was investigated by repeatedly drawing the ROIs in the same gamma camera image. It was found to be negligible with respect to the counting statistics because the resulting changes in the counts in the ROI were very small. The uncertainties for lobe are larger than for nodule, because the uptake is smaller and therefore the counting statistics are worse. Additionally, the lower uptake leads to a more smeared out edge of the lobe compared to the nodule which makes the definition of the ROI more uncertain.
The most important uncertainty arises from the assumption that the physiology does not change over time, i.e. that the uptake in this experiment at this time is representative for the uptake at other times. However, the physiology that governs the metabolism of the thyroid is highly variable. This intra-individual variability can not be quantified but can

be included in the global estimate of the uncertainty because the variance model is model based as described in chapter 4.3.2.
Therefore a fractional standard deviation of 5 % for all nodule uptake data and of 10 % for all lobe uptake data was chosen for this study.

4.5.3 Uncertainties in blood sample data

The counting statistics, as described above, also contribute to the uncertainty of the measured activity in blood samples. It accounts for about 1 % uncertainty in most samples except in samples taken later than two weeks after administration. There it can account for up to 5 % because the low activity in those samples leads to low counting rates.
Further sources of uncertainty are the possible adsorption of iodine to the walls of the sample collection vial or the inhomogeneous distribution of iodine in the liquid and coagulated parts of the blood.
The uncertainty in the measurement of the volumes of the blood samples is given by the scale that was used to weigh the samples. The volume was then calculated by dividing by the density of blood. The uncertainty from the scale is negligible as it is a very exact instrument (± 0.1 mg). Considering all this and allowing for the individual physiological variability, an uncertainty value (of at least 5 %) was chosen individually for all blood samples in this study.

4.5.4 Uncertainties in urine sample data

Three parameters are measured for a urine sample. The activity concentration, the volume of the sample and the time it took to accumulate the excreted activity in the bladder.
The uncertainties for the first are mainly from the counting statistics. In this study, small aliquots of less than a milliliter and often a long time of several days between collection and measurement lead to uncertainties in the counts of up to 2 %.
One source for uncertainties in the volume comes from the possibility that not all excreted urine was collected but some was spilled. This leads to a systematic underestimation of the volume. The second source are the beakers that were used in this case to collect the urine and to measure its volume. They have a scaling of 5 ml that led to large uncertainties of more than 25 % in cases where less than 20 ml were collected. Additionally there is an uncertainty of 1 % in the volumes of the measured aliquots introduced by the pipette that was used to take the aliquots from the samples.
The time it took to accumulate the urine (and the activity) in the bladder is the time interval between the last voiding and the sample collection. If this last voiding did not happen in the clinic, the time interval is unknown and the accumulation time had to be estimated. This was the case in 30 out of 55 urine samples in this study. Most of those

samples were collected in the late morning around nine. It was assumed that the previous voiding occurred before the departure to the clinic, roughly 1.5 hours before the sample collection. This assumption is supported by the finding that most excreted volumes are around 100 ml.
Therefore the measured activity in urine is associated with a very high uncertainty (of at least 20 %) that was estimated individually for each measurement. This was done by adding ten percent points to the uncertainty calculated from the collected volume in order to account for the uncertainties that could not be quantified.

4.5.5 Uncertainties in model parameters

The modeling process in itself is a source for uncertainties and errors. The compartmental models describe the very complex biological and physiological processes in the human body, and especially in the thyroid, by quite simple linear equations. Furthermore the modeling tries to describe processes that can vary widely between humans with a single set of parameters. These simplifications introduce a large uncertainty in the model prediction that is hard to quantify, additionally to that caused by uncertainties in the measurements. To investigate the consequences of these uncertainties of the model on the model output the method developed by Li 2009 [Li2010] was applied.
ADAPT 5 provides for each estimated parameter a population mean value together with a standard deviation. These are calculated from the intra-individual variability, i.e. the uncertainties connected with the measured data, and from the inter-individual variability, i.e. the differences between the subjects in the study.
In this approach this information and the differential equations characterizing the model are used to sample the model output 1000 times for 500 different time points during the experiment. In this case this means e.g. 1000 values for the uptake value of radioiodine in the nodule at 500 time points. For the sampling, each model parameter value is randomly chosen within the 90 % confidence interval defined by the standard deviation given by ADAPT 5. The sampling method employed is Latin Hypercube Sampling. For the resulting sampled outputs the mean, the 2.5 % and the 97.5 % confidence levels are calculated. This gives the 95 % confidence interval for the chosen model output (i.e. the uptake in nodule or lobe, the concentration in blood, ...).

5 Measured data and model development

5.1 Measured data

In this chapter the measured data are presented to visualize the distribution and the general time course of activity in the thyroid, in blood and in excreted urine.

The measured nodule masses ranged from 4.2 to 45.1 g with a mean of 15.0 g. The measured lobe masses ranged from 2.1 to 20.9 g with a mean of 6.9 g. The uptake and retention of radioiodine in the nodule was measured in all patients, but activity in the lobe was found in only 31 of the 43 patients.

All patients show a similar behavior, but the magnitude of uptake and retention varies widely. While the patient with the least uptake in the nodule during therapy reaches a maximum at about 10 %, the patient with the highest uptake reaches a maximum at about 40 %. The patients show the same trends during therapy and diagnostics. There are differences in the uptake in nodule and lobe. The uptake in nodule is much larger than in lobe, but the patient with the highest uptake in nodule does not have the highest uptake in lobe.
The measured uptake of activity in nodule and lobe is shown on the example of three selected patients. Patient 6 was selected because she shows a very high uptake in the nodule during therapy, patient 40 because she shows a very low uptake, and patient 9 was selected to show a medium uptake. The complete set of patient data is shown in the appendix.

Uptake of activity in nodule and lobe during diagnostics is shown in figures 5.1 and 5.2. The data for nodule and lobe during therapy are shown in figures 5.3 and 5.4. The uptake is normalized to the administered activities and values are given as percentage of that initial amount. In these plots the uptake during diagnostics is lower than during therapy. This is because the half-life of ^{123}I is much shorter than that of ^{131}I.

Activity concentration in blood was measured in two patients during diagnostics and in three patients during therapy. The measured activities in blood during diagnostics and therapy are shown in figures 5.5 and 5.6, respectively. The values are given as percentage of the initially administered activity per liter.

The activity concentration measured in urine samples during therapy is shown in figure 5.7. The excretion is given as percentage of the initially administered activity per milliliter.

The cumulative excreted activity could not be calculated because activity excreted in urine was not measured continuously. Patients could only be asked to collect excreted urine when they were in the clinic for administration of radioiodine or for subsequent gamma camera scans. The time it took to accumulate the urine (and the activity) in the bladder is the time interval between the last voiding and the sample collection. If this last voiding did not happen in the clinic, the time interval is unknown and the accumulation time had to be estimated as described in chapter 4.5.4. This was the case in 30 out of 55 urine samples.

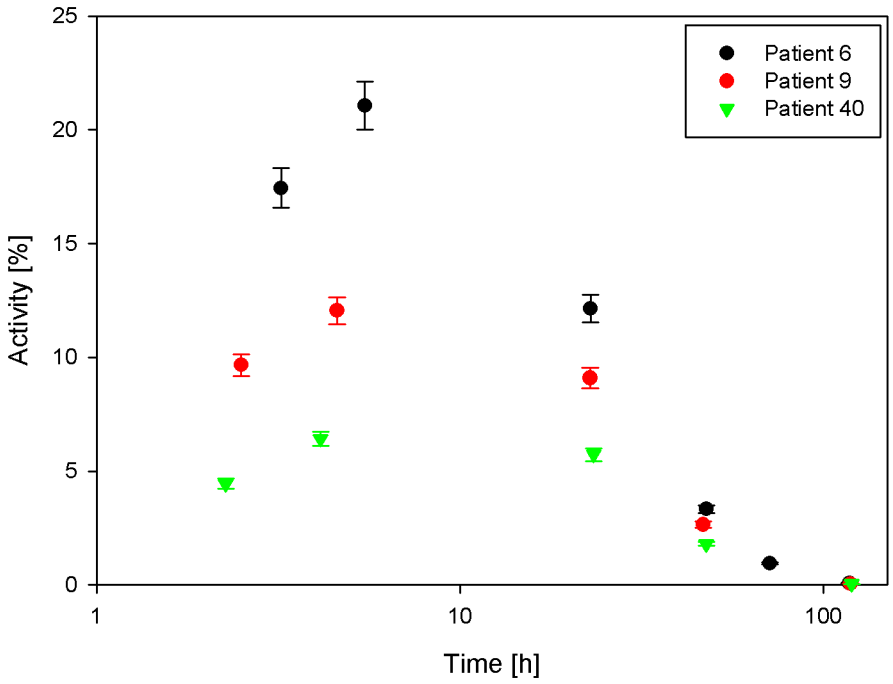

Figure 5.1: The measured ^{123}I activity in the nodule during diagnostics as percent of the administered activity.

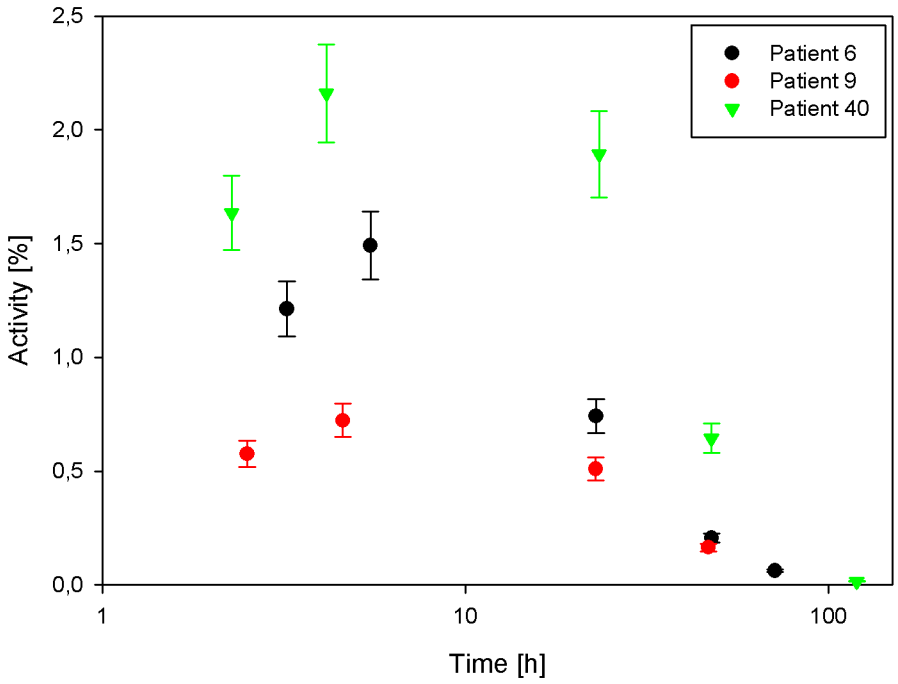

Figure 5.2: The measured ^{123}I activity in the lobe during diagnostics as percent of the administered activity.

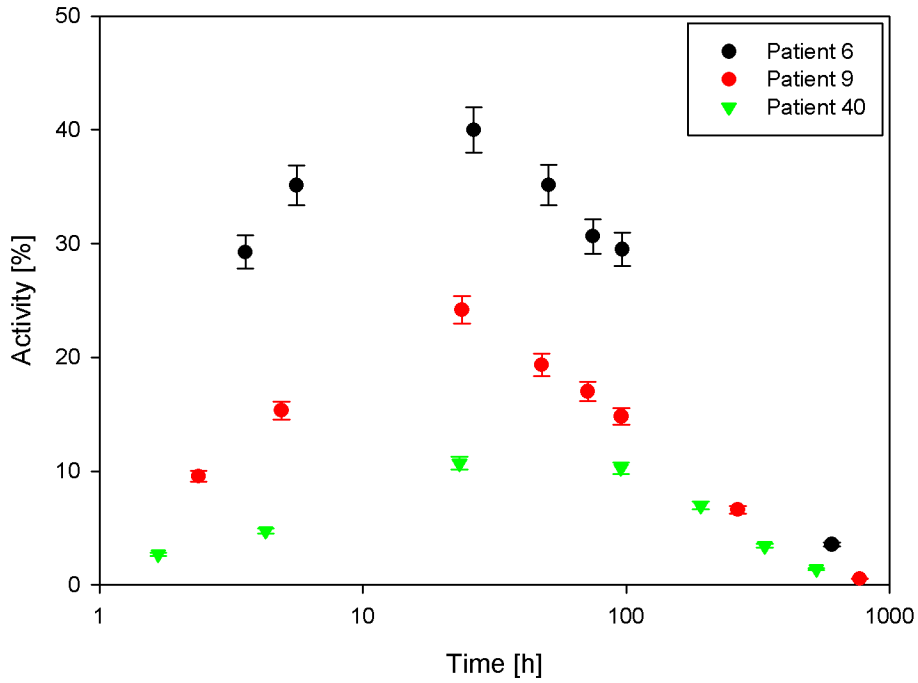

Figure 5.3: The measured ^{131}I activity in the nodule measured during therapy as percent of the administered activity.

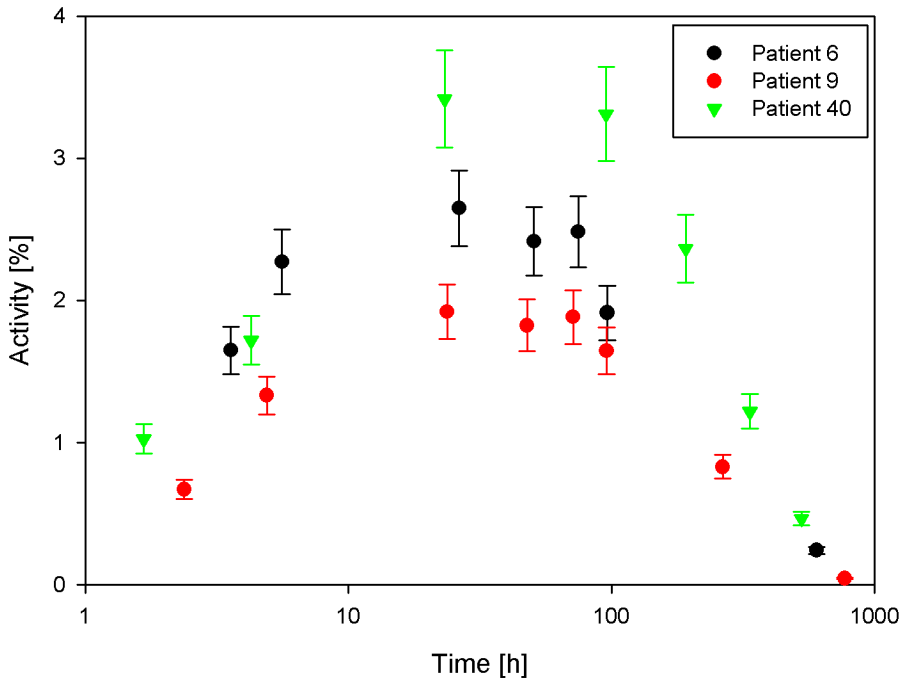

Figure 5.4: The measured ^{131}I activity in the lobe measured during therapy as percent of the administered activity.

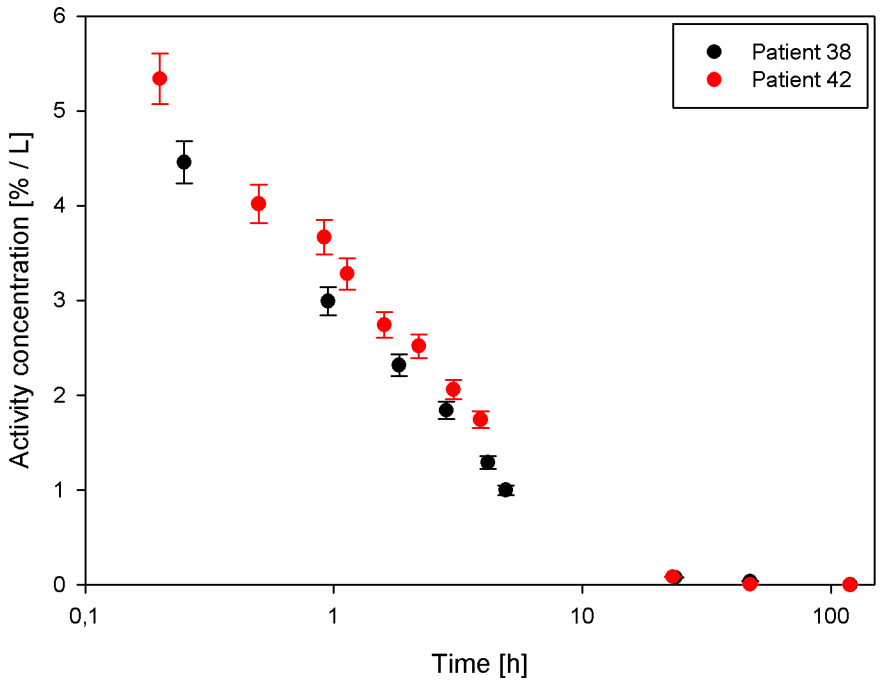

Figure 5.5: The measured activity concentration in blood during diagnostics as percent of the administered activity per liter.

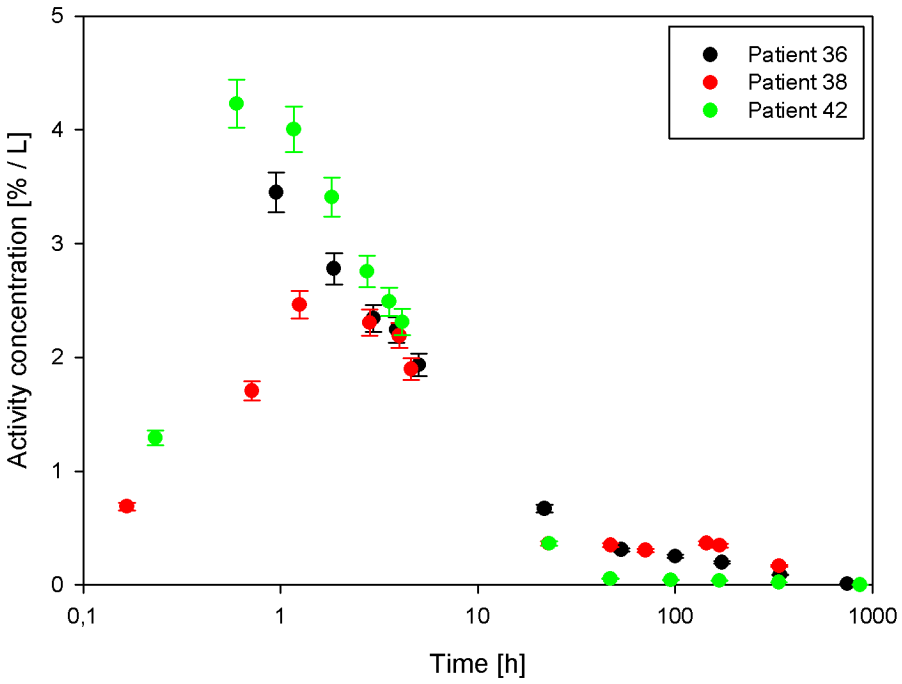

Figure 5.6: The measured activity concentration in blood during therapy as percent of the administered activity per liter.

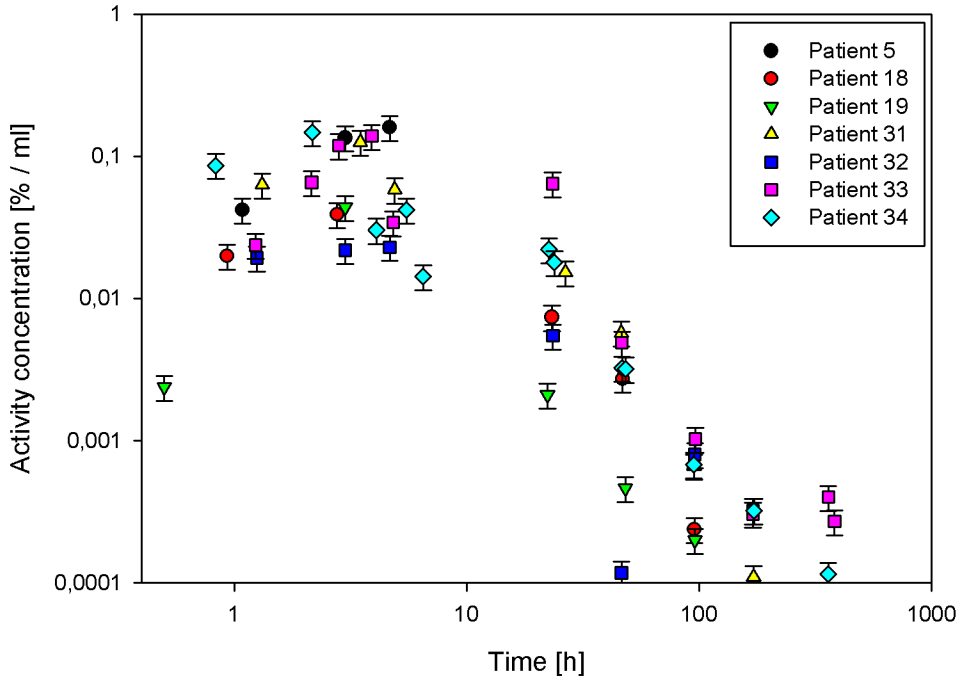

Figure 5.7: The measured activity concentration in urine during therapy as percent of the administered activity per milliliter (ml).

5.2 Development of a specific biophysical model structure for iodine in AFTN patients

The models for the kinetics of iodine introduced in chapter 4.3.3 are generally not made for specific diseases, but are derived from studies with healthy volunteers. A specific model structure for AFTN, that represents the peculiarities of this disease, helps to model the kinetics in the nodule and in the healthy lobe more realistically. Therefore, based on the general models describing the kinetics of iodine, models dealing specifically with AFTN were published. One of the first of those models was published by Giussani et al. (see fig. 5.8) [Giussani2002]. In this model direct uptake of the iodine into blood is assumed. From there it is either distributed into Nodule, Lobe or Rest of Body or it is directly excreted into Bladder. Iodine taken up by the Nodule is recycled to Blood while iodine in the Lobe is excreted subsequently. Iodine in Rest of Body is excreted via the Bladder. The model was developed using data from a preliminary subset of the patients presented here. The activity in both, the diseased nodule tissue and the healthy contralateral lobe, was measured in these patients. Therefore the main new feature was that the nodule and the lobe are modeled as separate units. With this approach the dose to the diseased and the healthy part of the thyroid could be evaluated separately.

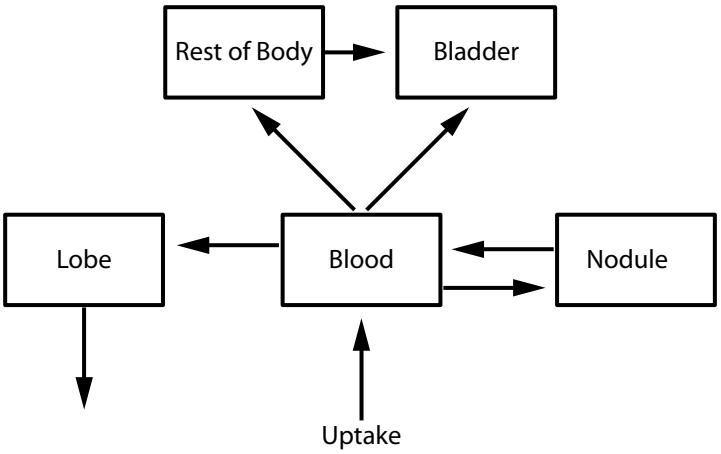

Figure 5.8: The compartmental model by Giussani et al. [Giussani2002].

Based on the results of this first model the measurement schedule was altered to get better data from subsequent patients. Analysis of these new data led to an improved model shown in figure 5.9. A split of the nodule and lobe compartments was introduced. With these appended compartments, the short- and long-term retention of iodine in the thyroid could be modeled more realistically. Further changes are the added possibility of recycling from Rest of Body to Blood and the direct excretion from Rest of Body. This model was presented by Giussani et al. in 2006 in Montpellier [Giussani2006] and by

Janzen et al. at the 2008 EANM Congress in Munich.

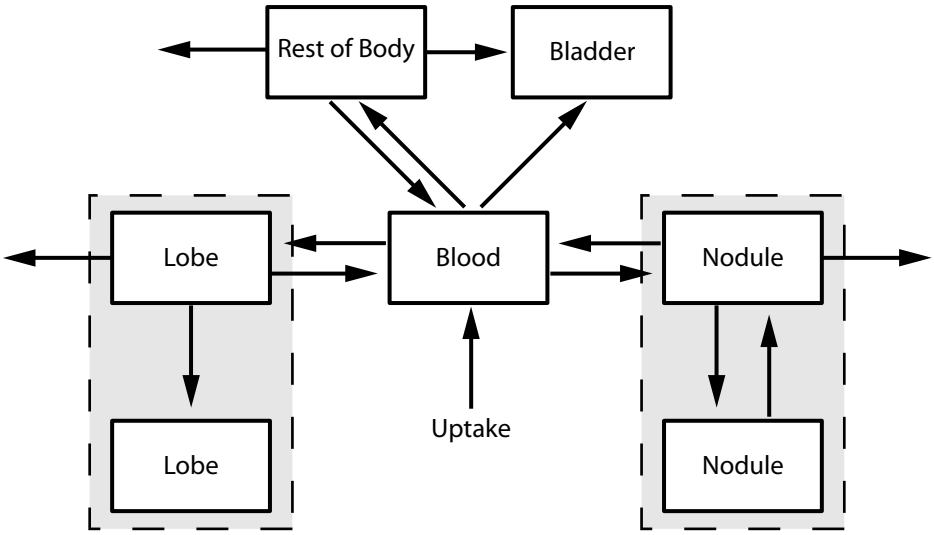

Figure 5.9: The compartmental model with split thyroid compartments.

This split of the thyroid compartments was interpreted subsequently as a representation of the different states of iodine in the organism, the elemental iodide and the organically bound iodine. Thus the idea to build a physiologically more realistic model structure emerged.
The basic idea of this last step in the model development was to differentiate in the model between not organically bound iodide and organically bound iodine. This is achieved by separate compartments for iodide and iodine in nodule, lobe and blood. Thus the kinetics of iodide in blood, nodule and lobe, the metabolism of iodine in the thyroid, the synthesis of the thyroid hormones and the distribution and metabolism of the hormones are now part of the model.

The resulting model structure is shown in figure 5.10. It is an expansion of the previous model with compartments for Nodule, Lobe and Blood and additionally a compartment Bladder for the urinary excretion. A compartment Alimentary Tract is introduced for the uptake of orally administered iodine during therapy. This compartment represents all parts of the alimentary tract in which iodine can be absorbed to blood, e.g. the stomach and the small intestines.
The uptake of iodide into the organism is modeled in two different ways to account for the different clinical protocols of administration for diagnostics and therapy. The uptake is modeled by a direct bolus intake into the Blood-I compartment for diagnostics because there iodide is administered by an intravenous injection. For modeling the kinetics during therapy, the iodide is given as a bolus into the Alimentary Tract compartment because there it is administered orally to the patient. From there it can either be taken up into

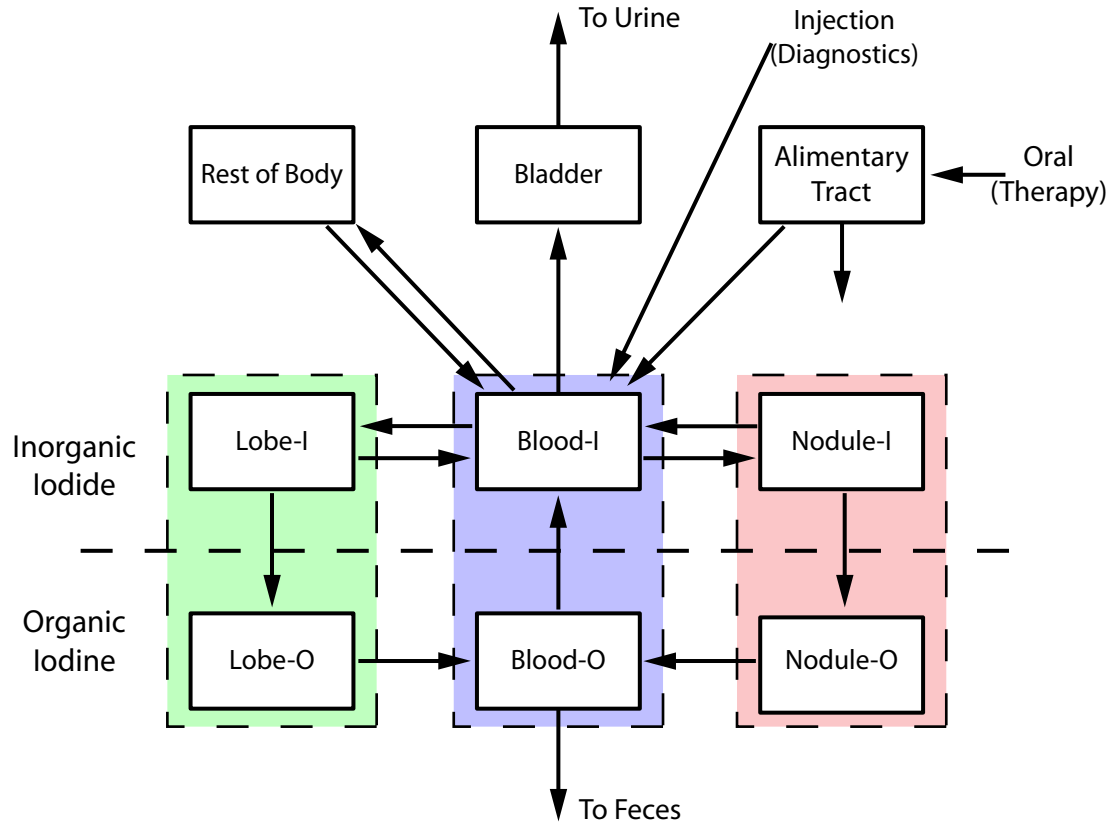

Figure 5.10: The complete compartmental model with separate compartments for inorganic iodide and organically bound iodine.

Blood-I or it remains in the gastro-intestinal tract and is excreted subsequently.
As before, an exchange compartment called Rest of Body is connected to the Blood-I compartment. It represents the not organically bound iodide in the body that is not in blood or the thyroid. The excretion of iodide via the urinary pathway through the Bladder is only possible from Blood-I and no longer from Rest of Body. The thyroid is modeled by four compartments to represent the not organically bound iodide and organically bound iodine in nodule and lobe. There are two compartments for the AFTN and two for the healthy contralateral lobe. Iodide is taken up from Blood-I into Nodule-I and Lobe-I and can be recycled back into Blood-I. The synthesis of thyroid hormones is modeled by the transfer from Nodule-I and Lobe-I to Nodule-O and Lobe-O respectively. The latter contain the organically bound iodine. The thyroid hormones are released from Nodule-O and Lobe-O into Blood-O that also represents all sites where the hormones are metabolized. Iodine from the hormones can either be excreted via feces or can be recycled as iodide to Blood-I where it is available again for uptake and hormone synthesis in the thyroid.
The adjustable parameters of this model are the transfer rates between the compartments

as shown in figure 5.10 and the rates of loss from Alimentary Tract and from Blood-O. Measurements in blood are available as activity concentrations. The volume within which the administered radiopharmaceutical is distributed is considered as an additional model parameter to be determined since its value is unknown.
With nine compartments and sixteen parameters the model is very complex. With the help of the GLOBI software it was possible to demonstrate that this model structure is identifiable when data for nodule, lobe, blood and urine are available simultaneously.

5.2.1 Model parameter estimation for the complete model

For all modeling in this work the data were used as they were measured in the patients. Therefore radioactive decay had to be included in the model as described in chapter 4.4.2. The additional compartments are not shown in the figures of the models. They do not increase the complexity of the model because they add no adjustable parameters.

The following analyses of the complete model structure for AFTN were performed only with data measured during therapy. Therapy data were used because of the longer half-life of ^{131}I, so that measurements over a longer period of time are available compared to the case of diagnostics. This makes the results obtained more reliable, especially when biological processes are investigated that are slower than the physical half-life of the radiopharmaceutical.

Unfortunately, due to practical restrictions mainly dictated by the health status of the patients, it was possible for none of them to perform the complete experimental schedule consisting in measuring the activity uptake in nodule and lobe and collecting urine and blood samples. So the complete model structure could not be fitted to data from one single patient.
A population kinetics analysis was also not possible for this model because there were too few subjects available. A rule of thumb for population kinetic analysis is that the ratio of subjects in the study to adjustable parameters should be at least two. With a lower ratio no information on the inter-individual (population) variability can be obtained. So with only three sets of blood samples and seven sets of urine samples this approach would give no reliable or meaningful results.
However the software SAAM II provides the possibility to simultaneously fit the model to data measured during different experiments. Considering the data of the three patients (36, 38, 42) with measurements in blood and the seven patients (5, 18, 19, 31, 32, 33, 34) with urine samples as ten different studies in one fictional patient, it was possible to test whether the proposed model structure can describe the data. An overview of the available datasets is given in table 5.1.

In figures 5.11 to 5.14 the measured data in nodule, blood and urine and the corresponding fitted curves of the model are plotted together. The error bars are omitted in

Table 5.1: Overview of available urine and blood datasets taken during therapy.

	Nodule	Lobe	Urine	Blood
Patient 5	y	y	y	
Patient 18	y	y	y	
Patient 19	y		y	
Patient 31	y		y	
Patient 32	y	y	y	
Patient 33	y	y	y	
Patient 34	y	y	y	
Patient 36	y	y		y
Patient 38	y			y
Patient 42	y			y

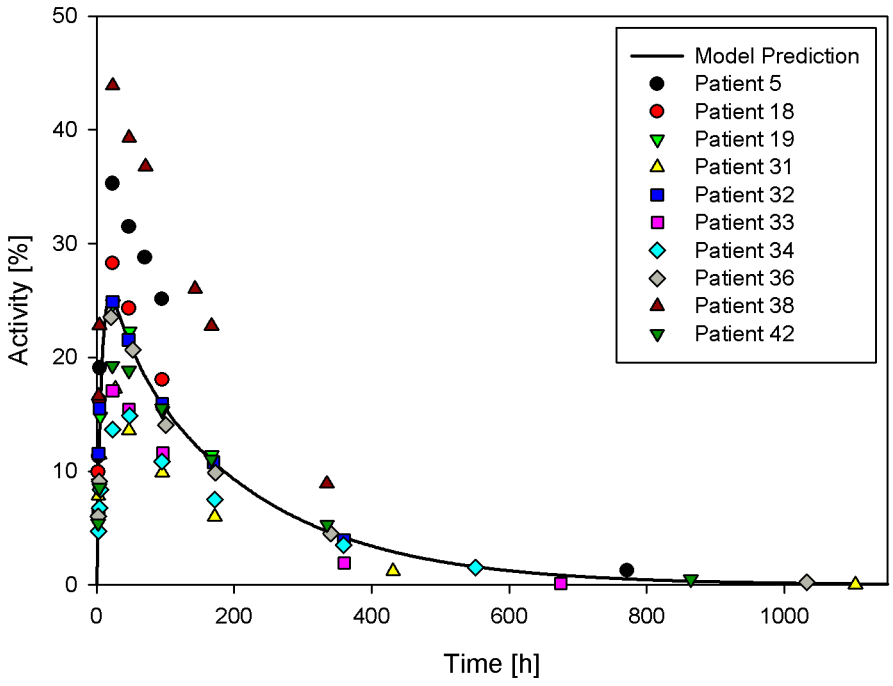

Figure 5.11: Fit of the complete compartmental model to the nodule data of the fictional patient; activity is given in percent of the administered activity.

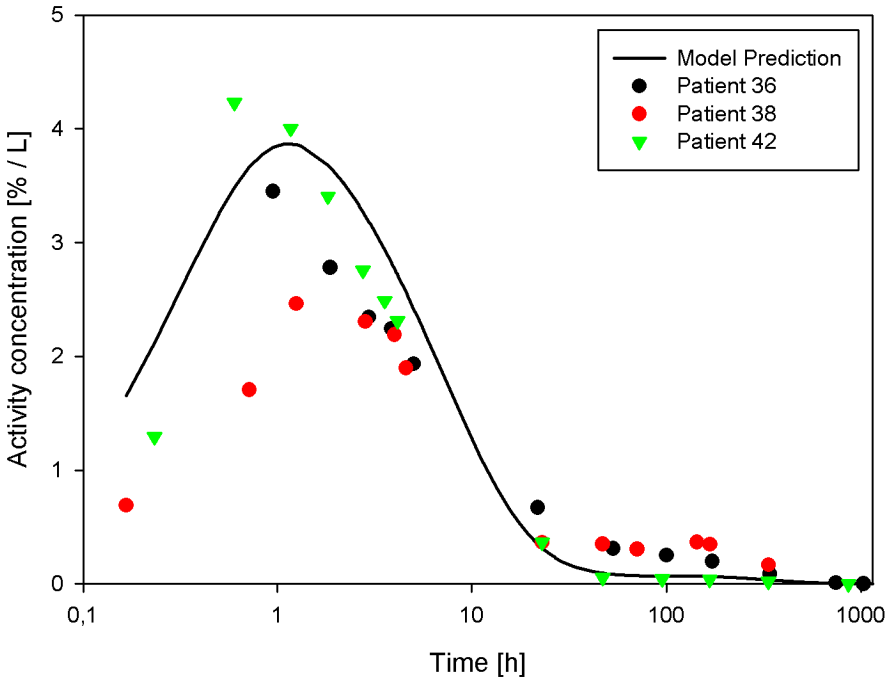

Figure 5.12: Fit of the complete compartmental model to the blood data of the fictional patient; activity conc. is given in percent of the administered activity per liter.

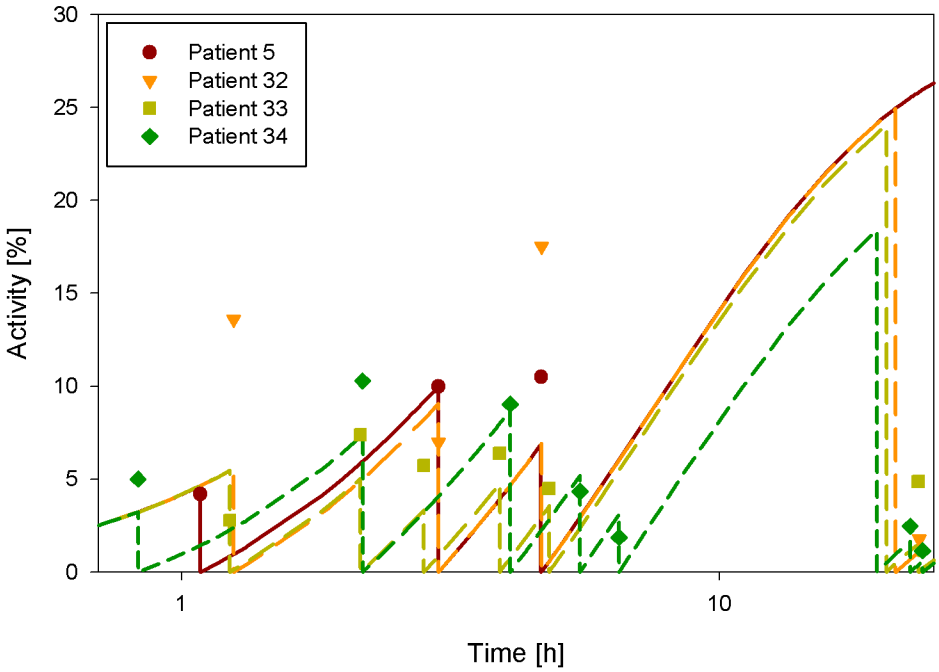

Figure 5.13: Fit of the complete compartmental model to the first part of the urine data of the fictional patient; activity is given in percent of the administered activity.

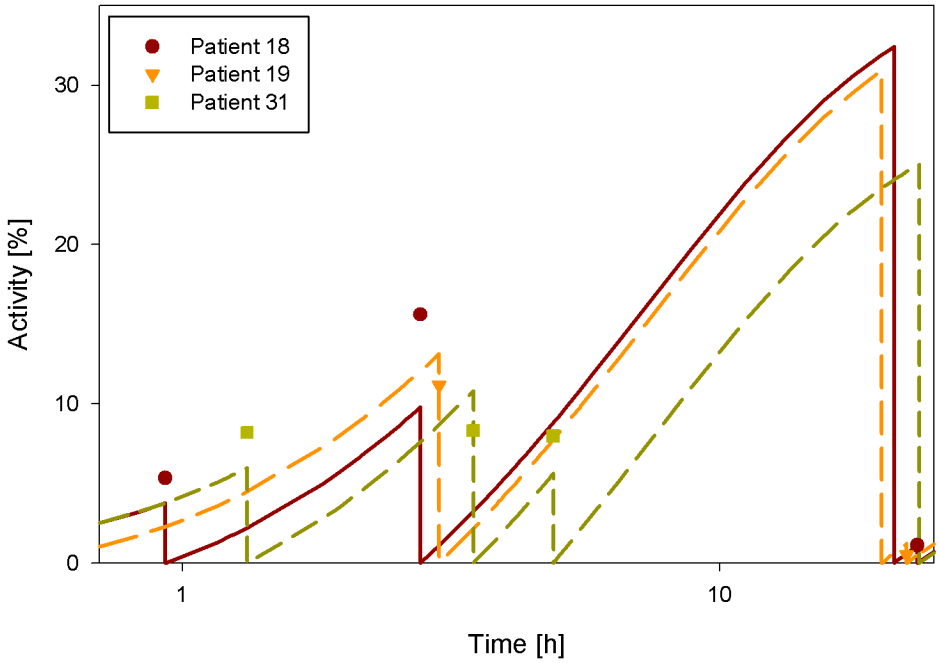

Figure 5.14: Fit of the complete compartmental model to the second part of the urine data of the fictional patient; activity is given in percent of the administered activity.

the plots for the sake of clarity. The urine data and corresponding fits are only shown in the first 25 hours after administration also for the sake of clarity. The activity excreted at later times is very low (less than 0.1 % IA) and could not be visualized on this scale. There is a fit curve for each patient because the voiding times of the bladder are different for each patient. Each curve rises as the activity accumulates in the bladder over time. Measurements are made when the bladder is voided. The abrupt drops in the fitted curves correspond to the voidings of the bladder.
Due to differences in uptake between the patients the data are spread. Therefore an exact correspondence of model prediction and data was not the aim of this analysis and would anyway be impossible to achieve with a single set of model parameters. The aim of the fit was rather to show the ability of the model structure to qualitatively describe the measured data. The model curves reproduce the trend of the measured data well. So it is demonstrated that the chosen model structure is a good description of the iodine kinetics in AFTN patients. The experiment indicates that a unique set of parameters can be found with which the model describes the data sufficiently if the necessary number of datasets is available.

After proving thus that the model is suitable to describe the kinetics of radioiodine, SAAM II was used to fit the model to the patient data individually.

5.2.2 Model parameter estimation: patients with blood samples

As was mentioned above, no patient had all data needed for the model to be identifiable. Therefore the model had to be reduced, i.e. compartments had to be omitted according to which data sets were missing.
For the case that blood had been sampled but no urine samples were available, the model used was like that in figure 5.10 but without the bladder compartment, that was replaced by a simple loss from inorganic Blood. The fA value defining the ratio of absorption into Blood-I to loss from the alimentary tract was fixed at 0.99. This value was chosen because it is recommended in the ICRP publications. Furthermore, in the previous analysis of the fictional patient the value of this parameter also settled at 0.9986.
For the case that urine had been sampled but no blood samples were available, the Alimentary Tract compartment was omitted. Instead direct uptake of iodine into the blood was assumed. Also the Rest of Body compartment was not considered in order to lower the number of parameters and thus make a solution possible.
For the patients that had no uptake in the lobe, the two lobe compartments were also omitted in the model.

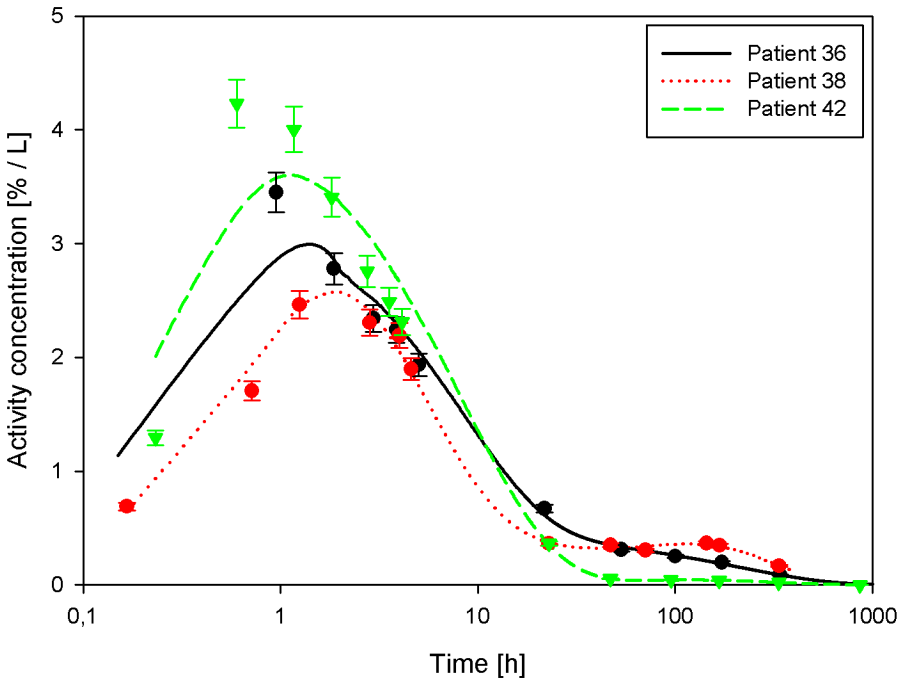

Figure 5.15: Fit of the model to individual blood data of patients with blood data; activity conc. is given in percent of the administered activity per liter.

Three patients (36, 38 and 42) that had blood samples taken were investigated with this reduced model. Patient 36 had data for uptake in lobe, patients 38 and 42 did not.

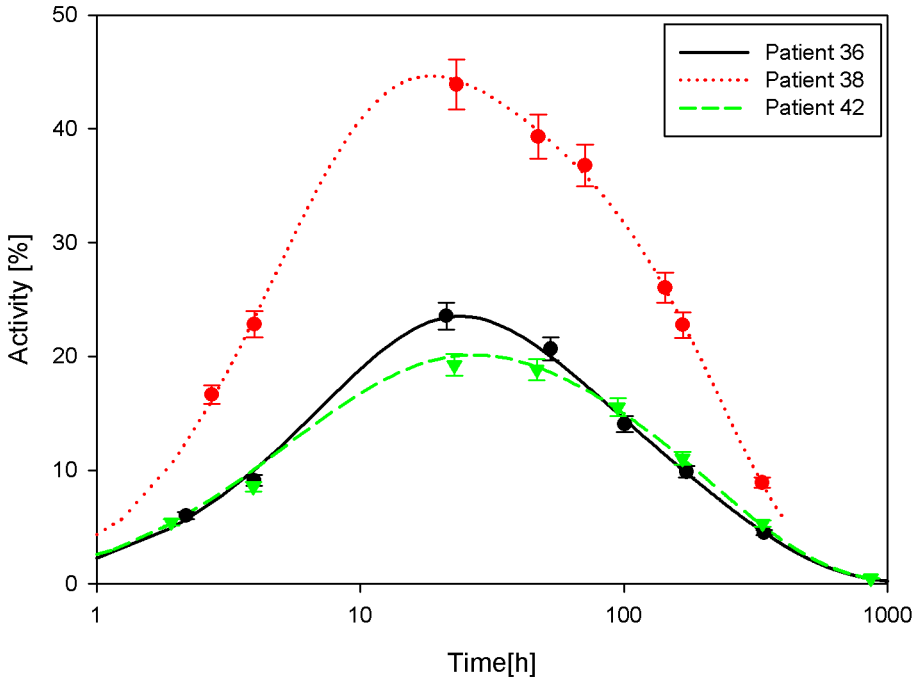

Figure 5.16: Fit of the model to individual nodule data of patients with blood data; activity is given in percent of the administered activity.

The fitted curves describe the uptake in the nodule very well in all patients (figure 5.16). The activity in blood later than one hour after administration is also well reproduced as shown in figure 5.15. For earlier kinetics of iodine in blood however, the fitted curves in patients 36 and 42 correspond not exactly to the measured data.
The resulting model parameters for therapy data of patients 36, 38 and 42 are compared in table 5.2. All parameters are given as transfer rate per hour, except for volume which is given in liters, and the associated standard deviations are given as the percental coefficients of variation. Parameters that settled at zero during the fitting process were considered as fixed parameters (parameter values can not be smaller than zero) and were therefore not evaluated in the fit. Only few parameters are similar over all patients. One is the transfer from Blood to Rest of Body, another is Volume. With values between 20 and 30 liters this is not only the blood volume, but the entire volume of distribution including e.g. the extracellular or interstitial fluids. Further parameters that have similar values for all patient are Loss from Alimentary Tract and Alimentary Tract to Blood-I. For all other parameters a common value or a common trend is not observable mainly because in many cases the parameter settles at zero for one of the patients. These differences between the patients are due to the large inter-individual differences in uptake.

Table 5.2: Parameter values for the analysis of patient 36, 38 and 42 with the reduced model including the Alimentary Tract. Volume is given in liters, all other values are 1/h. The standard deviation is given as % coefficient of variation. In some cases the parameter was not evaluated (-) because the corresponding data set was not available. AT represents Alimentary Tract and RoB represents Rest of Body.

Parameter	Patient 36		Patient 38		Patient 42	
	Value [1/h]	SD [%]	Value [1/h]	SD [%]	Value [1/h]	SD [%]
Volume	30.3	6	27.3	5	23.8	1
Loss from Blood-I	6.1e-3	11	0	-	0	-
Loss from AT	2.9e-2	16	1.2e-2	8	2.9e-2	4
Loss from Blood-O	0	-	1.1e-2	15	1.9e-3	157
Nodule to Blood-I	2.2e-2	8	2.8e-2	24	1.0e-1	56
Lobe to Blood-I	2.5e-2	17	-	-	-	-
AT to Blood-I	2.8	16	1.18	8	2.86	4
Blood-O to Blood-I	0	-	1.6e-3	165	1.1e-2	32
RoB to Blood	1.2e-2	13	1.5e-2	25	0	-
Blood to Nodule-I	3.5e-2	5	1.1e-1	6	4.1e-2	8
Blood to Lobe-I	5.7e-3	11	-	-	-	-
Nodule-I to -O	0	-	1.8e-2	72	1.7e-1	40
Lobe-I to -O	8.2e-4	38	-	-	-	-
Nodule to Blood-O	0	-	6.5e-3	24	1.18e-3	3
Lobe to Blood-O	0	-	-	-	-	-
Blood to RoB	5.3e-2	12	7.7e-2	15	8.4e-2	2

5.2.3 Model parameter estimation: patients with urine samples

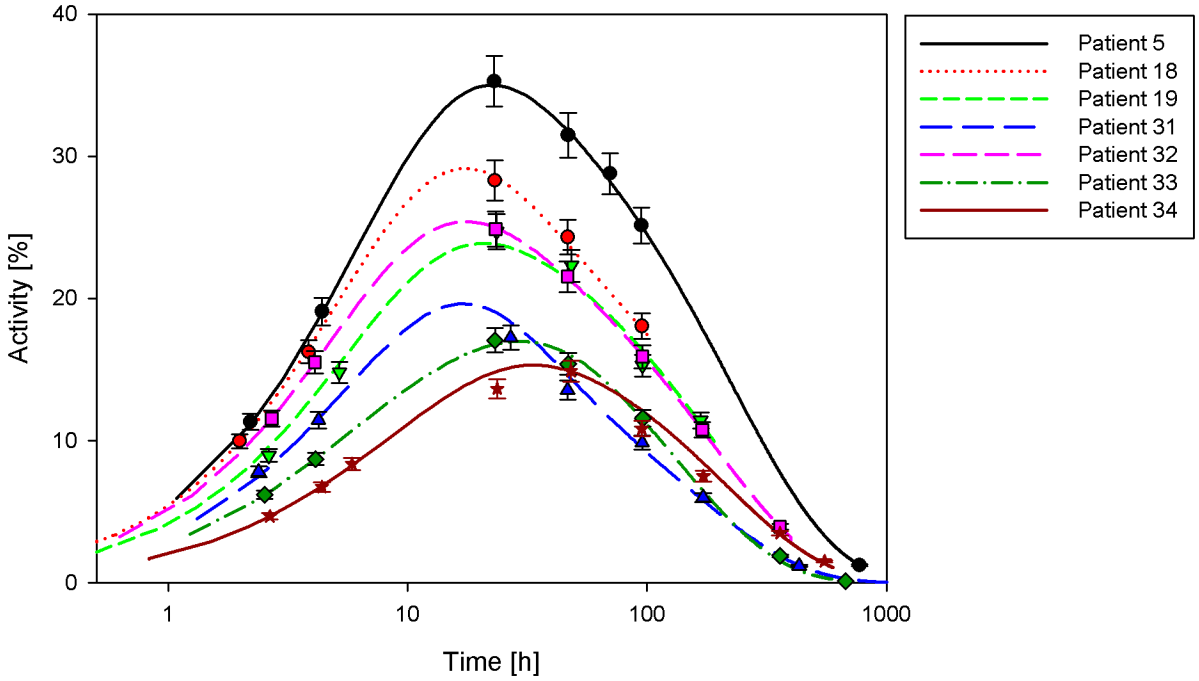

Figure 5.17: Fit of the model to individual nodule data of patients with urine data; activity is given in percent of the administered activity.

Seven patients (5, 18, 19, 31, 32, 33 and 34) who had collected urine samples after the administration of the therapeutic activity were investigated with the reduced model described above. Patients 5, 18, 32, 33 and 34 had data for uptake in lobe, 19 and 31 did not.

The fitted curves describe the uptake in the nodule very well in all patients (figure 5.17). Figures 5.18 and 5.19 show the fitted curves for the activity accumulated in the bladder with the corresponding urine data. In some patients the fitted curve corresponds satisfactory to the measured urine data, like in patients 31 and 34, while in others like 19 or 32, it fails to get even close to a proper description.

The model parameters for these fits to therapy data are listed in table 5.3. All parameters are given as transfer rate per hour and the associated standard deviations are given as the percental coefficients of variation. For patients 5 and 18 the parameter Loss from Blood-O had to be fixed to some high value and also the parameter Blood-O to Blood-I in patient 5 had to be fixed to 0.001 in order to reach convergence, in these cases also no standard deviations are available. Also in this case it is not possible to find a common set of parameters that describe approximately all patient data. This is again due to large inter-individual differences. Only three parameters showed similar values in a majority of the six patients: Blood to Nodule-I, Blood to Lobe-I and Blood to Bladder. This last

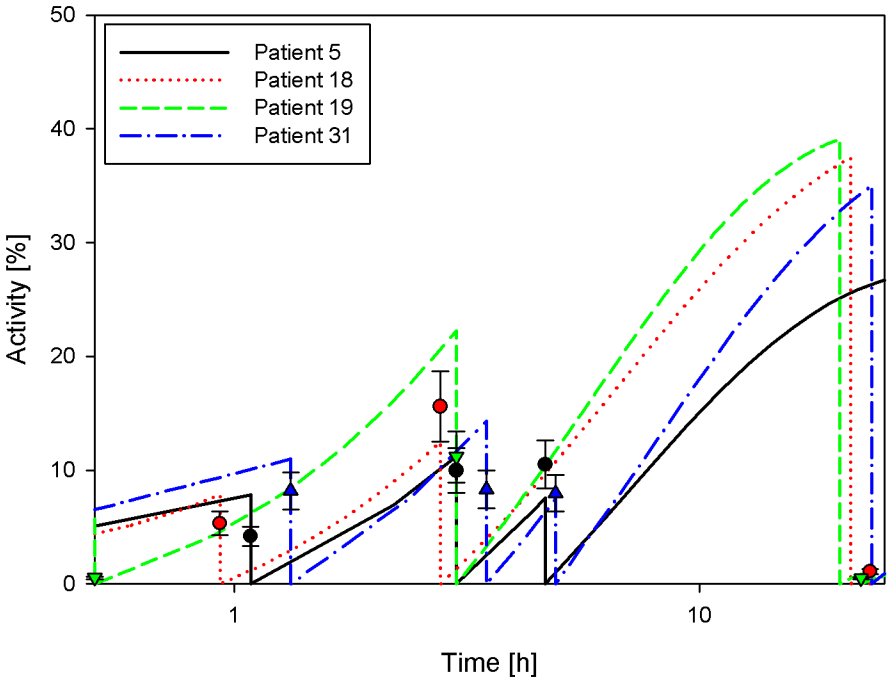

Figure 5.18: Fit of the model to individual urine data of patients with urine data; activity accumulated in the bladder is given in percent of the administered activity.

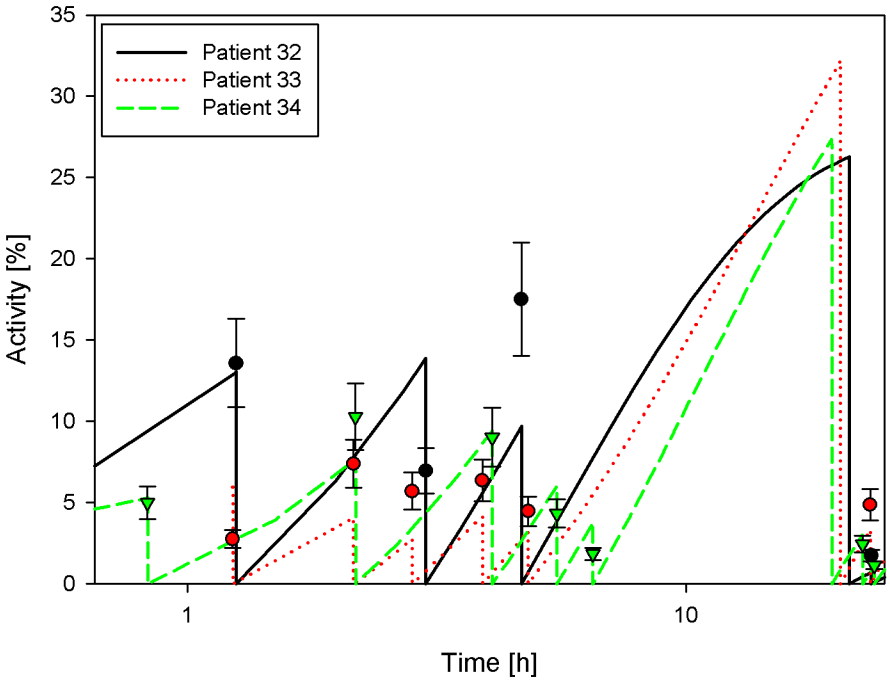

Figure 5.19: Fit of the model to individual urine data of patients with urine data; activity accumulated in the bladder is given in percent of the administered activity.

Table 5.3: Parameter values for the analysis of patient 5, 18, 19, 31, 32, 33 and 34 with the reduced model including the bladder. All parameter values are given as 1/h. The standard deviation is given as % coefficient of variation.

Parameter	Patient 5		Patient 18		Patient 19		Patient 31		Patient 32		Patient 33		Patient 34	
	Value	SD	Value	SD	Value	SD	Value	SD	Value	SD	Value	SD	Value	SD
Loss from Blood-O	35	-	5	-	0	-	3.5e-3	39	0	-	0	-	0	-
Nodule-I to Blood-I	7.8e-3	114	2.1e-2	13	3.1e-3	13	2.8e-2	12	9.8e-3	33	1.4e-1	153	9.0e-2	172
Lobe-I to Blood-I	5.2e-2	541	4.0e-2	47	-	-	-	-	1.0e-2	129	4.3e-1	96	1.0e-2	39
Blood-O to Blood-I	0	-	1.0e-3	-	0	-	6.1e-3	28	1.0e-1	-	1.0e-1	-	9.2e-2	402
Blood-I to Nodule-I	6.0e-2	5	6.0e-2	4	4.6e-2	3	3.8e-2	4	5.5e-2	0.7	3.2e-2	28	2.2e-2	18
Blood-I to Lobe-I	1.9e-3	31	1.7e-3	9	-	-	-	-	8.1e-3	6	2.8e-3	42	4.8e-3	6
Nodule-I to -O	2.6e-2	173	2.3e-2	8	8.6e-3	11	2.0e-2	10	2.7e-2	26	1.2e-1	122	2.5e-1	111
Lobe-I to -O	2.3e-1	399	3.4e-2	51	-	-	-	-	4.3e-2	195	1.4e-1	57	1.2e-2	56
Nodule-O to Blood-O	8.1e-4	17	5.0e-4	-	1.4e-3	61	2.6e-3	3	2.4e-3	3	5.5e-3	7	1.6e-3	6
Lobe-O to Blood-O	5.8e-4	31	5.0e-4	-	-	-	-	-	2.9e-3	17	7.6e-3	5	9.8e-4	42
Blood-I to Bladder	7.9e-2	7	9.0e-2	5	1.2e-1	4	9.1e-2	4	1.2e-1	5	5.1e-2	19	6.6e-2	4

parameter has a lower value only in patient 32 corresponding to the bad fit of the model prediction to the measured urine data.

5.2.4 Model parameter estimation: population analysis of reduced model

For the patients for which neither blood nor urine data were available, the model was reduced further by omitting the compartments for Alimentary Tract and Bladder now assuming an instant bolus uptake into blood and a direct excretion from Blood-I. Also the compartment for Rest of Body is left out. The reduced model is shown in figure 5.20. It only consists of the six compartments for blood, nodule and lobe. For the analysis of this model only the data measured in nodule and lobe were used. The activity in the nodule was measured in all 43 patients and in 31 of them also the activity in the lobe could be measured. This makes the use of the population kinetics approach possible. Therefore the data of all patients were used to analyze the reduced model to determine the parameter values that describe the data of all patients in this study and thus values that can be generalized for all patients suffering from AFTN.

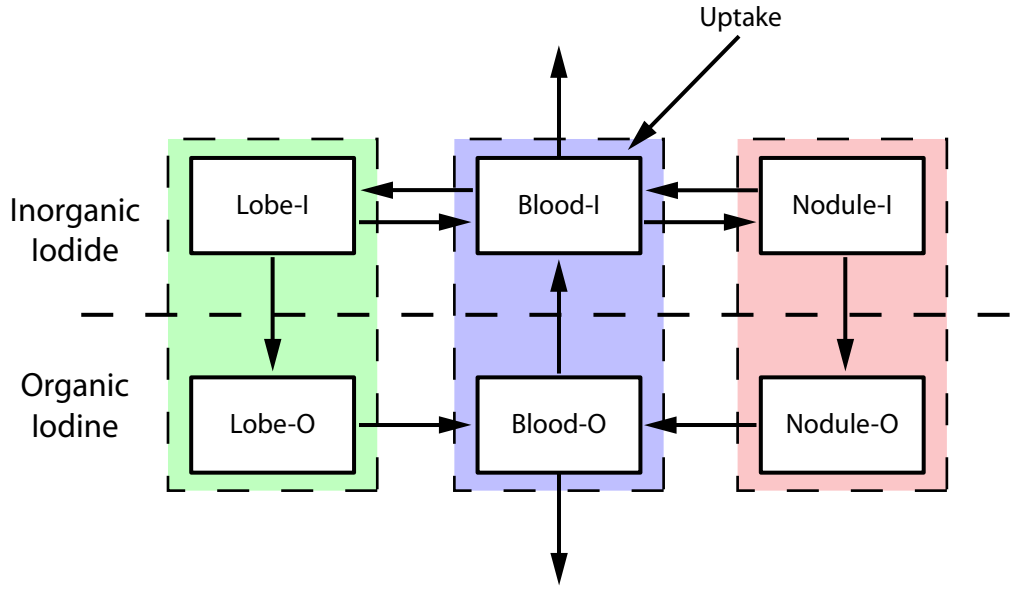

Figure 5.20: The reduced compartmental model.

This was done with the MLEM routine in ADAPT 5 described on pages 26 ff. A normal distribution of the parameter values was assumed and the full covariance matrix was calculated. 100 EM iterations with 2000 samples per iteration were chosen. Tests had shown that this number is sufficient for the parameters to converge at stable and reliable values.

Table 5.4: Population mean parameter values for the MLEM ADAPT 5 analysis of all patients with the reduced model, all values are 1/h. The standard deviation is given as % coefficinent of variation.

Parameter	Population	
	Value [1/h]	SD [%]
Loss from Blood-I	2.4e-2	40
Loss from Blood-O	5.0e-2	34
Nodule to Blood-I	9.7e-2	50
Lobe to Blood-I	1.0e-1	40
Blood-O to Blood-I	1.0e-1	31
Blood to Nodule-I	5.5e-2	52
Blood to Lobe-I	3.8e-3	52
Nodule-I to -O	1.9e-2	56
Lobe-I to -O	2.3e-2	40
Nodule to Blood-O	1.5e-3	66
Lobe to Blood-O	1.3e-3	87

The population mean parameters found are shown in table 5.4. The value of Blood to Nodule-I are similar in this analysis to the ones in the analysis of the individual patients with urine data and to most of those with blood data. Except for the transfers of hormones from thyroid to Blood-O all parameters have standard deviations of around 50 % or less. This means that the population mean values are well defined and that the model with these parameters can describe the data sufficiently well.
Figures 5.21 and 5.22 also show that this solution of the model can describe the measured data well. The model fits for nodule and lobe are shown with the respective 95 % confidence intervals and all patient data. Nearly all data are covered by the confidence interval and the fit curves pass through the middle of the population.

So far the model was only investigated with data acquired during therapy with ^{131}I. In the next chapter it will be investigated whether this model can also describe the kinetics during diagnostics with ^{123}I and whether there are differences in the kinetics during therapy and diagnostics.

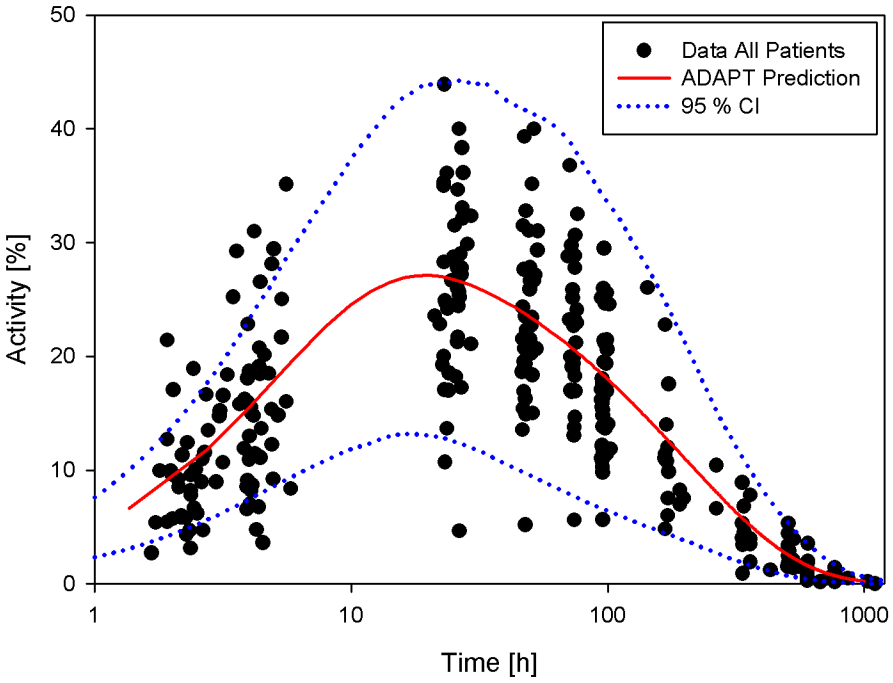

Figure 5.21: Fit of the reduced model to nodule data; activity is given in percent of the administered activity.

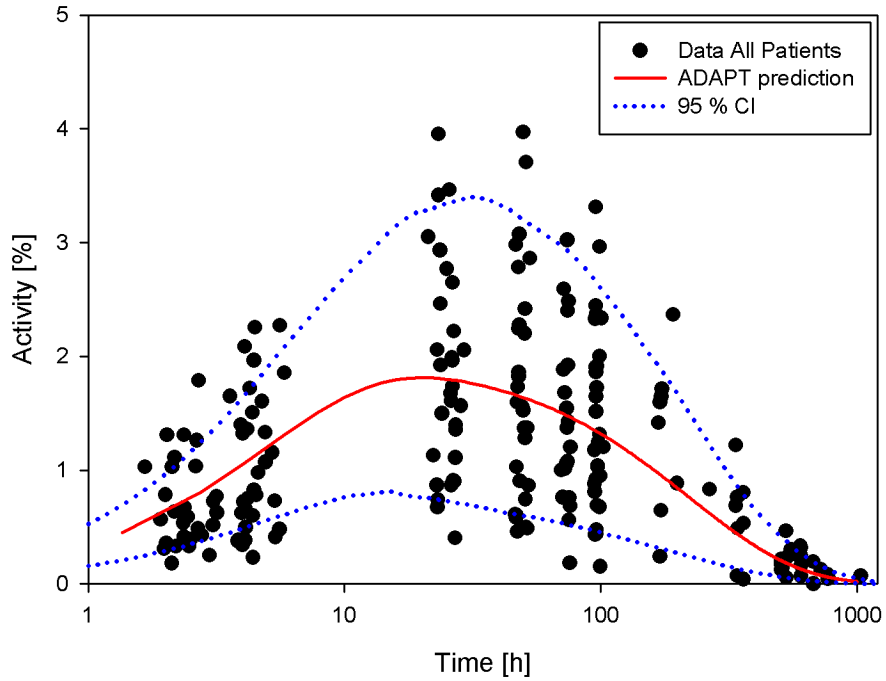

Figure 5.22: Fit of the reduced model to lobe data; activity is given in percent of the administered activity.

5.3 Comparison of biokinetics during diagnosis and therapy

In this study the uptake of iodine in the thyroid has been measured in all patients during diagnostics and therapy. The diagnostic measurements are used for therapy planning assuming that the kinetics do not change in the time between. The validity of this assumption is still discussed controversially as shown below. Therefore a test was performed with the data in this study to investigate if the kinetics show differences.
The kinetics are easily compared because the model parameters are independent of the isotope used. This is because the radioactive decay is included in the model by the introduction of additional compartments as described in chapter 4.4.2. Therefore each set of estimated model parameter can be used to describe the kinetics of both isotopes if the respective decay constant is used for the transfer rates into the additional compartments.

5.3.1 Differences between diagnostics and therapy - literature review

This phenomenon of differences in iodine uptake during treatment planning and therapy is widely discussed in the field of thyroid cancer therapy. There the activities used are much higher than in the therapy of AFTN because the aim is to remove all possibly malignant thyroid tissue with a high dose. Another difference to the therapy of AFTN is that ^{131}I is used for the diagnostics and the therapy.
The effect of the diagnostic activity on the thyroid is called stunning which refers to the (temporary) loss of function. While some studies did not find this phenomenon [Morris2001][Dorn2003] others have proposed two possible explanations. One is that the dose from the diagnostic activity damages the tissue and thus reduces functionality during therapy [Yeung2000]. The other is that the high therapeutic activities of 1 GBq or more damage the thyroid early during therapy [Sisson2006]. As all studies were performed in patients after near-total thyroidectomy it is quite hard to estimate the volume of remaining lesions and thus to do a dosimetric analysis. Several authors tried to circumvent the stunning problem by using ^{123}I for tracer studies, assuming that the pure gamma emitter would result in less absorbed dose and thus no stunning [Siddiqi2001][Cohen2004][Urhan2007]. Two studies investigated stunning using in vitro approaches with porcine thyroid cancer cells [Postgard2002] and rat thyroid cancer cells [Meller2008] respectively. They found a reduction of the iodine transport capacity of viable thyroid cells due to a down regulation of the NIS transporter system, the cells iodide transport mechanism, that was radiation induced and dose dependent. The stunning starts already at low doses of a few Gy but was found to be reversible in proliferating cells.

The effect has also been described in studies with patients suffering from benign thyroid diseases like Graves' disease or AFTN. In those studies uptake measurements have been made for diagnostics and therapy and a common observation is that on comparison uptake is lower during therapy than it was during diagnostics [Bockisch1993][Reinhardt2002] [Canzi2006]. The investigation if these differences can also be found in the data in the present study is described in the following chapter.

5.3.2 Results of this study

In chapter 5.2 a compartmental model has been developed and the model parameters have been estimated using the data from therapy. The population analysis of this same model (figure 5.20) with the diagnostics data of all patients was used to test whether the model is also suitable to describe the kinetics during diagnostics and to investigate if there are differences in the kinetics. Although only measurements in the first five days are available during diagnostic, the model is identifiable in the population approach.
The MLEM routine in ADAPT 5 was used to estimate the population mean parameter for the diagnostics data in an approach similar to the one above (see chapter 5.2.4). A normal distribution of the parameter values was assumed and the full covariance matrix was calculated. 100 EM iterations with 2000 samples per iteration were chosen.

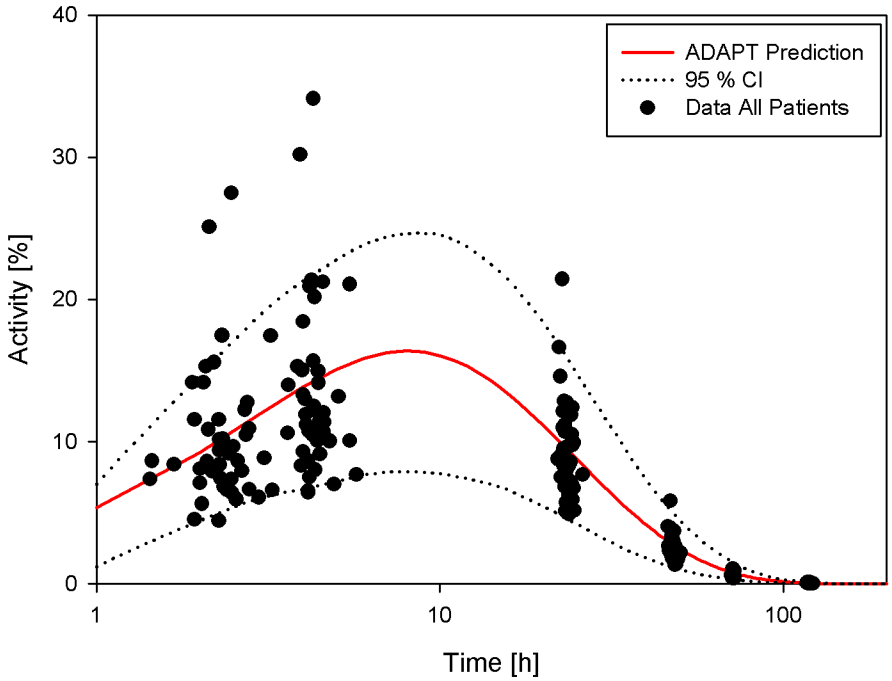

Figure 5.23: Fit of the reduced model to diagnostic nodule data; activity is given in percent of the administered activity.

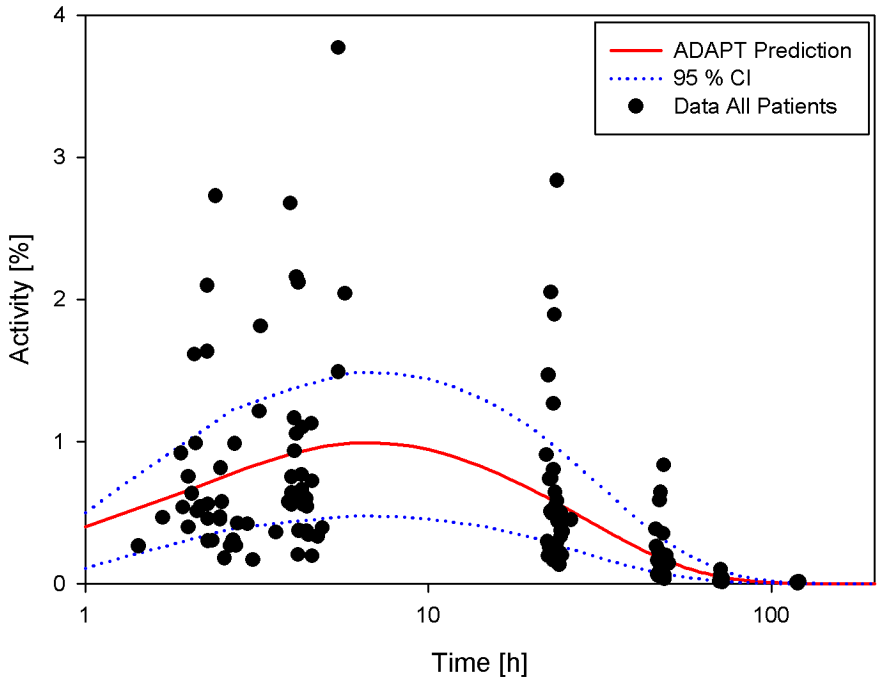

Figure 5.24: Fit of the reduced model to diagnostic lobe data; activity is given in percent of the administered activity.

The resulting fits and 95 % confidence intervals for nodule and lobe are shown in figures 5.23 and 5.24. The data for nodule are described well with almost all measurements within the confidence interval. For the lobe the fit curve is also in the middle of the data points but there are more measurements outside the confidence interval. The confidence interval calculation is based on the model structure and the standard deviations of the parameter values given by the software. In this case it can not reproduce the wide variability in the individual uptake of iodine in the lobe. However, the model is also suitable to represent the kinetics of iodine during diagnostics.

The resulting parameters are shown in table 5.5 together with the values estimated for the therapy data. The population mean values and their standard deviations are compared using a t-test for each parameter. The the t-values are listed in the last column. T-values larger than one indicate that the parameter values for therapy and diagnostics are not from the same distribution. The values for diagnostics and therapy are generally similar taking into account the uncertainties connected to the population mean values. But five parameters show large differences:

- The differences in the transition rates from of Lobe-I to Blood and to Lobe-O can be explained by the large uncertainty in the measured lobe data and with the wide spread of the data between patients.
- The differences in the parameters describing the release of organically bound iodine

Table 5.5: Population mean parameter values for the ADAPT 5 analysis of diagnostic and therapy data with the reduced model, all values are 1/h. The standard deviation is given as % coefficinent of variation. The differences between the parameter values are compared by a t-test.

Parameter	Diagnostic		Therapy		t-value
	Value [1/h]	SD [%]	Value [1/h]	SD [%]	
Loss from Blood-I	9.1e-3	46	2.4e-2	40	1.42
Loss from Blood-O	6.7e-2	36	5.0e-2	34	0.58
Nodule to Blood-I	1.3e-1	21	9.7e-2	50	0.59
Lobe to Blood-I	2.5e-1	20	1.0e-1	40	2.34
Blood-O to Blood-I	1.4e-1	34	1.0e-1	31	0.70
Blood to Nodule-I	6.2e-2	50	5.5e-2	52	0.17
Blood to Lobe-I	5.0e-3	64	3.8e-3	52	0.32
Nodule-I to -O	2.3e-2	38	1.9e-2	56	0.29
Lobe-I to -O	6.3e-2	32	2.3e-2	40	1.81
Nodule to Blood-O	1.1e-2	44	1.5e-3	66	1.92
Lobe to Blood-O	2.0e-2	44	1.3e-3	87	2.11

from the thyroid to Blood-O are due to the short measurement time scale during diagnostics. The excretion of thyroid hormones is a very slow metabolic process that takes much longer than the half-life of ^{123}I. Therefore these parameters can not be estimated realistically based on the data available during diagnostics. The standard deviation of the population mean values of these parameters is larger for therapy than for diagnostics because it is computed in respect to the measured data and there are no measurements at late times during diagnostics.

- The Loss from Blood-I is also dependent on the long term retention of iodine and therefore the values are different in diagnostics and therapy.

Although five of the eleven parameters have different values for therapy and diagnostics, the kinetics are very similar when the fitted curves are compared. In figure 5.25 the nodule kinetics of ^{123}I predicted by the therapy parameter set (conf. table 5.4) and the diagnostics parameter set are compared. Both curves are similar and well in the middle of the measurements, the main difference is the uptake in the first ten hours. The area under the curve for the kinetics during therapy is 10 % less than that of the diagnostics. This is within the uncertainties of the predicted model parameters and the measured data.
So the effect of the differences in the population mean parameters is not apparent in the predicted kinetics. This test confirms that the kinetics during diagnostics and therapy

are not significantly different in this study.

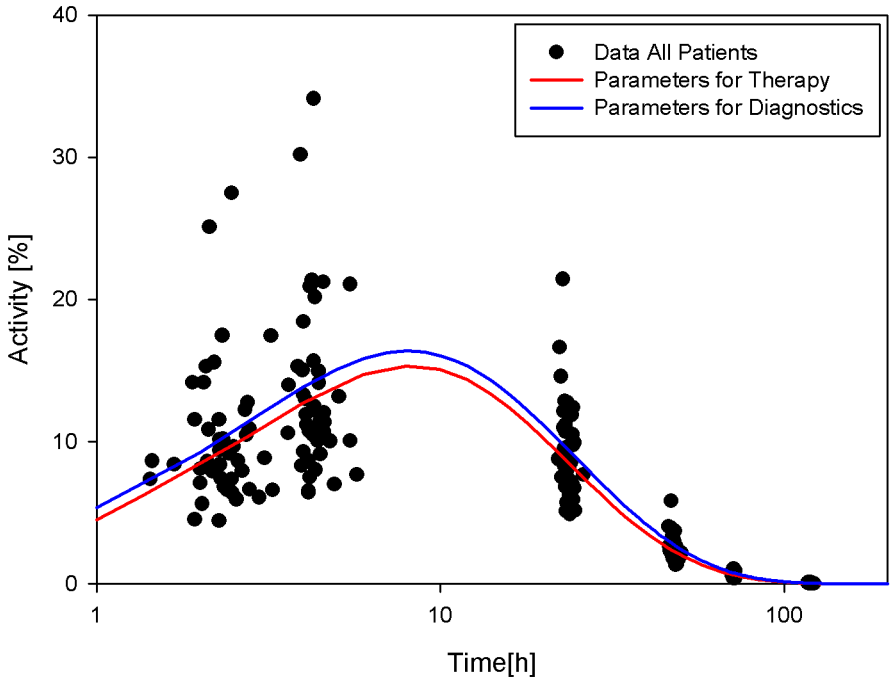

Figure 5.25: Activity in the nodule predicted by the population mean parameters for therapy and diagnostics compared to measured ^{123}I activity in the nodule during diagnostics; activity is given in percent of the administered activity.

6 Development of an optimized sampling schedule for routine applications

The aim of the analysis presented in this chapter is to identify the minimal number and the optimal time points of measurements that are necessary to describe the kinetics correctly. As was shown in the previous chapter, the kinetics are not significantly different for diagnostics and therapy. Therefore uptake measurements of ^{123}I made during diagnostics can be used to predict the kinetics for therapy planning. In clinical practice, diagnostics with ^{123}I measurements are only feasible during the first five days. This time frame is given a special attention in the following paragraphs. The measurement schedule was investigated analyzing population data as well as data from a fictional model subject representative for the population. Furthermore the schedule is investigated using data from therapy and from diagnostics.

6.1 Population analysis of the sampling schedule

In the population analysis of the sampling schedule, the general idea of this approach is to select patients with large data sets over a long time period, neglect data at certain time points, fit the model to the reduced data and investigate if the resulting model parameters can still describe the kinetics. To investigate the role of late measurements and the possible need for long term measurements, data from therapy with ^{131}I were used rather than data from diagnostic scans with ^{123}I. As has been shown in the previous chapter the results for ^{131}I can be transferred to ^{123}I. 34 patients with the largest data sets, i.e. at least seven measurements of uptake in the nodule over at least 14 days, were selected. The model for this analysis was the reduced model used in the last part of chapter 5.2.4 and shown in figure 5.20.

By omitting the measurements after certain cut-off times in all patient data sets, five different reduced data sets were generated. As cut-off times were chosen: 15 days (set A), 5 days (set B), 4 days (set C), 3 days (set D) and 2 days (set E). A sixth set of data (set F) was generated by taking the three measurements on the first two days together with one measurement taken between 12 and 25 days after administration, according to what data was available for the respective patient. Thereby all data taken at very late times were ignored. A seventh set of data (set G) was built by selecting the data of the

Table 6.1: Data included in the reduced data sets for the investigation of the measurement schedule.

Data Set	Time of measurement								
	2 h	4 h	24 h	3 d	4 d	5 d	7 d	14 d	other
A (Cut-off 15 d)	x	x	x	x	x	x	x	x	
B (Cut-off 5 d)	x	x	x	x	x	x			
C (Cut-off 4 d)	x	x	x	x	x				
D (Cut-off 3 d)	x	x	x	x					
E (Cut-off 2 d)	x	x	x						
F	x	x	x						One between 12 and 25 d
G	x	x	x						All data after day 11

first and second day together with all data after the eleventh day. The main difference between sets F and G are five data points instead of four in nine patients. In table 6.1 the data contained in the reduced data sets are listed.

For all these data sets the fit and parameter estimation was done with the population kinetics software ADAPT 5. The resulting fits for the nodule are shown in figures 6.1 to 6.5 and are compared against the fit done with all available data at the end of chapter 5.2. The latter is seen as the reference, assuming that the use of all available data gives the most accurate description of the kinetics of iodine. In all plots the reference curve is shown in blue. The fits are shown as solid curves together with the respective 95 % confidence intervals as dotted curves. In the first three figures the fits of data sets generated by omitting all data after a certain cut-off time are presented. The curves for cut-off at three and four days are not shown because they lie between the curves for cut-off at two and five days and give no further information.

From these figures it is clear that the more data are used the closer the fits get to the reference curve. Only the data set generated by cut-off after 15 days with six or seven measurements per patient can adequately describe the kinetics at longer times. With less data the retention of iodine in the thyroid is underestimated.
The fit of the model to data acquired in the first five days (set B) follows the reference curve for the first four days and then drops below. For times points later than 12 days after the administration the reference curve is outside the confidence interval of the fit for this data set B. The area under the fitted curve is 25 % smaller than that of the reference curve. So the absorbed dose is largely underestimated as this measure is related to the number of nuclear transitions and therefore to the dose. If this schedule was used for treatment planning, it would result the administration of too much activity in order to reach the prescribed dose.

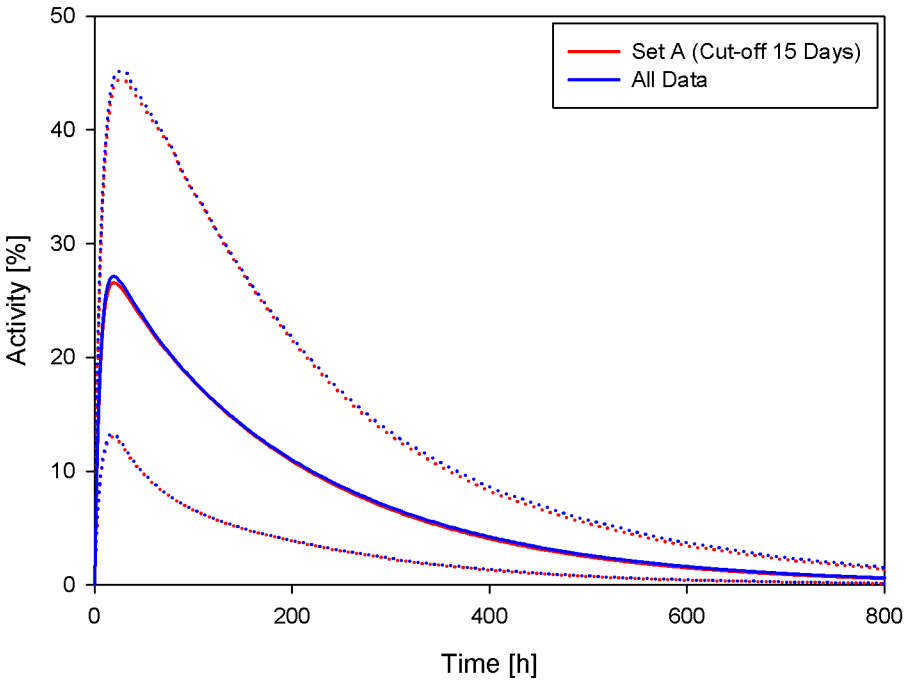

Figure 6.1: Comparison of model fits obtained with the full amount of data and data cut-off at 15 days. The dotted curves indicate the 95 % CI.

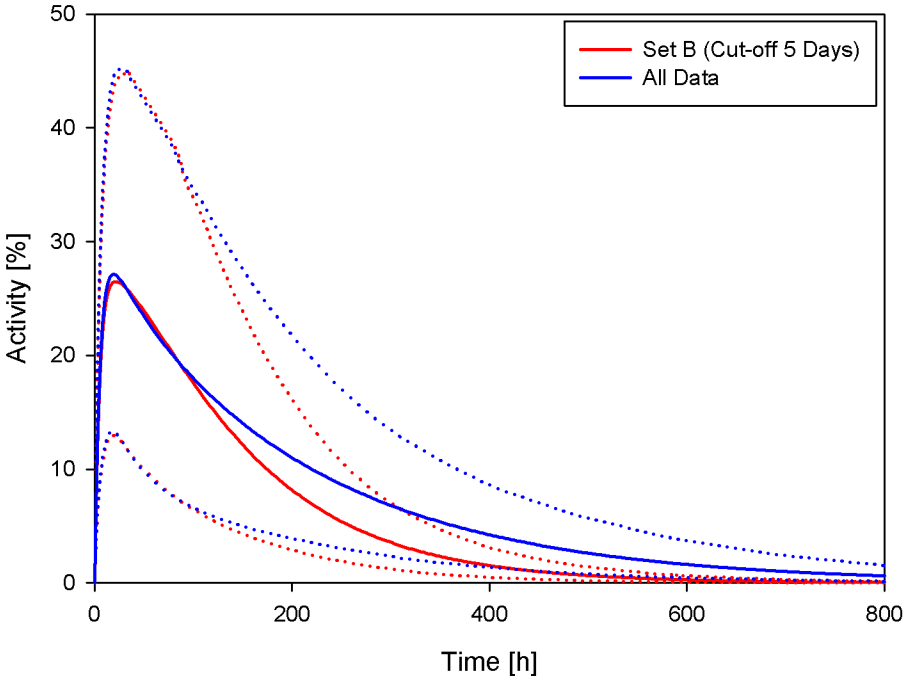

Figure 6.2: Comparison of model fits obtained with the full amount of data and data cut-off at five days. The dotted curves indicate the 95 % CI.

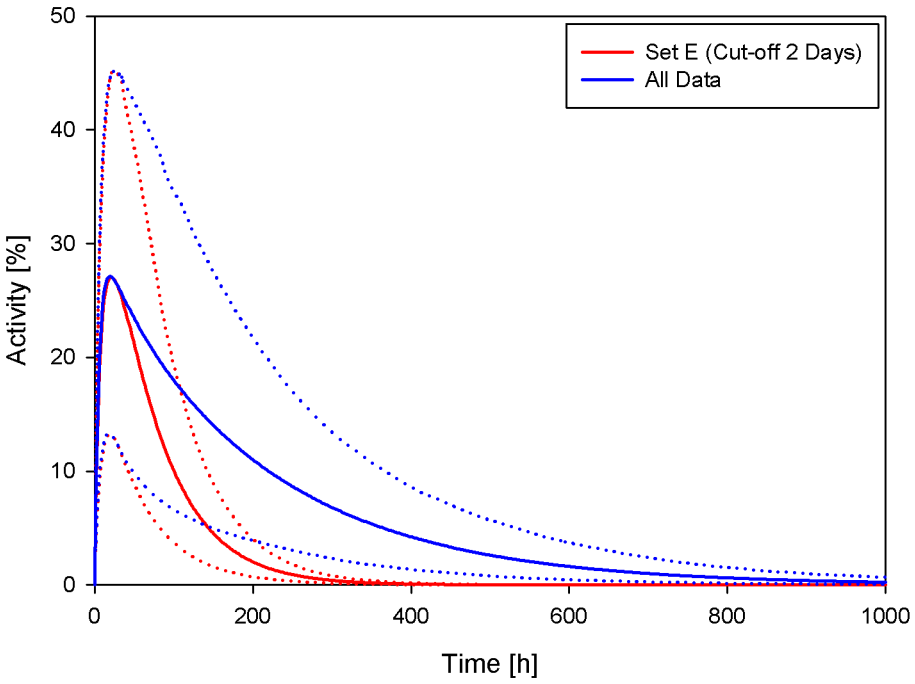

Figure 6.3: Comparison of model fits obtained with the full amount of data and data cut-off at two days. The dotted curves indicate the 95 % CI.

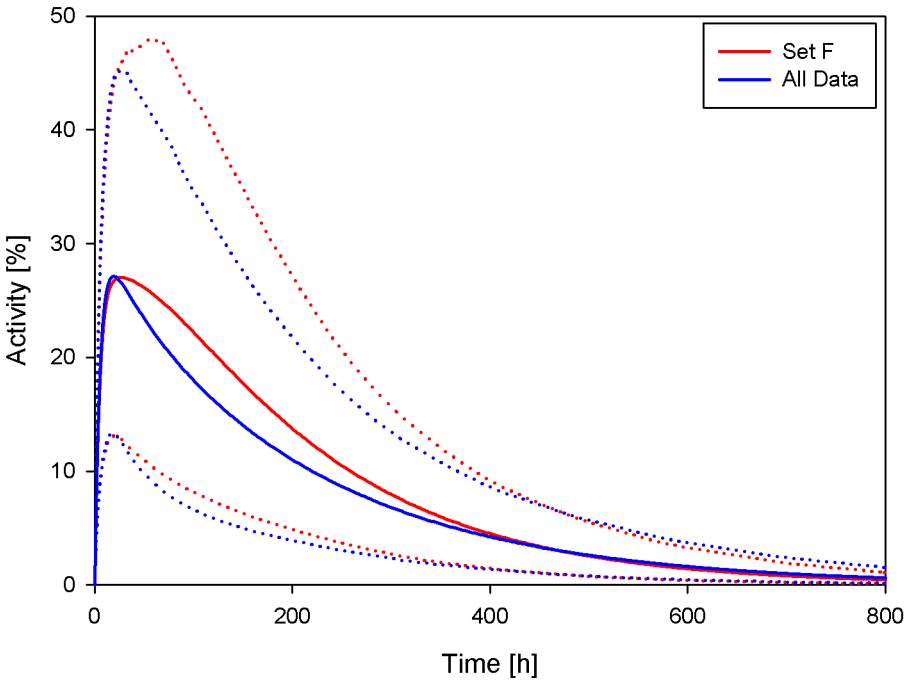

Figure 6.4: Comparison of model fits obtained with the full amount of data and data set F. The dotted curves indicate the 95 % CI.

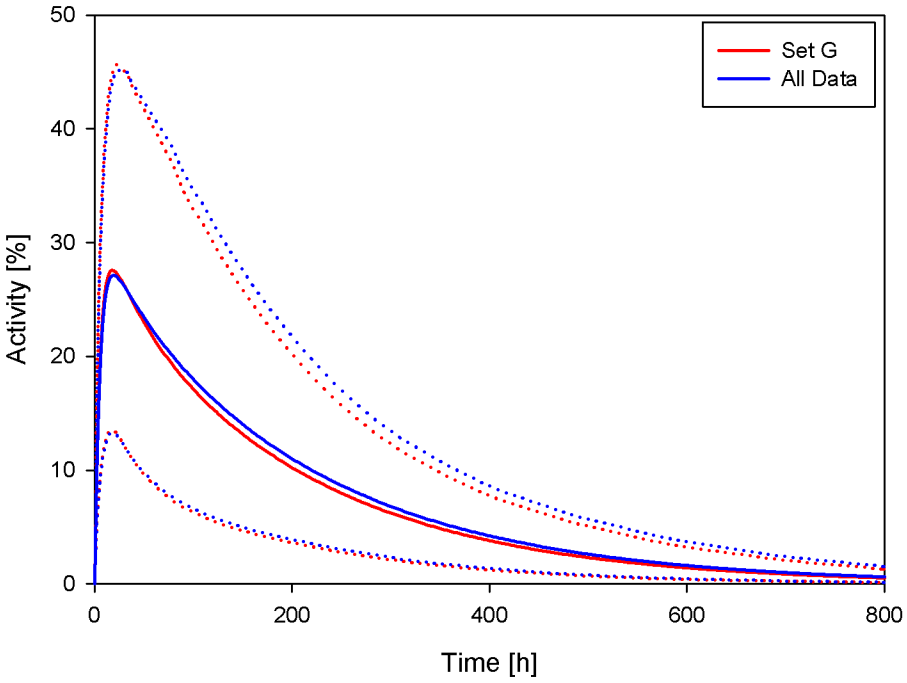

Figure 6.5: Comparison of model fits obtained with the full amount of data and data set G. The dotted curves indicate the 95 % CI.

Using only data measured in the first two days, the fit reproduces the reference curve only over the first 30 h and then drops below. The reference curve is outside the confidence interval of the fitted curve for times later than four days. Here the area under the fitted curve is 57 % smaller than that under the reference curve. So this amount of data is completely useless to determine the kinetics of iodine realistically.
Figure 6.4 shows the fit obtained with data set F, where only one late measurements in the time between 12 days and 25 days is included additionally to the three measurements in the first two days. The fit to data set F overestimates the uptake slightly, the area under the curve is 13 % larger than that of the reference curve. The last fit (fig. 6.5) has been obtained with data set G where measurements between three days and 11 days are omitted. Although it is only a little larger than the one before, it follows the reference curve very closely. However the broad confidence intervals indicate that both sets of data are sufficient to describe the kinetics. They are significantely better in describing the long term retention than the data sets with data from late measurements missing.

In table 6.2 and in figure 6.6 the population mean model parameters of the three data sets A, F and G that can describe the kinetics best are compared to the parameters from the reference fit. In the figure the relative differences in percent of the reference value are given for each parameter. The parameter values for the reduced data sets are generally similar to the reference values. However, the parameters for cut-off at 15 days (blue

crosses) and for the set G (red X) are in better agreement with the reference values than in the case of only four data per patient (triangles).

The result of this analysis of the measurement schedule is therefore that five measurements are necessary to estimate the kinetics of iodine with this model using population kinetics: Measurements between three days and two weeks are not necessary. With the three measurements in the first two days and two further measurements, one around two weeks after administration and one later than three weeks, the kinetics can be described well.
But this schedule is not feasible in the clinical practice if the kinetics for treatment planning are determined by diagnostics with ^{123}I. Furthermore the estimation of the kinetics for treatment planning is based on measurements in a single patient. Therefore an approach more suited to the clinical routine is chosen in the next chapter to investigate possibilities for an optimized measurement schedule.

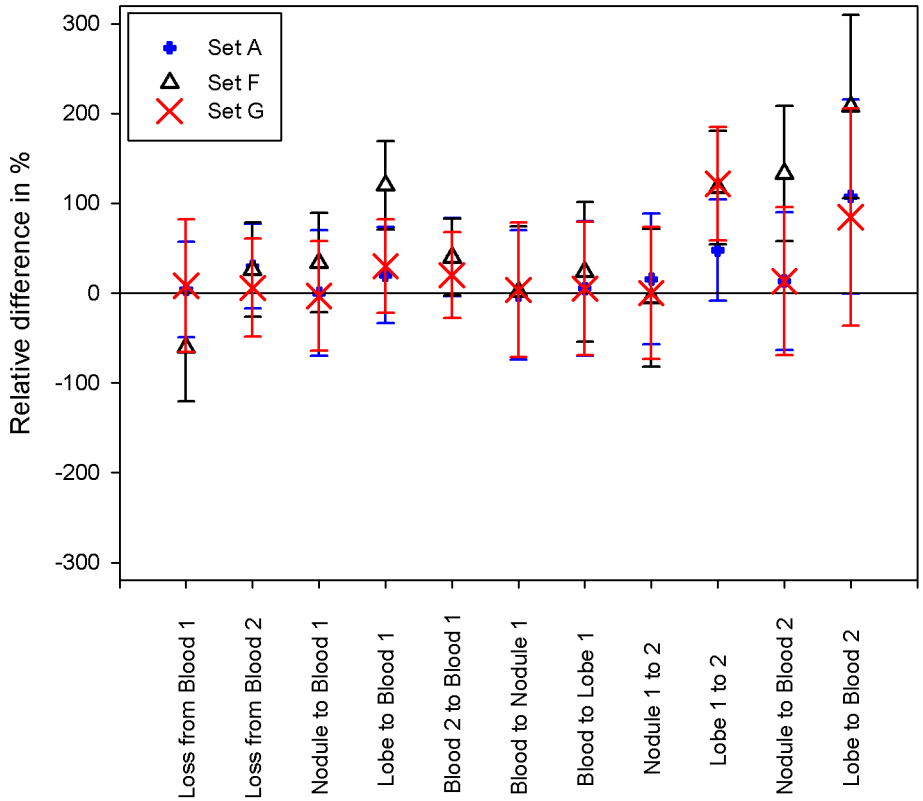

Figure 6.6: Relative difference of the population mean model parameters obtained with the reduced data sets A, F and G and the reference parameters obtained with all data.

Table 6.2: Population mean parameter values for the three best fits (data sets A, F and G) and the reference, all values are 1/h. The standard deviation is given as % coefficient of variation.

Parameter	All data		Cut-off 15 d		1. & 2. d + 1 in 12-25 d		1. & 2. d + all after 11 d	
	Value [1/h]	SD [%]	Value [1/h]	SD [%]	Value [1/h]	SD [%]	Value [1/h]	SD [%]
Loss from Blood-I	2.4E-02	40	2.5E-02	35	9.5E-03	45	2.6E-02	62
Loss from Blood-O	5.0E-02	34	6.5E-02	33	6.3E-02	40	5.3E-02	43
Nodule to Blood-I	9.7E-02	50	9.7E-02	49	0.13	24	9.4E-02	35
Lobe to Blood-I	0.10	40	0.12	36	0.22	29	0.13	33
Blood-O to Blood-I	0.10	31	0.14	31	0.14	30	0.12	36
Blood to Nodule-I	5.5E-02	52	5.4E-02	50	5.6E-02	51	5.7E-02	54
Blood to Lobe-I	3.8E-03	52	4.0E-03	54	4.7E-03	58	4.0E-03	53
Nodule-I to -O	1.9E-02	56	2.2E-02	47	1.8E-02	52	1.9E-02	48
Lobe-I to -O	2.3E-02	40	3.4E-02	40	5.0E-02	49	5.1E-02	49
Nodule to Blood-O	1.5E-03	66	1.7E-03	39	3.5E-03	36	1.7E-03	49
Lobe to Blood-O	1.3E-03	87	2.7E-03	64	4.0E-03	53	2.4E-03	84

6.2 Individual analysis of the sampling schedule

In the clinical practice, data of a single patient are used to model the kinetics of iodine for therapy planning. Therefore, the sampling schedule was investigated for an individual subject. The kinetic described by the population mean model parameters derived in chapter 5.2.4 was used to generate a representative data set. Sampling time points were 2, 4 and 24 hours, 2, 4, 5, 7, 14, 21 and 28 days. As before, these are data from therapy, chosen because the influence of long-term measurements on the modeling can only be investigated with those.

Four different data sets were generated from this initial set by omitting data at certain time points. With respect to the findings in the previous population analysis the following data sets were generated: one set with three data points in the first two days and one data point at 21 days (set AA) and a second set with three data points in the first day and data points at 14 and 21 days (set BB). Two further data sets were generated using only data points in the first five days because diagnostic measurements with ^{123}I are only made in this time range. So the third dataset includes the first six time points (set CC), while the fourth set includes data points in the first two days and one on day five (set DD). In table 6.3 the data contained in the reduced data sets are listed.

Fitting the model used in the previous population approach to these data sets is impossible because the eleven model parameters are not identifiable with so few data. Two approaches were chosen to solve this problem. In the first some model parameters were set to values resulting from the solution of the final model structure as shown in table 5.4. The parameters for 1) excretion from Blood-O, 2) Blood-O to Blood-I, 3) Nodule-O to Blood-O and Lobe-O to Blood-O were successively set to the population mean value and the fitting process was initiated each time. If the fit converged no further parameters were excluded from estimation.
In the second approach the model was further reduced to the three minimal compart-

Table 6.3: Data included in the reduced data sets for the investigation of the measurement schedule.

Data Set	Time of measurement								
	2 h	4 h	24 h	2 d	4 d	5 d	7 d	14 d	21 d
AA	x	x	x						x
BB	x	x	x					x	x
CC	x	x	x	x	x	x			
DD	x	x	x			x			

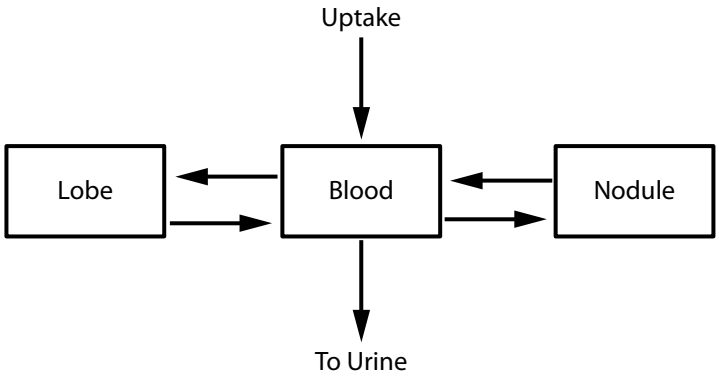

Figure 6.7: The minimal model for the individual analysis of the schedule optimization.

ments shown in figure 6.7. For this model no a priori information are needed, because it is simple enough to be identifiable with only four uptake measurements in both, nodule and lobe.

The resulting fits for the time-course of activity in the nodule are shown in figure 6.8. The solid lines are the fits of the data to the minimal model, the dashed lines are the fits to the full model with less adjustable parameters. In all four cases the fits describe the data well. This is in contrast to the findings from the population approach because it shows that no data acquired beyond one week are necessary to describe the kinetics. Even four measurements in the first five days (data set DD) are enough with the minimal model. The time range of five days is especially interesting for the kinetics of iodine because during the diagnostics with ^{123}I only measurements in this time range are possible due to the short half-life of about 13 h of the isotope. Therefore data sets CC and DD are of special interest as they represent measurement schedules that can possibly be implemented in the clinical practice.
The minimal model performs as good as or better than the full model, especially when data set DD is used. The minimal model can most probably not predict correctly the kinetics in blood and the urinary excretion. But these are anyways not measured in the usual clinical protocols. Hence, the schedule represented in set DD with the minimal model is the most practical and most efficient schedule for treatment planning because it involves only few measurements and a simple model.

So far data acquired during therapy have been used. In the next step, diagnostic data were used to verify the above findings. The kinetic described by the population mean model parameters for diagnostics derived in chapter 5.3.2 was used to generate a representative data set. Sampling time points were 2, 4 and 24 hours, 2, 4 and 5 days. Two data sets were generated corresponding to the schedules for sets CC and DD. The minimal model was fitted to these two sets. In figure 6.9 the resulting fits for the nodule

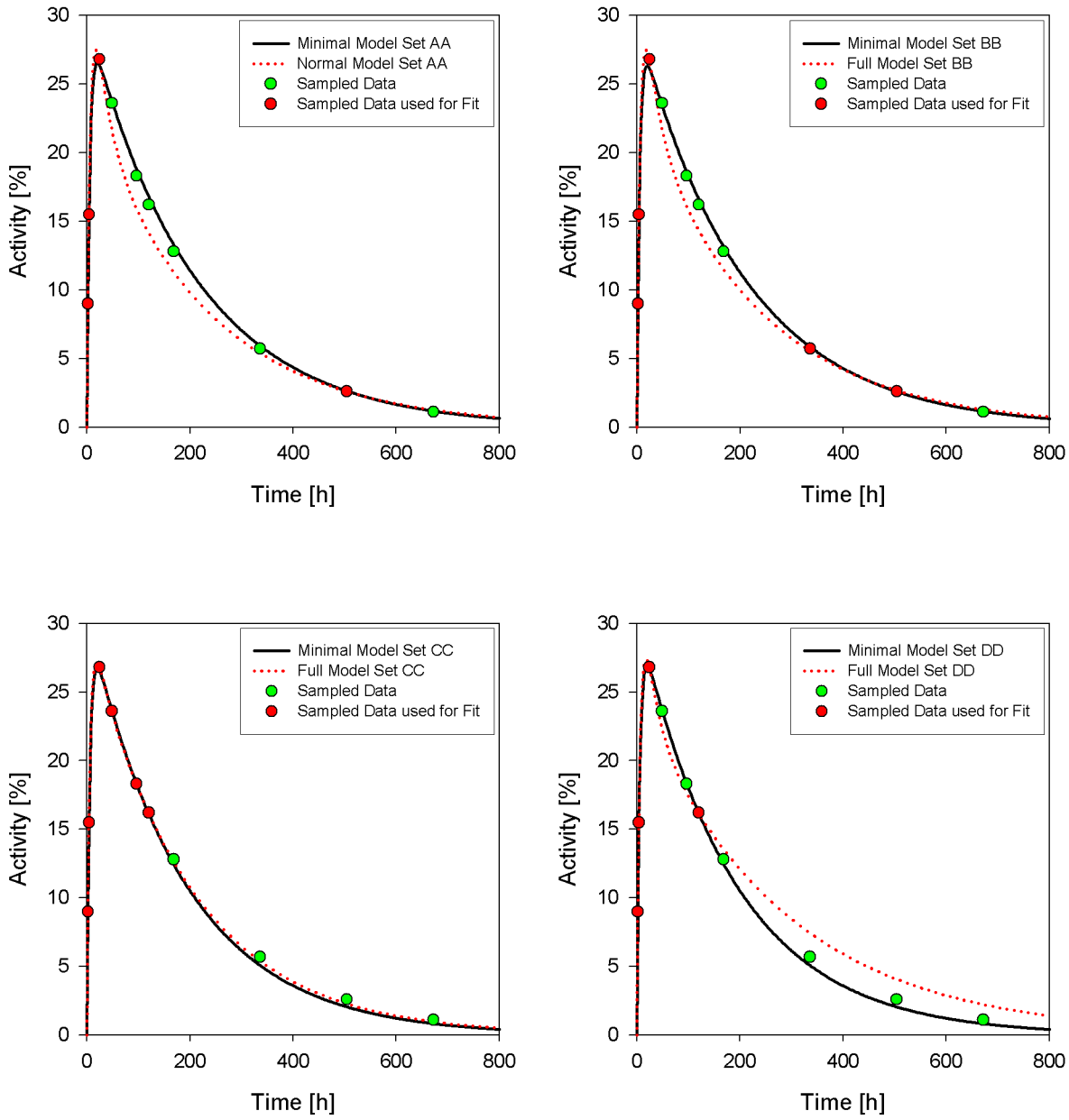

Figure 6.8: Schedule optimization with individual analysis: Fit of the full model and the minimal model to four different data sets for therapy.

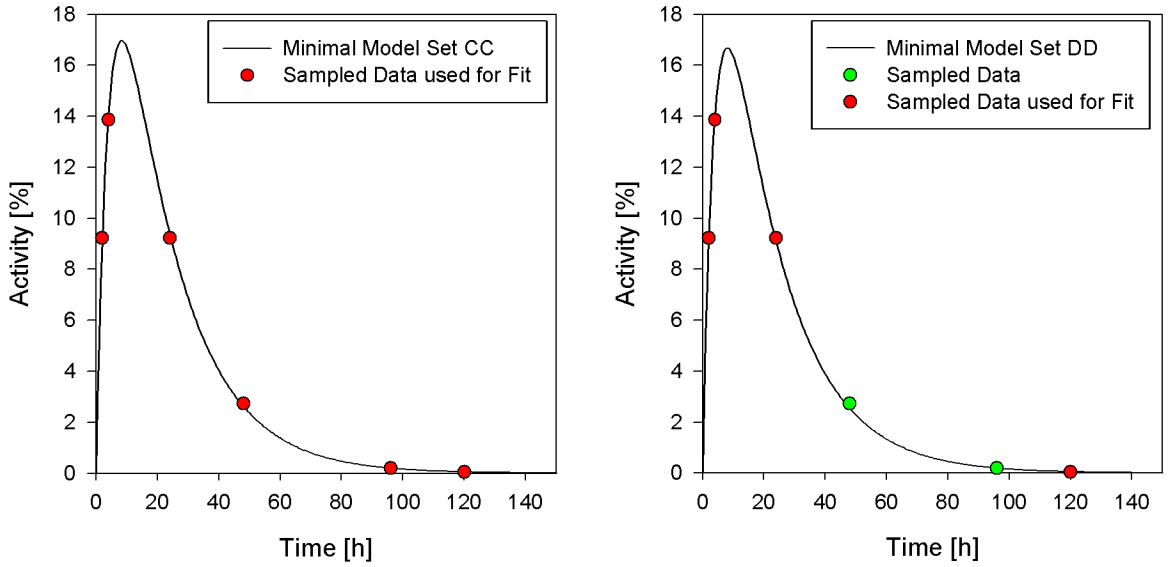

Figure 6.9: Schedule optimization with individual analysis: Fit of the minimal model to two different data sets for diagnostics.

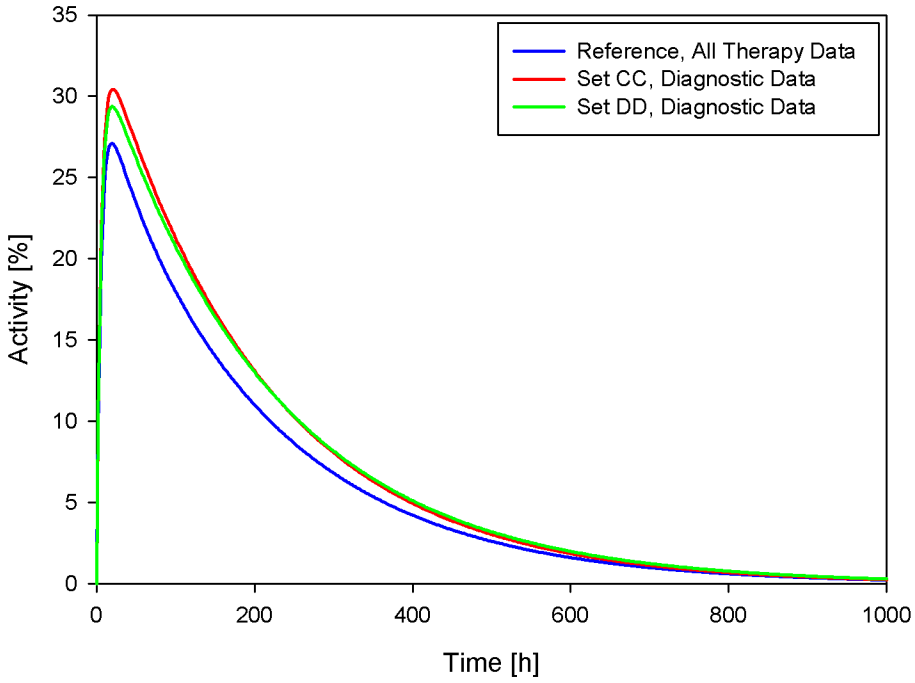

Figure 6.10: Schedule optimization with individual analysis: Fit of the full model to all data and the minimal model to two different reduced data sets.

are shown. They both reproduce the data very well. Furthermore both diagnostic schemes give very similar results in parameter values. The resulting model parameters together with the half life of ^{131}I were used to simulate the therapy kinetics with the diagnostic parameter set as described at the end of chapter 5.3.2. In figure 6.10 these curves are compared to the reference curve describing the kinetics during therapy derived from the population analysis of all data with the full model.

Both schedules result in very similar curves that overestimate the uptake slightly in comparison to the reference curve. The area under the curve for the set DD is 16 % larger than the area under the reference curve. Although only data measured in the first five days together with the minimal model are used, the kinetics at late times are modelled very realistically. The differences between the curves are in any case smaller than the uncertainties connected with the model parameters.

Up to now the schedule was based on the experience and the intuition of the physicists and physicians at the clinic. There was no systematic analysis what is actually needed to describe the kinetics correctly and do the treatment planning. In some procedures no diagnostic measurements were taken at all.
The availability of patients for measurements and the limited resources at the clinic like staff time and machine time restrict the schedule. Also the half -life of the isotope used and the activity given have an influence. In our case the diagnostic scan was done with ^{123}I and therefore the measurements were only feasible in the first five days after administration.

This analysis has shown that four measurements collected in the first five days can correctly predict the kinetics with a very simple model. This procedure is feasible in an clinical setting and is well suited for treatment planning.

7 Evaluation of the relation between absorbed dose and outcome of the therapy

7.1 Dose calculation for individual patients

The dose absorbed by nodule and healthy lobe during therapy was calculated for each patient. The dose was compared to the outcome of the treatment for each patient in this study to assess the success of the treatment planning approach used here.
The absorbed doses in nodule and, if present, in lobe were calculated for self-irradiation according to the method described in chapter 4.4.2. In these calculations the simplifying assumption was made that radiation is absorbed only in the same structure in that it is emitted. This means e.g. that only radiation emitted in the lobe is absorbed in the lobe and the crossfire from the activity in the nodule is ignored. The results are shown in table 7.1.

Table 7.1: Administered activity and absorbed dose in nodule and lobe during therapy calculated individually. For some patients no activity in the lobe was measured (-).

Number	Activity [MBq]	Dose Nodule [Gy]	Dose Lobe [Gy]
1	274	127.32	13.90
2	111	151.81	14.13
3	163	98.40	16.60
4	444	167.50	27.07
5	266	111.70	17.77
6	307	168.77	33.60
7	518	108.27	-
8	389	128.41	29.28
9	300	114.41	42.19
10	488	136.69	13.39
11	470	151.26	-
12	252	198.74	57.50
13	152	108.12	24.70
14	259	160.27	18.75

continued on next page...

Table 7.1: (continued)

Number	Activity [MBq]	Dose Nodule [Gy]	Dose Lobe [Gy]
15	352	131.24	-
16	155	152.04	23.62
17	318	143.24	34.80
18	315	154.68	12.41
19	333	127.37	36.01
20	189	90.57	-
21	370	133.17	26.75
22	180	117.28	9.57
23	277	114.62	16.11
24	451	158.47	16.83
25	337	101.72	6.53
26	340	251.14	7.49
27	189	112.48	-
28	218	127.92	17.63
29	311	195.89	15.17
30	359	45.32	30.51
31	315	123.75	-
32	196	118.39	60.37
33	274	165.66	15.37
34	315	86.56	13.54
35	611	135.63	23.43
36	197	125.60	31.37
37	607	193.87	-
38	66	123.98	-
39	481	154.69	-
40	870	98.24	-
41	164	99.82	-
42	851	146.70	-
43	198	132.17	59.33
Mean	331	135	25
Median	311	128	18
Minimum	66	45	6
Maximum	870	251	60

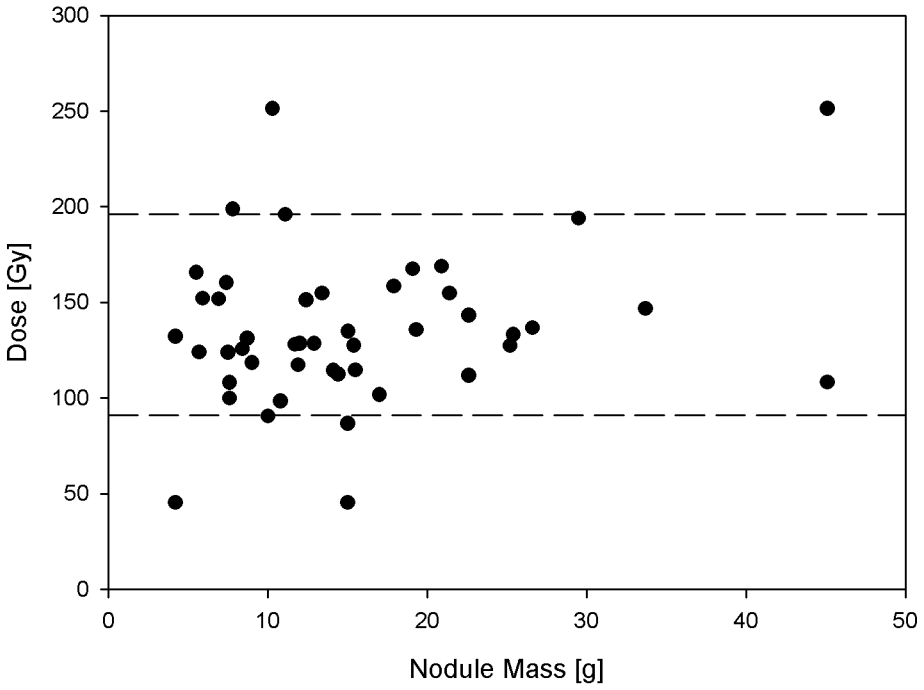

Figure 7.1: The nodule mass and the dose absorbed in the nodule. The two dashed lines represent the 5th and 95th percentile of the dose distribution.

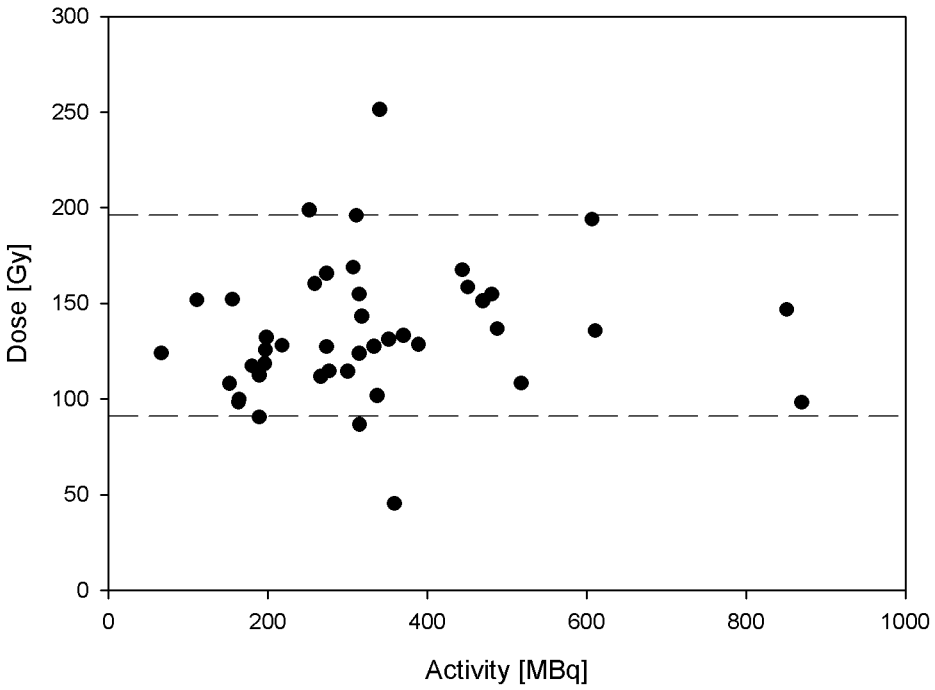

Figure 7.2: The administered activity and the dose absorbed in the nodule. The two dashed lines represent the 5th and 95th percentile of the dose distribution.

The doses absorbed by the nodules range from 45 Gy to 251 Gy, but 90 % of the patients received doses between 91 Gy and 196 Gy with a median of 128 Gy and a mean of 135 Gy. The absorbed doses in the contralateral lobe range from 6 Gy to 60 Gy with a median of 18 Gy and a mean of 25 Gy. In all cases the dose to the lobe is smaller than that to the nodule.

In figures 7.1 and 7.2 the absorbed dose is shown in relation to the thyroid mass and to the administered activity respectively. All patients got treated roughly with the same dose of about 130 Gy independently of the activity or the mass. Doses were neither correlated with the administered activity nor with the mass of the diseased tissue. This confirms the validity of the treatment planning approach because each patient is treated according to her or his individual iodine kinetics and nodule size. In 90 % of the patients the dose prescribed by the physicians was administered. In only very few cases this clinical procedure led to under- or overtreatment in respect to the absorbed dose.

The absorbed doses calculated in this chapter were derived for the simplified case that only self-irradiation occurred. In the next chapter the influence of this simplification is investigated by comparing the calculated dose values with values derived in a Monte Carlo simulation.

7.2 Dose calculation with Monte Carlo

The distribution of the absorbed dose during radioiodine therapy of AFTN was calculated in a Monte Carlo simulation as described in chapter 4.4.3. The energy spectrum of the radiation emitted by ^{131}I was used. In this simulation, the activity was homogeneously distributed in the nodule structure, uptake in the healthy tissue was neglected. Three different nodule sizes (cases) were simulated: 5, 10 and 20 grams. The total mass of the thyroid structure (31.8 g) and thus the total number of voxels (7097) for nodule and healthy tissue was the same in all three cases. Five million histories were calculated for each case.
The focus in this simulation was on the crossfire from nodule to lobe. The aim was to estimate how much dose was absorbed in the healthy tissue through irradiation from activity in the nodule.

The dose distributions for all three cases are shown in table 7.2. In this table the maximum dose absorbed in one voxel is set as 100 %. The dose in every other voxel in the thyroid structure is evaluated as percent of the maximum dose. For each case the number of voxels of either structures that fall into a certain dose range are summed.
In all three cases no voxel of the healthy tissue got more than 30 % of the maximum dose while all voxels of the nodule got more than 70 % of the maximum dose. This means that there is a very sharpe edge in the dose distribution separating the healthy tissue from the

Table 7.2: Frequencies of voxels with doses in per cent of the maximum dose in one voxel.

Percent	5 g Nodule		10 g Nodule		20 g Nodule	
	Healthy tissue	Nodule	Healthy tissue	Nodule	Healthy tissue	Nodule
0 - 10	5848	0	4395	0	1695	0
10 - 20	135	0	412	0	831	0
20 - 30	1	0	63	0	118	0
30 - 40	0	0	0	0	0	0
40 - 50	0	0	0	0	0	0
50 - 60	0	0	0	0	0	0
60 - 70	0	0	0	0	0	0
70 - 80	0	53	0	128	0	258
80 - 90	0	176	0	337	0	671
90 - 100	0	884	0	1762	0	3524
Sum	5984	1113	4870	2227	2644	4453

nodule. Furthermore, the dose distribution within the nodule is homogeneous with 80 % of the voxels in the nodule getting between 90 and 100 % of the maximum dose. For the 5 g nodule 98 % of the healthy voxels get less than 10 % of the maximum dose, for the 10 g nodule 90 % and for the 20 g nodule still 64 %.

Therefore the dose absorbed by the healthy tissue from irradiation by activity in the nodule is negligible for smaller nodules. This simulation indicates that this is not the case for larger nodules of more than 10 g. But it has to be considered that simulating large nodules in this voxel phantom leads to difficulties. The total mass of the thyroid could not be changed in the model. Therefore the 20 g nodule occupied voxels in both lobes. This differs significantly from the situation found in the patients in this study. In patients with large nodules of more than 15 g the total thyroid volume was enlarged due to the adenoma and the nodules did not extend into both lobes. So the simulation was in this case not as realistic as in the others due to the properties of the voxel phantom.

In table 7.3 SEE values and absorbed doses originating from the Monte Carlo calculation and those computed for individual patients are compared. For each of the three cases a patient with approximately the same nodule size was selected: patient 33 with a 5.5 g nodule, patient 20 with a 10 g nodule and patient 35 with a 19.3 g nodule. To get comparable dose values the number of nuclear disintegrations that occurred in the nodules of these patients were also used for the dose calculation in the corresponding Monte Carlo simulation. The values for both methods are in good agreement considering that the morphology differed in the patient and in the voxel model. A further reason for the

Table 7.3: Comparison of the SEE values computed in the Monte Carlo simulation and those calculated for patients with similar nodule masses. Additionally the resulting dose for the number of nuclear transitions in the respective patient is listed.

Nodule mass	Monte Carlo		Patient	
	SEE [J/kg]	Dose [Gy]	SEE [J/kg]	Dose [Gy]
5 g / Pat 33	4.92e-12	176	5.51e-12	166
10 g / Pat 20	3.23e-12	95	3.08e-12	91
20 g / Pat 35	1.61e-12	135	1.62e-12	136

small differences is the assumption of homogeneously distributed activity in the nodule during the simulation.

This comparison was only done for the nodule because there the dose from self-irradiation is computed in both cases. The doses calculated with the two methods are not comparable for the healthy tissue. In one method only self-irradiation is considered, in the second method only the dose from irradiation by an external source, i.e. the nodule, is considered.
In the Monte Carlo simulation the dose to the healthy tissue amounted to 3.7, 4.4 and 11.6 Gy for 5, 10 and 20 g nodules respectively. The mean dose from self-irradiation in the patients was 25 Gy. So the dose contribution by the external irradiation does not significantly change the total absorbed dose to the healthy tissue for small nodules. In the case of the large 20 g nodule the same difficulties for the reliability of the results as before have to be considered. In that case the nodule is too large for the thyroid structure it is set into. Therefore larger parts of the healthy tissue are near the nodule than would be in a real patient. This leads to an increased dose in the healthy thyroid tissue compared to a more realistic setting.

The Monte Carlo calculations have confirmed that the doses calculated for the individual patients are reasonable and realistic. Considering all the uncertainties in the measurements and modeling that are included in these calculations, disregarding the crossfire leads to no significant changes in the final dose estimate.

7.3 Evaluation of the outcome of the therapy

To investigate the outcome of the treatment, all patients had clinical follow-up examinations. In these the hormonal status of each patient was investigated by analyzing the TSH levels in blood samples. Thus the long term effects of the therapy could be determined.

These examinations were scheduled one, three, six and twelve months after the therapy, thereafter annually.
Of the 43 patients in this study, 36 patients became euthyroid after the therapy. Five patients developed hypothyroidism between three and six month after the therapy. They had medium sized nodules (10-17 g) and received between 45 Gy and 117 Gy of dose in the nodule and between 6 Gy and 42 Gy in the lobe, if present. These values are very similar to the mean values in our population. Other patients with similar nodule masses who were treated with similar doses became euthyroid after the therapy. So an overtreatment is not likely the reason for the hypothyroidism. Three of those five patients had been previously treated with ethanol injections. In the whole patient population in this study only five patients had undergone previous ethanol treatment. So there could be a causal relation between the previous treatment and the hypothyroidism after radioiodine therapy, but the numbers are too small to allow a statistically reliable conclusion.
Two patients remained hyperthyroid one year after the therapy. They had nodule masses of 15 g and 34 g and received 127 Gy and 147 Gy respectively. These values are also in the normal range for our patient population and thus a undertreatment is not likely the reason for the treatment failure.

Apparently the inability to reach an euthyroid status in these seven patients is not connected with too much dose to the healthy tissue or not enough dose to the diseased nodule. But the available data give no reliable insight into other factors that might influence the outcome of the therapy. Taking into consideration that hypothyroidism can be easily controlled by suppling the patient with artificial thyroid hormones only two out of 43 patients had to be treated further. This is an excellent result of this treatment procedure if compared to recurrence rates in the literature: Kok et al. [Kok2000] report an incidence of recurrence in 20 % of patients, Erdogan et al. [Erdogan2004] found that 12 % were still hyperthyroid after the therapy and Leslie et al. [Leslie2003] report that 23 % of the patients experienced recurrant hyperthyroidism.

8 Conclusions and outlook

In this work a biophysical compartmental model of the biokinetics of iodine in patients suffering from AFTN was developed. This is the first model to deal specifically with this disease. The kinetics of iodine were modeled for both the healthy and the diseased parts of the thyroid. It describes in a physiologically realistic way the actual metabolic pathway of iodine,i.e. the uptake and retention of iodine in the thyroid and the synthesis of thyroid hormones. It also includes the release from the thyroid and the metabolism of the hormones and finally the recycling and excretion of the iodine.

The model parameters were estimated using measured biokinetic data from 43 AFTN patients. The data were collected during the clinical diagnostic and therapeutic routine procedures with radioiodine isotopes. The model can describe all data measured during diagnostics and therapy, the activity concentration in urine and blood samples and the activity measured in the nodule and healthy tissue.

The model was used to optimize the measurement schedule during diagnostics. The model together with information collected during this pretherapeutical study can predict the individual iodine kinetics of a patient. These are used to treat the patient with the amount of activity that in his case cures the hyperthyroidism but preserves as much of the healthy thyroid tissue as possible. The minimal number and the optimal time points for diagnostic measurements were found. Applying this schedule can help to increase the efficiency of the clinical procedures by reducing the work load of the staff and the usage of the machines. Also the patients can profit from the optimization because the treatment can be adapted individually to the personal iodine biokinetics.

In the last part of this work it was shown that the personalized treatment leads to excellent results of the therapy. The absorbed dose to the diseased nodule was calculated for each patient because it is closely related to the outcome of the therapy. The results of the dose calculations were validated with a Monte Carlo simulation and found to be realistic. In 90 % of the patients the dose was administered as prescribed. The therapy failed to cure the patient only in two out of 43 patients.

The optimized time schedule for diagnostic measurements developed in this work together with the new model have the potential to facilitate the personalized treatment of AFTN patients. To validate this and test the application of this treatment planning approach in a clinical setting a further patient study would be needed in the future.

Appendix

Complementary to the data shown in chapter 5.1, the activites measured in the thyroid in all patients included in this study are graphically shown in the appendix. For each patient there are graphs for the activity in the nodule and, if present, in the healthy lobe during both diagnostics and therapy. All graphs are available on the included CD as pdf-files.

Bibliography

[Alexander2002] E. K. Alexander and P. R. Larsen. High dose of ^{131}I therapy for the treatment of hyperthyroidism caused by Graves' disease. *Journal of Clinical Endocrinology and Metabolism*, 87(3):1073–1077, 2002.

[Allahabadia2001] A. Allahabadia, J. Daykin, M. C. Sheppard, S. C. L. Gough, and J. A. Franklyn. Radioiodine treatment of hyperthyroidism-prognostic factors for outcome. *The Journal of Clinical Endocrinology & Metabolism*, 86(8):3611–3617, 2001.

[Angerstein2005] W. Angerstein, editor. *Grundlagen der Strahlenphysik und radiologischen Technik in der Medizin*. H. Hoffmann GmbH Berlag, Berlin, 5th edition, 2005.

[Audoly1997] S. Audoly and L. D'Angio. *Globi2 - software for GLOBal Identifiability.* Gruppo Biomed Mod. Padova, Italy, 1997.

[Barrett1998] P. H. Barrett, B. M. Bell, C. Cobelli, H. Golde, A. Schumitzky, P. Vicini, and D. M. Foster. SAAM II: Simulation, analysis, and modeling software for tracer and pharmacokinetic studies. *Metabolism*, 47(4):484–492, 1998.

[Berg1996] G. E. B. Berg, A. M. K. Michanek, E. C. V. Holmberg, and M. Fink. ^{131}I treatment of hyperthyroidism: Significance of effective half-life measurements. *Journal of Nuclear Medicine*, 37(2):228–232, 1996.

[Berkovski1999a] V. Berkovski. *Radioiodine biokinetics in the mother and fetus. Part 1. Pregnant woman. In: Radiation and Thyroid Cancer.* World Scientific Publishing, 1999. Publication No. EUR 18552 EN of the European Commission, pp. 319-325.

[Berkovski1999b] V. Berkovski. *Radioiodine biokinetics in the mother and fetus. Part 2. Fetus. In: Radiation and Thyroid Cancer.* World Scientific Publishing, 1999. Publication No. EUR 18552 EN of the European Commission, pp. 327-332.

[Berman1968] M. Berman, E. Hoff, M. Barandes, D. V. Becker, Sonenber.M, R. Benua, and D. A. Koutras. Iodine kinetics in man - a model. *Journal of Clinical Endocrinology and Metabolism*, 28(1):1–14, 1968.

[Bockisch1993] A. Bockisch, T. Jamitzky, R. Derwanz, and H. J. Biersack. Optimized dose planning of radioiodine therapy of benign thyroidal diseases. *Journal of Nuclear Medicine*, 34(10):1632–1638, 1993.

[Bolch1999] W. E. Bolch, L. G. Bouchet, J. S. Robertson, B. W. Wessels, J. A. Siegel, R. W. Howell, A. K. Erdi, B. Aydogan, S. Costes, E. E. Watson, A. B. Brill, N. D. Charkes, D. R. Fisher, M. T. Hays, and S. R. Thomas. MIRD pamphlet No. 17: The dosimetry of nonuniform activity distributions–radionuclide S values at the voxel level. Medical Internal Radiation Dose Committee. *Journal of Nuclear Medicine*, 40(1):11S–36S, Jan 1999.

[Bolch2009] W. E. Bolch, K. F. Eckerman, G. Sgouros, and S. R. Thomas. MIRD pamphlet No. 21: A generalized schema for radiopharmaceutical dosimetry–standardization of nomenclature. Medical Internal Radiation Dose Committee. *Journal of Nuclear Medicine*, 50(3):477–484, 2009.

[Brenner2002] W. Brenner. Is thyroid stunning a real phenomenon or just fiction? *Journal of Nuclear Medicine*, 43(6):835–836, 2002.

[Canzi2006] C. Canzi, F. Zito, and F. Voltini. Verification of the agreement of two dosimetric methods with radioiodine therapy in hyperthyroid patients. *Medical Physics*, 33(8):2860–2867, 2006.

[Carson1983] E. R. Carson, C. Cobelli, and L. Finkelstein. *The mathematical modeling of Metabolic and Endocrine systems*. John Wiley & Sons, New York, 1983.

[Catargi1999] B. Catargi, F. Leprat, M. Guyot, N. Valli, D. Ducassou, and A. Tabarin. Optimized radioiodine therapy of Graves' disease: analysis of the delivered dose and of other possible factors affecting outcome. *European Journal of Endocrinology*, 141:117–121, 1999.

[Clerc1995] J. Clerc, F. Dagousset, M. Izembart, J. P. Jais, H. M. Heshmati, A. Alcais, A. Chevalier, A. F. Leger, and L. Barritault. Radioiodine therapy of the autonomous thyroid-nodule in patients with or without visible extranodular activity. *Journal of Nuclear Medicine*, 36(2):217–223, 1995.

[Cohen2004] J. B. Cohen, J. E. Kalinyak, and I. R. McDougall. Clinical implications of the differences between diagnostic ^{123}I and post-therapy ^{131}I scans. *Nuclear Medicine Communications*, 25:129–134, 2004.

[DArgenio2009] D. Z. DArgenio, A. Schumitzky, and X. Wang. *ADAPT 5 Users Guide: Pharmacokinetic/Pharmacodynamic Systems Analysis Software*. Biomedical Simulations Resource, Los Angeles, 2009.

[Deleu2000] S. Deleu, Y. Allory, A. Radulescu, I. Pirson, N. Carrasco, B. Corvilain, I. Salmon, B. Franc, J.E. Dumont, J. Van Sande, and C. Maenhaut. Characterization of autonomous thyroid adenoma: metabolism, gene expression, and pathology. *Thyroid*, 10:131–140, 2000.

[Dorn2003] R. Dorn, J. Kopp, H. Vogt, P. Heidenreich, R. G. Carroll, and S. A. Gulec. Dosimetry-guided radioactive iodine treatment in patients with metastatic

differentiated thyroid cancer: Largest safe dose using a risk-adapted approach. *Journal of Nuclear Medicine*, 44:451–456, 2003.

[Erdogan2004] M. F. Erdogan, N. O. Kücük, C. Anil, S. Aras, D. Ozer, G. Aras, and N. Kamel. Effect of radioiodine therapy on thyroid nodule size and function in patients with toxic adenomas. *Nuclear Medicine Communications*, 25:1083–1087, 2004.

[Franklyn1995] J. A. Franklyn, J. Daykin, R. Holder, and M. C. Sheppard. Radioiodine therapy compared in patients with toxic nodular or Graves' hyperthyroidism. *QJM-Monthly Journal of the Association of Physicians*, 88(3):175–180, 1995.

[Giussani2002] A. Giussani, M. C. Cantone, and U. Asaro. Radioiodine therapy of the autonomous functioning thyroid nodule: a compartmental model for individual dose estimation. European IRPA Congress 2002, Firenze, Italy.

[Giussani2006] A. Giussani, C. Canzi, and P. Gerundini. The contribution of compartmental modelling for optimization of radioiodine therapy in patients with atn syndrome. Workshop on Internal Dosimetry of Radionuclides. Occupational, public and medical exposure. Montpellier, France, 2-5 October 2006.

[Grzesiuk2006] W. Grzesiuk, J. Nieminuszczy, M. Kruszewski, T. Iwanienko, M. Plazinska, M. Bogdanska, E. Bar-Andziak, L. Krolicki, and E. Grzesiuk. DNA damage and its repair in lymphocytes and thyroid nodule cells during radioiodine therapy in patients with hyperthyroidism. *Journal of Molecular Endocrinology*, 37:527–532, 2006.

[Guhlmann1995] C. A. Guhlmann, J. Rendl, and W. Borner. Radioiodine therapy of autonomously functioning thyroid-nodules and of Graves' disease. *Nuklearmedizin*, 34(1):20–23, 1995.

[Haase2000] A. Haase, M. Bhre, I. Lauer, B. Meller, and E. Richter. Radioiodine therapy in Graves' hyperthyroidism: determination of individual optimum target dose. *Exp Clin Endocrinol Diabetes*, 108(2):133–137, 2000.

[Hall2000] E. J. Hall. *Radiobiology for the radiologist*. J.B. Lippincott Williams & Wilkins, Philadelphia, 5 edition, 2000.

[Hays1965] M. T. Hays and D.H. Solomon. Influence of the gastrointestinal iodide cycle on the early distribution of radioactive iodide in man. *Journal of Clinical Investigation*, 48:1114–1123, 1965.

[Hays2001] M. T. Hays. Estimation of total body iodine content in normal young men. *Thyroid*, 11(7):671–675, 2001.

[Hoffman1982] D. A. Hoffman, W. M. McConahey, J. F. Fraumeni, and L. T. Kurland. Cancer incidence following treatment of hyperthyroidism. *International Journal of Epidemiology*, 11(3):218–224, 1982.

[Holm1991] L. E. Holm, P. Hall, K. Wiklund, G. Lundell, G. Berg, G. Bjelkengren, E. Cederquist, U. B. Ericsson, A. Hallquist, and L. G. Larsson. Cancer risk after iodine-131 therapy for hyperthyroidism. *Journal of the National Cancer Institute*, 83(15):1072–1077, 1991.

[ICRP1977] International Commission on Radiological Protection. *Recommendation of the International Commission on Radiological Protection*. ICRP Publication 26 (Annals of the ICRP Vol. 1(3)). Pergamon Press, Oxford, UK.

[ICRP1979] International Commission on Radiological Protection. *Limits for intakes of radionuclides by workers*. ICRP Publication 30, Part 1 (Annals of the ICRP Vol. 2(3-4)). Pergamon Press, Oxford, UK.

[ICRP1983] International Commission on Radiological Protection. *Radionuclide Transformations: Energy and Intensity of Emissions*. ICRP Publication 38 (Annals of the ICRP Vols. 11-13). Pergamon Press, Oxford, UK.

[ICRP1987] International Commission on Radiological Protection. *Radiation dose from radiopharmaceuticals*. ICRP Publication 53 (Annals of the ICRP Vol. 18(1-4)). Pergamon Press, Oxford, UK.

[ICRP1989] International Commission on Radiological Protection. *Age-dependent doses to members of the public from intake of radionuclides Part 1*. ICRP Publication 56 (Annals of the ICRP Vol. 20(2)). Pergamon Press, Oxford, UK.

[ICRP2001] International Commission on Radiological Protection. *Doses to the embryo and fetus from intakes of radionuclides by the mother*. ICRP Publication 88 (Annals of the ICRP Vol. 31(1-3)). Pergamon Press, Oxford, UK.

[ICRP2006] International Commission on Radiological Protection. *Human Alimentary Tract Model for Radiological Protection*. ICRP Publication 100 (Annals of the ICRP Vol. 36(1-2)). Pergamon Press, Oxford, UK.

[ICRP2008] International Commission on Radiological Protection. *Nuclear Decay Data for Dosimetric Calculations*. ICRP Publication 107 (Annals of the ICRP Vol. 38(3)). Pergamon Press, Oxford, UK.

[Johansson2003] L. Johansson, S. Leide-Svegbirg, S. Mattsson, and B. Nosslin. Biokinetics of iodide in man: Refinement of current ICRP dosimetry models. *Cancer Biotherapy & Radiopharmaceuticals*, 18(3):445–450, 2003.

[Jonsson2004] H. Jönsson and S. Mattsson. Excess radiation absorbed doses from non-optimised radioiodine treatment of hyperthyroidism. *Radiation Protection Dosimetry*, 108(2):107–114, 2004.

[Kawrakow2009] I. Kawrakow and D. W. O. Rogers. The EGSnrc code system: Monte Carlo simulation of electron and photon transport. PIRS Report 701, 5th edn (Ottawa: National Research Council of Canada), 2009. Available online at

http://www.irs.inms.nrc.ca/inms/irs/EGSnrc/pirs701.pdf; visited on October 1st 2010.

[Kok2000] S. W. Kok, J. W. Smit, A. J. M. De Craen, B. M. Goslings, B. L. F. Van Eck-Smit, and J. A. Romijn. Clinical outcome after standardized versus dosimetric radioiodine treatment of hyperthyroidism: an equivalence study. *Nuclear Medicine Communications*, 21:1071–1078, 2000.

[Leslie2003] W. D. Leslie, L. Ward, E. A. Salamon, S. Ludwig, R. C. Rowe, and E. A. Cowden. A randomized comparison of radioiodine doses in Graves' hyperthyroidism. *The Journal of Clinical Endocrinology & Metabolism*, 88:978–983, 2003.

[Li2010] W. B. Li and C. Hoeschen. Uncertainty and sensitivity analysis of biokinetic models for radiopharmaceuticals used in nuclear medicine. *Radiation Protection Dosimetry*, 139(1-3):228–231, 2010.

[Lucignani2007] G. Lucignani. Long-term risks in hyperthyroid patients treated with radioiodine: is there anything new? *European Journal of Nuclear Medicine and Molecular Imaging*, 34:1504–1509, 2007.

[Matheoud2003] R. Matheoud, C. Canzi, E. Reschini, F. Zito, F. voltini, and P. Gerundini. Tissue-specific dosimetry for radioiodine therapy of the autonomous thyroid nodule. *Medical Physics*, 30(5):791–798, 2003.

[Mattsson2006] S. Mattsson, L. Johansson, H. Jönsson, and B. Nosslin. Radioactive iodine in thyroid medicine - how it started in sweden and some of today's challenges. *Acta Oncologia*, 45:1031–1036, 2006.

[Meier2002] D. A. Meier, D. R. Brill, D. V. Becker, S. E. M. Clarke, E. B. Silberstein, H. D. Royal, and H. R. Balon. Procedure guideline for therapy of thyroid disease with ^{131}I. *Journal of Nuclear Medicin*, 43:856–861, 2002.

[Meller2008] B. Meller, E. Gaspar, W. Deisting, B. Czarnocka, M. Baehre, and B. E. Wenzel. Decreased radioiodine uptake of FRTL-5 cells after ^{131}I incubation in vitro: molecular biological investigations indicate a cell cycle-dependent pathway. *European Journal of Nuclear Medicine and Molecular Imaging*, 35(6):1204–1212, 2008.

[Metso2004] S. Metso, P. Jaatinen, H. Huhtala, T. Luukkaala, H. Oksala, and J. Salmi. Long-term follow-up study of radioiodine treatment of hyperthyroidism. *Clinical Endocrinology*, 61(5):641–648, 2004.

[Metso2007a] S. Metso, P. Jaatinen, H. Huhtala, A. Auvinen, H. Oksala, and J. Salmi. Increased cardiovascular and cancer mortality after radioiodine treatment for hyperthyroidism. *Journal of Clinical Endocrinology and Metabolism*, 92(6):2190–2196, 2007.

[Metso2007b] S. Metso, A. Auvinen, H. Huhtala, J. Salmi, H. Oksala, and P. Jaatinen. Increased cancer incidence after radioiodine treatment for hyperthyroidism. *Cancer*, 109(10):1972–1979, 2007.

[Morris2001] L. F. Morris, A. D. Waxman, and G. D. Braunstein. The nonimpact of thyroid stunning: remnant ablation rates in ^{131}I-scanned and nonscanned individuals. *Journal of Clinical Endocrinology and Metabolism*, 86(8):3507–3511, 2001.

[NNDC2010] National Nuclear Data Center, Brookhaven National Laboratory. NuDat 2.5: Interactive Decay Radiation Search. Website, 2010. Available online at `http://www.nndc.bnl.gov/nudat2/`; visited on June 15th 2010.

[Nygaard1999] B. Nygaard, L. Hegedus, K. G. Nielsen, P. Ulriksen, and J. M. Hansen. Long-term effect of radioactive iodine on thyroid function and size in patients with solitary autonomously functioning toxic thyroid nodules. *Clinical Endocrinology*, 50(2):197–202, 1999.

[Parma1993] J. Parma, L. Duprez, J. Van Sande, P. Cochaux, C. Gervy, J. Mockel, J. Dumont, and G. Vassart. Somatic mutations in the thyrotropin receptor gene cause hyperfunctioning thyroid adenomas. *Nature*, 365:649–652, 1993.

[Postgard2002] P. Postgard, J. Himmelman, U. Lindencrona, N. Bhogal, D. Wiberg, G. Berg, S. Jansson, E. Nystrm, E. Forssell-Aronsson, and M. Nilsson. Stunning of iodide transport by ^{131}I irradiation in cultured thyroid epithelial cells. *Journal of Nuclear Medicine*, 43(6):828–834, 2002.

[Reinartz2003] P. Reinartz, M. Zimny, W. Schaefer, B. Mueller, U. Buell, and O. Sabri. Radioiodine therapy in patients with hyperthyroid disorder: standard versus dosimetric activity application. *Nuclear Medicine Communications*, 24:1247–1253, 2003.

[Reinhardt2002] M. J. Reinhardt, I. Brink, A. Y. Joe, D. von Mallek, S. Ezziddin, H: Palmedo, and T. M. Krause. Radioiodine therapy in Graves' disease based on tissue-absorbed dose calculations: effect of pre-treatment thyroid volume on clinical outcome. *European Journal of Nuclear Medicine and Molecular Imaging*, 29:1118–1124, 2002.

[Reschini1999] E. Reschini, R. Matheoud, C. Canzi, M. Castellani, M. Galelli, C. Ferrari, A. Paracchi, and P. Gerundini. Dosimetry study in patients with autonomous thyroid nodule who are candidates for radioiodine therapy. *Journal of Nuclear Medicine*, 40:1928–1934, 1999.

[Ross1984] D. S. Ross, E. C. Ridgway, and G. H Daniels. Successful treatment of solitary toxic thyroid nodules with relatively low-dose ^{131}I, with low prevalence of hypothyroidism. *Annals of Internal Medicine*, 101(4):488–490, 1984.

[SNM2005] E. B. Silberstein, A. Alavi, H. R. Balon, D.V. Becker, D. R. Brill, S. E. M. Clarke, C. Divgi, S. J. Goldsmith, R. J. Lull, D. A. Meier, H. D. Royal, J. A. Siegel, and A. D. Waxman. Society of nuclear medicine procedure guideline for therapy of thyroid disease with ^{131}I (sodium iodide), version 2.0. Website, 2005. Available online at `http://interactive.snm.org/docs/TherapyofThyroidDiseasewithIodine-131v2.0.pdf`; visited on May 3rd 2010.

[Siddiqi2001] A. Siddiqi, R. R. Foley, K. E. Britton, A. Sibtain, P. N. Plowman, A. B. Grossman, J. P. Monson, and G. M. Besser. The role of ^{123}I-diagnostic imaging in the follow-up of patients with differentiated thyroid carcinoma as compared to ^{131}I-scanning: avoidance of negative therapeutic uptake due to stunning. *Clinical Endocrinologyl (Oxf)*, 55(4):515–521, 2001.

[Singer1995] P. A. Singer, D. S. Cooper, E. G. Levy, P. W. Ladenson, L. E. Braverman, G. Daniels, F. S. Greenspan, I. R. McDougall, and T. F. Nikolai. Treatment guidelines for patients with hyperthyroidism and hypothyroidism. Website, 1995. Available online at `http://thyroid.org/professionals/publications/documents/GuidelinesHyperHypo_1995.pdf`; visited on May 3rd 2010.

[Sisson2006] J. C. Sisson, A. M. Avram, S. A. Lawson, P. G. Gauger, and G. M. Doherty. The so-called stunning of thyroid tissue. *Journal of Nuclear Medicine*, 47(9):1406–1412, 2006.

[Sisson2007] J. C. Sisson, A. M. Avram, D. Rubello, and M. D. Gross. Radioiodine treatment of hyperthyroidism: fixed or calculated doses; intelligent design or science? *European Journal of Nuclear Medicine and Molecular Imaging*, 34(7):1129–1130, 2007.

[Snyder1975] W. S. Snyder, M. R. Ford, G. G. Warner, and S. B. Watson. "S", Absorbed dose per unit cumulated activity for selected radionuclides and organs, 1975. MIRD Pamphlet No. 11. New York, NY: Society of Nuclear Medicine.

[Spitzweg2000] C. Spitzweg, A. E. Heufelder, and J. C. Morris. Thyroid iodine transport. *Thyroid*, 10(4):321–330, 2000.

[Stabin2000] M. G. Stabin and M. W. Konijnenberg. Re-evaluation of absorbed fractions for photons and electrons in spheres of various sizes. *Journal of Nuclear Medicine*, 41(1):149–160, 2000.

[Tezelman1994] S. Tezelman, R. F. Grossman, A. E. Siperstein, and O. H. Clark. Radioiodine-associated thyroid cancers. *World Journal of Surgery*, 18(4):522–528, 1994. 35th World Congress of the International Society of Surgery, 1993, Hong Kong, Hong Kong.

[Thyroid2000] L. E. Braverman and R. D. Utiger, editors. *Werner & Ingbar's The Thyroid: A Fundamental and Clinical Text*. Lippincott Williams & Wilkins, Philadelphia, 2000.

[Urhan2007] M. Urhan, S. Dadparvar, A. Mavi, M. Houseni, W. SChamroonrat, A. Alavi, and S. J. Mandel. ^{123}I as a diagnostic imaging agent in differentiated thyroid carcinoma: a comparison with ^{131}I posttreatment scanning and serum thyroglobulin measurement. *European Journal of Nuclear Medicine and Molecular Imaging*, 34:1012–1017, 2007.

[WHO2004] Joint FAO/WHO Expert Consultation. *Vitamin and mineral requirements in human nutrition*, chapter Iodine, pages 303–317. World Health Organization and Food and Agriculture Organization of the United Nations, Geneva, Switzerland, second edition, 2004.

[Weetman2007] A. P. Weetman. Radioiodine treatment for benign thyroid diseases. *Clinical Endocrinology*, 66:757–764, 2007.

[Yeung2000] H. W. D. Yeung, J. L. Humm, and S. M. Larson. Radioiodine uptake in thyroid remnants during therapy after tracer dosimetry. *Journal of Nuclear Medicine*, 41:1082–1085, 2000.

[Zankl2002] M. Zankl, U. Fill, N. Petoussi-Henss, and D. Regulla. Organ dose conversion coefficients for external photon irradiation of male and female voxel models. *Physics in Medicine and Biology*, 47(14):2367–2385, 2002.

[Zankl2003] M. Zankl, N. Petoussi-Henss, U. Fill, and D. Regulla. The application of voxel phantoms to the internal dosimetry of radionuclides. *Radiation Protection Dosimetry*, 105(1-4):539–548, 2003.

[Zingrillo2000] M. Zingrillo, M. Torlontano, M. R. Ghiggi, V. Frusciante, A. Varraso, A. Liuzzi, and V. Trischitta. Radioiodine and percutaneous ethanol injection in the treatment of large toxic thyroid nodule: A long-term study. *Thyroid*, 10(11):985–989, 2000.

Acknowledgment

First and foremost I thank Prof. Dr. Dr. Herwig G. Paretzke for the possibility to work on this topic under his supervision.

I thank Prof. Dr. Christoph Hoeschen for supporting and funding my work, for scientific guidance and stimulation through critical questions and the requisition for excellence.

My deepest gratitude is to Dr. Augusto Giussani who always had time for me for scientific guidance, for technical instructions on modeling and for advice and motivation in many fruitful discussions.

My thank goes to Dr. Christina Canzi and the staff at Fondazione IRCCS Ca' Granda - Ospedale Maggiore Policlinico in Milan, Italy for recruiting patients to volunteer for this study, for measurements and data acquisition and for their time to give me insight into the practical aspects of nuclear medicine and the clinical routine procedures.

I thank Maria Zankl for the simulation of AFTN in a voxel phantom and the Monte Carlo calculations.

I thank Dr. Weibo Li for the application of his uncertainty analysis software to my model and his advice on biokinetic modeling.

My thank goes to all members of the AMSD for the very friendly, amicable and relaxed working atmosphere, for scientific and moral support whenever needed and the good time together at the Helmholtz Zentrum.

I thank my family and friends for always supporting and helping me, for their lenience and patience.

This work was financially supported by the Collaborative Project "MADEIRA" (www.madeira-project.eu), cofunded by the European Commission through EURATOM Seventh Framework Programme (Grant Agreement FP7-212100).